國 立 交 通 大 學

電 子 工 程 學 系 電 子 研 究 所

碩 士 論 文

利用共鍍催化金屬與不同間距高度比之奈米碳管柱列改善氣體游離式感測器之特性研究

Study on the improvement of carbon nanotube gas ionization sensors via co-deposited catalyst and pillar array with different spacer / height ratios

研 究 生：黃 均 宇

指導教授：鄭 晃 忠 博士

中華民國 100 年 七 月

利用共鍍催化金屬與不同間距高度比之奈米碳管柱列改善氣體游離式感測器之特性研究

Study on the improvement of carbon nanotube gas ionization sensors via co-deposited catalyst and pillar array with different spacer / height ratios

研 究 生：黃均宇　　Student: Chun-Yu Huang

指導教授：鄭晃忠　博士　　Advisor: Dr. Huang-Chuang Cheng

國立交通大學

電子工程學系　電子研究所碩士班

碩士論文

A Thesis

Submitted to Department of Electronics Engineering & Institute of Electronics

College of Electrical and Computer Engineering

National Chiao Tung University

In Partial Fulfillment of the Requirements for the Degree of Master

in

Electronics Engineering

2011

Hsinchu, Taiwan, Republic of China

中華民國 100 年 七月

利用共鍍催化金屬與不同間距高度比之奈米碳管柱列改善氣體游離式感測器之特性研究

學生:黃均宇　　指導教授: 鄭晃忠 博士

國立交通大學

電子工程學系 電子研究所碩士班

摘　要

氣體游離式感測器是一種以氣體分子各自獨特的物理特性來分辨不同氣體的元件，傳統上，氣體游離式感測器受限於過大的結構（如火焰游離式感測器及光游離式感測器）、危險的高電壓操作並其伴隨而來的高功率消耗等因素。因此在本篇論文的實驗中，吾人嘗試利用奈米碳管較低的功函數、尖銳的特點以及在適當電場下能獲得極佳之游離待測氣體能力與穩定性等來改善氣體游離式感測器。

在本篇論文實驗的起頭，首先會討論不同表面型態的奈米碳管薄膜所造成的氣體崩潰特性之差異。由無定向之碳管薄膜的量測結果發現，其崩潰電壓十分不穩定且在高電壓區域的誤差有將近 100 伏特的變動。這些結果被認為與其表面碳管的長度不一有很大的關係。因為相對來說，均勻垂直之碳管薄膜就有較穩定的氣體崩潰特性。但是，對於這兩種表面型態不同的碳管薄膜來說，在經過穩定性測試的高電壓處理之後，它們的崩潰電壓漂移的情形都十分嚴重。無定向之碳管薄膜在經過 1000 次重複的穩定性測試之後，其崩潰電壓由起初的 365V 上升到 605V，相當於上升了 68%。而均勻垂直之碳管薄膜在經過相同 1000 次重複的穩

定性測試之後，其崩潰電壓則由 395V 上升到 575V，也就是上升了 45%。並且我們從掃描式電子顯微鏡圖中可觀察發現，崩潰電壓上升的主要原因跟碳管在高電壓下會有被拔除與燒結的現象有關。

因此，為了增進奈米碳管氣體游離式感測器之穩定性，吾人嘗試以鈷-鈦催化劑金屬共鍍的方式來改善碳管與基板之間的附著力及接觸阻抗。並且由實驗的結果可發現，以此方式合成之碳管薄膜確實有更穩定的崩潰特性，在經過同樣 1000 次重複的穩定性測試之後，其崩潰電壓僅由 375V 上升到 435V，只上升了 16%，與先前兩種碳管薄膜比較起來可說大有改進。

另外，為了改善氣體游離式感測器的功率消耗，減低其操作電壓是首先需要研究的。在這部份，則使用不同間距高度比的奈米碳管柱列來探討在多少的間距高度比下有最理想的表面電場分佈，以期達到有最好的拉電子能力並可最早達到氣體崩潰；也就是有最低的崩潰電壓。在實驗中，吾人嘗可在量測結果的統整中發現，在間距高度比約 2.91 附近有最低的崩潰電壓。因此此理想的陣列間距高度比可應用於降低氣體游離式感測器的操作電壓以及功率消耗。

接下來，這些理想化過後的碳管柱陣列被使用來探討在不同氣體環境下的氣體游離特性。這些不同的氣體因為具有不同的平均自由路徑、游離能及再結合率，因此會有各自獨特的 Paschen’s curve。利用這些 Paschen’s curve 並加上適當地選擇氣體壓力與間距的乘積值，則可製作出既操作在低電壓，又能有足夠寬的間隔來分辨不同氣體的崩潰電壓。最後，吾人探討不同比例的氫氣、二氧化碳與一般空氣混和之後的崩潰電壓變化：以間距高度比為 2.91 碳管柱陣列為例，當二氧化碳在空氣中的比例到達 15%時，則崩潰電壓上升會 60V，當氫氣在空氣中的比例到達 11%時，則崩潰電壓會下降 100V。

Study on the improvement of carbon nanotubes gas ionization sensors via co-deposited catalyst and pillar array with different spacer / height ratios

Student: Chun-Yu Huang Advisor: Dr. Huang-Chung Cheng

Department of Electronics Engineering & Institute of Electronics
National Chiao Tung University

Abstract

Gas ionization sensors are physical devices that work by fingerprinting the ionization characteristics of distinct gases. Conventional ionization sensors were limited by the huge and bulky architecture (ex: FID, PID), risky high-voltage operation and high power consumption. In this thesis, carbon nanotubes (CNTs) with relatively low work function, extremely sharp nanotips, and structural and chemical stability under high electrical field were therefore used to improve these issues of gas ionization sensors.

In the beginning of this thesis, the effects on gas breakdown characteristics of different surface morphology of CNTs film are presented. For the Random oriented CNTs film, the variations of the breakdown voltages are especially large at high voltage region and their error bars in the high voltage region are as wide as 100 volts. These variations are associated with the nonuniformity of the CNTs' length. On the other hand, the gas breakdown characteristics of the Uniform CNTs film were relatively stable from the measurement results. However, for both of the two samples,

the shift-up of their breakdown voltages (V_{br}) were fairly severe after the high-voltage process in stability tests. One could find that the V_{br} of the Random oriented CNTs film lifts up from 365V to 605V after 1000 cycles, i.e., 68% increase. And for the Uniform CNTs film, it lifts up from 395V to 575V after 1000 cycles, i.e., 46% increase. Observed from the SEM images, the pull-off and evaporation of CNTs resulted from the high local electric field difference were considered as the main reason for the shift-up of breakdown voltages.

In order to acquire a better stability in the CNTs gas ionization sensor, the improvement of the adhesion and the contact resistance between CNTs and substrate under high electric field was obtained using Co-Ti co-deposited catalyst structure. The V_{br} of the CNTs film synthesized from Co-Ti co-deposited catalyst lifts up from 375V to 435V after 1000 cycles, i.e., only 16% increase, which is much more reduced than that of the first two conventional CNTs film.

In addition, to improve the issue of high power consumption, pillar arrays of vertical aligned CNTs bundles with different spacer height ratios (R/H) were utilized to investigate the optimal local electrical field on the nanotubes that has the most efficient field emission, namely, the earliest gas breakdown and lowest breakdown voltage. In this thesis, the lowest breakdown voltages were approached by changing H while maintaining R and the optimal R/H ratio was around 2.91. This optimal R/H ratio would lessen the high operating-voltage and thus improve high power consumption issues of the ionization sensors.

Next, the optimized samples were exploited to explore their gas ionization characteristics under different gases environment. From the experiment, dissimilar trends of Paschen's curve for distinct gases was obtained due to that different gas molecules have different mean free path, ionization energy and recombination rate. With a proper selection of the p×d product value, CNT gas ionization sensor can not

only operate under low voltages but also provide enough space to distinguish between different gases.

Finally, the breakdown voltages of Ar and CO_2 gases in mixture with air as a function of concentration were investigated. Take the R/H = 2.91 optimized patterned sample for example. It was found that the V_{br} increases 50V as the concentration of CO_2 in the mixture with air reaches 15 %, and decreases 100V as the concentration of Ar in the mixture with air reaches 11 %.

Acknowledgments

一眨眼碩士班兩年的時間就這樣飛過去了，在即將完成這篇論文的同時心中浮現了許多想要感謝的人事物，首先最要感謝的是不辭辛勞費心指導我的恩師鄭晃忠老師，老師不僅在學術上給予許多寶貴的意見，也在為人處世上處處提點學生，尤其在我碩一為是否找尋共同指導教授時，老師的真知灼見也一針見血的讓學生明白了問題的癥結點，能夠順利完成碩士學業，實在是要感謝老師的諄諄教誨。

再來要感謝 309B 的學長姐、同學、學弟妹們，不管是逸哲、柏宇、昱智、宏顯、還是昭龍等各位學長，雖然我們不是同一個組，但在大咪時你們的意見都使這篇論文更加的完全，還要謝謝俊諭學長許多學術外的看法，每次和學長聊天都讓學弟我獲益良多。謝謝佳信常常幫忙我這愚拙的實驗室管理員，我實在應該要把薪水分你一半才對。也謝謝柏鈞在即將畢業的這段時間裡幫忙我許多。再來要感謝奈米組的各位，首先謝謝萬霖學長給予本論文多有專業的見解，許多的問題也在和學長的討論中才豁然開朗。接著感謝奈米組兩朵花，筠珊學姐及育荏，謝謝你們總是帶給大家歡樂，看見你們我總是能不自覺得嶄露笑容。也要感謝即將一起畢業的俊賢，那些在實驗中遇到的困難擊倒不了我們的，一起努力吧。還有冠宇跟湛宇，在二樓孤單的日子有你們陪伴真好，你們在研究上認真反倒是我的榜樣，還有瑋萱、桓民，加油吧，你們一定也可以順利畢業的！

還要謝謝指導我實驗並提供意見的加聰學長，我是個個性頑固的人，也常常不尊重學長，感謝學長許多的包容，不僅在研究上一步一步的帶領著我，還要忍受我一些不合理的作法跟主意，感謝學長不計較這些，還繼續不斷帶領著我。

並且要感謝我的家人，我親愛的父親黃明國先生跟三個弟弟，俊綑、俊福、偉峰，和姑姑、姑丈及其他所有的家人，你們的全力支持是我完成碩士學業的最大後盾。還有屬靈上的家人，新竹市召會的弟兄姊妹們，謝謝你們在主裡的扶持，

特別是409區的弟兄姊妹們，謝謝你們把我當親生兒子一樣的照顧，我永遠會想念在這裡的教會生活。希伯來書12:1「所以，我們既有這許多的見證人，如同雲彩圍著我們，就當脫去各樣的重擔，和容易纏累我們的罪，憑著忍耐奔那擺在我們前頭的賽程。」

最後，最要感謝的，是那以永遠的愛愛我的神-親愛的主耶穌，謝謝主在我還年輕的時候就來到我的生命中，使我得以享受祂一切的豐富。這份信仰伴隨著我走過高山低谷，不管是身體上的軟弱或心靈上的虛空，親愛的主都陪伴著我渡過。我知道，未來的人生祂也會陪伴我走下去。我所有的，所得的，都是恩典。願一切的榮耀和讚美都歸給祂，主必擴增，我必衰減，感謝主，阿們。

哥林多後書4：16~18「所以我們不喪膽，反而我們外面的人雖然在毀壞，我們裡面的人卻日日在更新。因為我們這短暫輕微的苦楚，要極盡超越的為我們成就永遠重大的榮耀。我們原不是顧念所見的，乃是顧念所不見的，因為所見的是暫時的，所不見得才是永遠的。」

Contents

Chapter 1：Introduction

Chapter 2：Experiment

Chapter 3：Results and Discussions

Chapter 4：Summary and Future prospects

Table Lists

Chapter 1

Chapter 2

Chapter 3

Figure Captions

Chapter 1:

Chapter 2:

Chapter 3:

Chapter 4:

Chapter 1

Introduction

1-1 Overview of Gas sensors

In recent age, interests in industry safety and environmental pollution have been growing in our life. The needs of prevention and control of air pollution and detection for toxic gases have gradually increased. Thus, researches and developments on the gas sensors are carried out rapidly. According to Frost and Sullivan, global gas sensor markets were worth $48.5 million in 2005; their forecast for 2012 is $80.6 million. And based on a new technical market research report (BCC Research) (**Fig. 1-1)**, the global market for gas sensors and gas metering is worth an estimated $3.9 billion in 2010, but is expected to increase to nearly $5.2 billion in 2015, for a 5-year compound annual growth rate (CAGR) of 5.9%.These data show how large, and still expanding, this market is. A gas sensor is a device which outputs the appropriate signals (the change of current, voltage and conductance) for detection and measurement when specific gas was released (**Fig. 1-2)**. In our daily life, most of the gases are colorless and smell-less. Moreover, the sense of smelling of human beings was not able to identify the amount and content of certain gases. Hence, people always become conscious that some toxic and harmful gases run out due to the inhalation of overdose that causes uncomfortableness. Therefore, an accurate, fast-reacting and stable gas sensor plays an important role to improve the safety in our life.

In the analysis of gases, conventional analytical instruments have many usage restrictions while gas sensor was more convenient. As shown in **Table. 1-1,** the data

precision of analytical instrument is absolute value, yet its data acquisition time is too long and the size is much larger, which means the low-cost gas sensor attracts much attention from researchers.

Generally, gas sensor was classified into the following kinds:

1) Catalytic combustion gas sensor,
2) Semiconductor-absorbing Gas sensor,
3) Electrochemical Gas sensor,
4) Field-effect transistor Gas sensor,
5) Infrared Gas sensor and
6) Gas ionization sensor.

The first three kinds of gas sensors must be heated to high temperature before detecting gas leakage. Besides, they have different reactive sensitivities and response time of distinct gases, which cause mistakes or inability in sensing specific gases.

The mechanism of Field-effect transistor Gas sensor is as follows. When target gas contacts with catalyst metals, chemical reaction occurs and the product (take H_2 for example) will tunnel through the catalyst metal layer to affect charge density in the channel. Sander J.Tans et al. [1] and R.Marel et al. [2] have used carbon nanotubes (CNTs) as the channel of field-effect transistor **(Fig. 1-3)**. By applying a voltage to a gate electrode, the nanotube can be switched from a conducting state to an insulating state. Generally, Source and Drain were fabricated by noble metals like Pt and Au, and doped Si was used as the back gate of transistor. Using the gate electrode, the conductance of a SWNT-FET could be modulated by more than 5 orders of magnitude. The sensitivity of this kind of gas sensor is three times higher than that of common gas sensors and the former has a good response time of two to ten seconds. However, there are still many limitations on Field-effect transistor Gas sensor. For example, it

takes high temperature to recover to the initial resistance after each gas sensing measurement. Also, the fabrication process is more complicated, and the improved response time is still too long to detect specific toxic gases.

The Infrared gas sensor, however, measures target gases by determining the absorption of an emitted infrared light source through a certain air sample [3]. Infrared gas analyzers usually have two chambers that one is a reference chamber while the other is a measurement chamber. Infrared light is emitted from some type of source on one end of the chamber, passing through a series of chambers that contain given quantities of the various gases in question. Target gases found in the atmosphere get excited under specific wavelengths found in the infrared range. The concept behind the technology can be understood when considering the greenhouse effect. As sunlight hits the earth surface, the incoming short wave radiation gets turned into long wave infrared radiation that is reflected back into space. If the planet has a thick atmosphere, much of this radiation is absorbed by the "greenhouse gases" in the atmosphere which acts as an isolative blanket. The infrared gas sensor operates on the similar principle. However, the response time of infrared gas sensor is still quite long. A gas sensor with very short response time was required to detect some poison gases.

Among all of these sensors, Gas ionization sensor meets the requirement of response time with a stable discharge current in microseconds to ppm-level gases by its breakdown effect. It shows good sensitivity and selectivity, and is unaffected by extraneous factors such as temperature, humidity, and gas flow [4]. The fundamental operation principle of Gas ionization sensor is as follows. When applying a high voltage between two parallel electrodes, the electrical-field-induced band bending of the Vacuum level forces electrons to tunnel through the electrode material onto the Vacuum level which is the so-called Field emission effect. Since there are neutral molecules in the path of electrons which are moving to the positive electrode by the

traction of electric field, impact ionization reaction would take place when the electrons receive enough kinetic energy to ionize the molecule from the electrical field. A positive gas ion and a negative electron would be generated after an effective impact ionization process, and the number of electrons gets doubled after each time of effective collision. The whole reaction could be described via **(eq. 1-1)** :

$$e^- + X_2 \rightarrow X_2^+ + 2e^- \quad (1\text{-}1)$$

The number of charged particles between two electrodes would increase rapidly when the reaction repeats perpetually. Once it reaches a certain amount, the original poor electrical conducting gases would turn out to cause the electrical breakdown and an unusual high current could be measured afterward. Due to different molecular physical properties of different gases, distinct breakdown voltage could be obtained when breakdown effect occurs. Although gas ionization sensor work by fast response time and fingerprinting the ionization characteristics of distinct gases, they are, however, limited by their huge architecture, risky high-voltage operation and high power consumption. Hence, the miniaturization of device size, the reduction of breakdown voltage, and the improvement of power consumption are the most important issues for this kind of gas sensor.

1-2 Overview of Carbon nanotubes Gas sensors

1-2-1 Structure and properties of Carbon nanotubes

Since the discovery of carbon nanotubes (CNTs) by Iijima in 1991, [5] CNTs have attracted considerable interests because of their unique physical properties and many potential applications [6]. From 1991 until the end of 2007, roughly 30 000 scientific reports have been published on this topic [7]. This explosion of CNT reports is

illustrated in (**Fig. 1-4)** with a histogram detailing the number of CNT publications per year. This large volume of CNT literature includes over 1200 reports that deal specifically with the application of CNTs in a sensing capacity. CNTs have numerous potential applications in nanoelectronics, nanometer-scale structural materials, hydrogen storage, field-emission devices, gas sensors, and so on. Among these applications, CNTs seem to be very promising as electron emitters.

CNTs can be divided into two categories. The first is called multi-walled carbon nanotubes (MWNTs). MWNTs are close to hollow graphite fibers [8], except that they have a much higher degree of structural perfection. They are made of sheets of carbon atoms with a cylindrical shape and generally consist of co-axially arranged 2 to 20 cylinders (**Fig. 1-5 (b))**. The interlayer spacing in MWNT ($d_{(002)}$ = 0.34 nm) is slightly larger than that in single crystal graphite ($d_{(002)}$ = 0.335 nm) [9]. This is attributed to a combination of tubule curvature and van der Waals force interactions between successive garphene layers. The second type of the nanotube is made up of only a single layer of carbon atoms. These nanotubes are called the single-walled nanotubes (SWNTs) and possess good uniformity in diameter about 1.2 nm **(Fig. 1-5 (a))**. They are close to fullerenes in size and have a single-layer cylinder extending from end to end [10,11].

Most experimentally observed CNTs are multi-walled structures with outer most shell diameters exceeding 10 nm. Since current conduction in a MWNT is known to be mostly confined to the outermost single-walled nanotube and since band gap of a SWCNT varies inversely with its diameter, MWNTs are metallic in nature. SWNTs can be either metallic or semiconducting depending on the way the roll-up of the graphene sheet occurs - an aspect termed as Chirality, and if all the roll-up types are realized with equal probability, 1/3 of the SWNTs end up being metallic and 2/3 semiconducting. The structure of a SWNT can be conceptualized by wrapping a

one-atom-thick layer of graphite called graphene into a seamless cylinder. The way of the graphene sheet is wrapped is represented by a pair of indices (n,m) called the chiral vector. The integers n and m denote the number of unit vectors along two directions in the honeycomb crystal lattice of graphene. If m=0, the nanotubes are called "zigzag". If *n=m*, the nanotubes are called "armchair". Otherwise, they are called "chiral". (**Fig. 1-6)** depicts these structures of a SWNT [12,13].

CNTs have been attracting much attention for their unique physical and chemical properties such as high mechanical strength, chemical stability, high aspect ratio, super-thermal conductivity, and electron emission properties [14,15]. CNTs could be one of the strongest and stiffest materials known, in terms of tensile strength and elastic modulus respectively. This strength results from the covalent sp^2 bonds formed between the individual carbon atoms. The highest tensile strength an individual multi-walled carbon nanotube has been tested to be is 63 GPa [16]. Under excessive tensile strain, the tubes will undergo plastic deformation, which means the deformation is permanent. This deformation begins at strains of approximately 5% and can increase the maximum strain the tube undergoes before fracture by releasing strain energy. For the thermal conductivity of CNTs , it is predicted that carbon nanotubes will be able to transmit up to 6000 watts per meter per kelvin at room temperature; compare this to copper, a metal well-known for its good thermal conductivity, which only transmits 385 W/m/K. The temperature stability of carbon nanotubes is estimated to be up to 2800 degrees Celsius in vacuum and about 750 degrees Celsius in air [17].

1-2-2 The synthesis methods of Carbon nanotubes

Carbon nanotubes (CNTs) have been extensively investigated for the synthesis using arc discharge, laser vaporization, pyrolysis, solar energy, and plasma-enhanced

chemical vapor deposition (CVD), for its unique physical and chemical properties and for applications to nanoscale devices. However, common methods of CNT synthesis include: (1) arc-discharge [18], (2) laser ablation [19], (3) thermal CVD [20-22], and (4) plasma enhanced CVD [23,24].

The laser ablation can synthesize pure carbon nanotubes in high fabrication temperature, but large scale display panel cannot be fabricated in the high fabrication temperature above the melting point of glass substrate. The arc discharge can synthesize carbon nanotubes in shorter fabrication times, but it has some issues, such as (1) poor purity, (2) hard to control growth orientations of carbon nanotubes, and (3) poor emission uniformity.

Compared to laser ablation and arc discharge, using CVD for carbon nanotube growth has some features, such as (1) high purity carbon nanotubes, (2) selective growth only for catalyst metal, (3) controlling growth direction, and (4) much suitable to semiconductor fabrication procedure.

1-2-3 Carbon nanotubes as the Chemical gas sensor

Carbon nanotubes (CNTs) are expected as a new material which has an outstanding high sensitivity and selectivity at relatively low temperature with a fast response time. Several kinds of gas sensors using CNTs have been proposed. They can be generally classified into two types: the absorption type gas sensor (chemical type) [25,26] and the ionization type gas sensor (physical type) [27].

The mechanism of a chemical type gas sensor using CNTs as the gas absorption material is based on the fact that CNTs show its semiconductor property, which their electrical resistance can be modified by the charge transfer between CNTs and oxidizing or reducing gas molecules absorbed on the CNT surfaces. Owing to the high surface area, nanometer size and hollow centre of CNTs, it seems to be an ideal

material for absorption and detection of gases. Nonetheless, this type of CNTs gas sensor has some limitations [28] such as the inability to detect gases with low absorption energy or low electro-negativity like inert gases. It's also difficult to distinguish between gases and gas mixtures with electrical resistance. (Gases in different concentrations could produce the same amount of net change in conductance as produced by a single gas.) In addition, nanotube conductance is very sensitive to environmental conditions like temperature, moisture and gas-flow velocity. Besides, chemisorptions could cause irreversible change in nanotube conductivity. All the limitations mentioned above make us pay more efforts in selecting ionization type gas sensor in order to overcome these disadvantages.

1-2-4 Carbon nanotubes as the Gas ionization sensor

The Gas ionization sensors working by fingerprinting the ionization characteristics of distinct gases that can ignore the magnitude of gas absorption energy have been reported recently [29]. The sharp tips of CNTs generate very high electrical fields at relatively low voltage, about several hundred volts, which is several-fold lower than the traditional metal electrodes [30]. The most crucial part of the operating mechanism of this type of gas sensor is the Field emission. And the field emitted electrons from a cold cathode have often played an important role in vacuum electronics as an alternative to the thermionic emitted electrons from a hot cathode with advantages such as higher efficiency, less scattering of emitted electrons, faster turn-on times and more compactness. As we have mentioned above, the Gas ionization sensor suffers from their risky high-voltage operation, high power consumption and huge architecture. However, with the employment of CNTs as the electrode, the sharp tips of CNTs can generate very high electric fields at relatively low voltage that hastens the breakdown process. CNTs also have high chemical

stability, high emission current density and good emission stability that make it an ideal material to fabricate the Gas ionization sensor.

Recently, this physical type CNT gas sensors has been proposed, which indicates that CNT gas ionization sensors (with proper calibration) show promising potential for room-temperature gas detection at extremely low percentage in mixtures with air and for fast response toward the application of the breakdown electric field resulting in a stable discharge within 20 μs [29,31].

1-3 Theory background

When using CNTs as electrode material of the Gas ionization sensor, the first mechanism needed to be realized is electron field emission. Electrons would receive enough energy to tunnel through the bended potential barrier caused by the high electric field around sharp tips of CNTs. After their tunneling, electrons might have the impact ionization with neutral molecules and generate lots of charged particles between two electrodes. And electrical gas breakdown would take place when achieving enough amounts of electrons. The total operation principles of gas ionization sensor can be described through the derivation of Townsend's discharge [32,33] and Paschen's law [34,35], which illustrate the relationship between Gas ionization sensor breakdown voltages and the gas pressure along with the distance between anode to cathode.

1-3-1 The Mechanism of electron emission

Generally speaking, it's not straightforward for an electron to escape from the surface of materials. A potential barrier (so-called Fermi level) exists at the surface of materials which prevents the electrons from escape unless certain conditions are satisfied so that electrons upon the metal could emit into the surrounding vacuum or

gases environment. That is, the binding electron is not able to flee away from the binding energy band of the atom's surface unless sufficient external energy is provided. The supplied external energy must be higher than the work function of electrode surface material (defined as the work needed to remove an electron from the surface). As electrons receive specific external energy to cross the potential barrier of the work function and reach the vacuum, this phenomenon is called electron escape or electron emission.

In general, the electron emission mechanism can be classified into two types, thermionic emission and field emission. Their operating mechanisms are to use either temperature or electrical field to provide the external energy of electron emission, respectively. These two mechanisms can be described by the band diagram **(Fig. 1-7)**.

Thermionic emission is the heat-induced flow of charge carriers from a surface or over a potential-energy barrier. This happens because the thermal energy applied to the carrier overcomes the potential barrier, also known as work function of the metal **(Fig. 1-7 (a))**. In the beginning, all electrons were bound under the Fermi level (EF) when the temperature is at 0°K**.** However, part of electrons might acquire kinetic energy from the thermal heating as the temperature increases gradually. When the temperature is high enough, electrons might escape from Fermi level to Vacuum level with high probabilities. This mechanism accomplishes the electron emission without applying any bias voltages at the cost of the thermal energy supplied. In most cases, the thermionic electron is emitted under considerably high temperature, which is based on the different work functions of different materials. The average temperature is about 1500 to 2000 ℃.

On the other hand, the field emission (FE) (also known as Fowler-Nordheim tunneling) is an emission mechanism of electrons induced by external electric fields, which implies that heating was not necessary for the cathode materials. Ab initio,

most of electrons would remain under the Fermi level at low temperatures. The external electric field would lead to band bending of the Vacuum level, which induces gradual narrowing of the effective potential barrier width **(Fig. 1-7 (b))**. As soon as it was thin to some extent, the electron tunneling effect occurred and the electron might tunnel to the Vacuum level, namely the well-known Fowler-Nordheim tunneling. Because this mechanism provides the main escape energy of emitting electrons to the vacuum level by electrical field, it is thus called the field emission.

The throughout thesis will focus on this mechanism of electron emission as our main research issues.

1-3-2 Electron field emission

In quantum mechanical, electron field emission is a tunneling phenomenon of electrons extracted from the conductive solid surface, such as a metal or a semiconductor, where the surface electrical field is extremely high.

If a sufficient electrical field is applied on the emitter surface, electrons will be emitting through the surface potential barrier into vacuum, even under a very low temperature. On the other hand, thermionic emission is the hot electron emission under high temperature and low electric field. **(Fig. 1-8 (a))** demonstrates the band diagram of a metal-vacuum system.

Here W_0 is the energy difference between an electron at rest outside the metal and an electron at rest inside, whereas W_f is the energy difference between the Fermi level and the bottom of the conduction band. The work function ϕ is defined as $\phi = W_0 - W_f$. If an external bias is applied, vacuum energy level is reduced and the potential barrier at the surface becomes thinner as shown in **(Fig. 1-8 (b))**.

Then, an electron having energy “W” has a finite probability of tunneling through

the surface barrier. Fowler and Nordheim derive the famous F-N equation **(eq. 1.2)** as follow [36]:

$$J = \frac{aE^2}{\phi t^2(y)} \exp[-b\phi^{\frac{3}{2}} v(y)/E], \tag{1-2}$$

where J is the current density (A/cm^2). E is the applied electric field (V/cm), ϕ is the work function (in eV), a = 1.56×10^{-6}, b = -6.831×10^{-7}, y = 3.79x10^{-4}×10^{-4}E$^{1/2}$/ϕ, t^2(y)~1.1 and v(y) can be approximated as [37]

$$v(y) = \cos(0.5\pi y), \tag{1-3}$$

or

$$v(y) = 0.95 - y^2. \tag{1-4}$$

Typically, the field emission current I is measured as a function of the applied voltage V. Substituting relationships of J = I/α and E = βV into **(eq. 1.2),** where α is the emitting area and β is the local field enhancement factor of the emitting surface, the following equation can be obtained

$$I = \frac{A\alpha\beta^2 V^2}{\phi t^2(y)} \exp[-bv(y)\frac{\phi^{\frac{3}{2}}}{\beta V}]. \tag{1-5}$$

Then taking the log. form of **Eq. (1-5)** and v(y) ~ 1

$$\log(\frac{I}{V^2}) = \log[1.54\times10^{-6}\frac{\alpha\beta^2}{\phi t^2(y)}] - 2.97\times10^7(\frac{\phi^{3/2}v(y)}{\beta V}), \tag{1-6}$$

from **Eq. (1-6)**, the slope of a Fowler-Nordheim (F-N) plot is given by

$$S \equiv slope_{FN} = 2.97\times10^7(\frac{\phi^{\frac{3}{2}}}{\beta}), \tag{1-7}$$

The parameter β can be evaluated from the slope S of the measured F-N plot if the work function ϕ was known

$$\beta = -2.97\times10^{7}\left(\frac{\phi^{\frac{3}{2}}}{S}\right)(\mathrm{cm}^{-1}), \tag{1-8}$$

The emission area α can be subsequently extracted from a rearrangement of **(eq. 1-6)**

$$\alpha = \left(\frac{I}{V^{2}}\right)\frac{\phi}{1.4\times10^{-6}\beta^{2}}\exp\left(\frac{-9.89}{\sqrt{\phi}}\right)\exp\left(\frac{6.53\times10^{7}\phi^{\frac{3}{2}}}{\beta V}\right)(\mathrm{cm}^{2}). \tag{1-9}$$

For example, the electric field at the surface of a spherical emitter of radius r concentric with a spherical anode (or gate) of radius r+d can be represented analytically by

$$E = \frac{V}{r}\left(\frac{r+d}{d}\right), \tag{1-10}$$

Though a realistic electric field in the emitter tip is more complicated than above equation, we can multiply **(eq. 1-10)** by a geometric factor $\beta`$ to approximate the real condition.

$$E_{tip} \equiv \text{function of (r,d)} = \beta`\frac{V}{r}\left(\frac{r+d}{d}\right), \tag{1-11}$$

where r is the tip radius of emitter tip, d is the emitter-anode(gate) distance and $\beta`$ is a geometric correction factor [38].

1-3-3 Operation principles of electron impact ionization

For the application of Gas ionization sensor, an electron would move along the electric field to the anode after it was emitted from the cathode. However, if the distance from anode to cathode is much larger than the average mean free path of an

electron, the electrical field may induce accelerated electrons to collide with neutral molecules or atoms in its path to anode. Normally, there are three kinds of reactions for an electron to impact on a neutral molecule, which are the dissociation reaction **(eq. 1-12)**, the activation reaction **(eq. 1-13)** and the ionization reaction **(eq. 1-14)**.

$$e^- + X_2 \rightarrow 2X + e^- \quad (1\text{-}12)$$

$$e^- + X \rightarrow X^* + e^- \quad (1\text{-}13)$$

$$e^- + X_2 \rightarrow {X_2}^+ + 2e^- \quad (1\text{-}14)$$

The most notable reaction among the above is the ionization reaction (eq. 1-14), which depicts the increment of the number of electrons after the reaction. An ionized electron would be produced whenever an effective collision occurs. Moreover, an ionized positive ion would receive kinetic energy from the acceleration of electric field and collide with the cathode, which would produce more ionized electrons. And the electrical gas breakdown would take place when the amount of ionized electrons was up to a certain quantity.

What's more, the excited atom of (eq. 1-13) would emit photons and then return to ground state which could be expressed as (eq. 1-15),

$$X^* \rightarrow X + h\nu \quad (1\text{-}15)$$

where h is the Plank Constant and ν is the frequency of radiation light. That's the reason why spark and glare can be seen when the electric gas breakdown occurs on the microstructure of electrodes with high voltages applied **(Fig. 1-8)**[39].

1-3-4 The fundamental mechanism of gas ionization breakdown

The magnitude of breakdown voltage of gas ionization sensors is based on Paschen's law, which points out that the breakdown characteristics of a gap between two electrodes are a function (generally not linear) of the product of the gas pressure and the gap length, which is usually denoted as Vbr= f(pd). Nevertheless, before this

law was deduced, the mechanism of applying high voltage among anode and cathode has to be described below.

From **(Fig. 1-10)**[40], it shows that the processes of gas ionization via positive nanotip could be separated into three parts, which are molecule ionization via nanotip, impact ionization effect, and electron recombination along with γ-process[41]. As one can see in **(Fig. 1-10)**, in process 1, when CNTs were used as positive electrode, the high voltage among anode and cathode would generate a strong local electric field around nanotips, where neutral molecule was ionized and an electron was released simultaneously. The ion would move to the negative electrode under the electrostatic force and the electron would be absorbed concurrently on the positive nanotip. Here suppose that the ionization rate induced by the ion's moving to the negative electrode is small so that it could be ignored. On the surface of the negative electrode, the ion would recombine with an electron and revert to molecule. However, the release energy of recombination and the kinetic energy of the ion would promote the electron emission from the negative electrode in the process III. This process is the so-called γ-process. The electron released from the negative electrode would get enough energy to make other gas molecule ionized during its moving to the positive electrode. This is the electron impact ionization effect (process II). Thus, the pre-breakdown current was generated mainly by the molecule ionization via positive nanotips when utilizing CNTs as the positive electrode. The current could be continued and magnified in processes I and II to result in high current to cause electric breakdown. Therefore, the application of CNTs as positive electrode could enhance the gas ionization process, lower the working voltage, and improve the sensitivity of the sensor.

When CNTs were used as negative electrode, as shown in **(Fig. 1-11)**, in process I, electrons would emit via negative nanotips. Then they move to the positive electrode while obtaining kinetic energy from electrical field. As soon as they receive

enough energy to make a molecule ionized, the impact ionization occurs and produces more electrons and ions as desired. This is the process which we mentioned above (process II). Similarly, the ions also induce recombination of electron and γ-process (process III). These three processes would duplicate unceasingly and the breakdown would occur when the number of generated electrons was sufficient. Therefore, the application of CNTs as negative electrode would enhance the emission current, lower the working voltage, and improve the sensitivity of the sensor.

1-3-5 Townsend discharge and Paschen's law

As mentioned above, an electron moves beyond the average mean free path along the electrical field might acquire sufficient kinetic energy to ionize a neutral molecule into a positive ion and a free electron. This means that the number of free electrons get doubled if we take the original colliding electron into account. As this mechanism proceeds again, these two electrons might collide with two neutral molecules and become two positive ions and four electrons in totality. Therefore, the number of charged particles increases exponentially like a snow avalanche as it repeats continually, which is the well-known Avalanche breakdown effect.

As depicted in **(Fig. 1-12)**, assume the number of electrons after impact ionization is **Ne,** then

$$\mathrm{Ne} = 2^0 \text{、} 2^1 \text{、} 2^2 \text{、} 2^3 \text{、} 2^4 \text{、} 2^5 \text{、} 2^6 \text{、} 2^7 \ldots \quad (1\text{-}16)$$

Note that the number of collisions is related to average mean free path λ. Suppose that the distance of electron to the anode is X, then Ne can be described as

$$\mathrm{Ne(x)} \approx 2^{\frac{x}{\lambda_i}} = e^{\frac{x}{\lambda_i}\ln 2} = e^{\alpha x} \quad (1\text{-}17),$$

where α is the Townsend's first ionization coefficient, which tells the average number of ionizing collisions are made by an electron as it travels 1cm in the direction of the

electric field.

And

$$\alpha \approx \frac{\ln 2}{\lambda_i} = Ap \exp\left(\frac{-Bp}{E}\right) \quad (1\text{-}18).$$

Here A and B are the constants which depend on gaseous species. E is electrical field strength and p is gaseous pressure. From (eq. 1-17), one can easily realize the exponential relationship between Ne and α. That is, Ne will grow exponentially as the value of α increase. This is the well-known Townsend discharge which illustrates that initially a very small amount of free electrons, accelerated by a sufficiently strong electric field, give rise to electrical conduction through a gas by the avalanche multiplication.

In order to describe the mechanism of gas breakdown, we have to assume that $\gamma(e^{\alpha d} - 1)$ electrons will be generated when $(e^{\alpha d} - 1)$ positive ions impact on the cathode. They are referred to the Secondary electrons.

Now, if the electrical field flux is Γ_e, the unit volume density is n_e and ν_e is the electron velocity, then

$$\Gamma_e = n_e \nu_e \quad (1\text{-}19),$$

The unit of Γ_e is $[m^{-2} \cdot s^{-1}]$, n_e is $[m^{-3}]$, ν_e is $[m \cdot s^{-1}]$, and

$$\nu_e = \mu_e \cdot E \quad (1\text{-}20),$$

where μ_e is the electron mobility, E is the magnitude of **e**lectrical field between two electrodes.

Therefore, the current between two electrodes (I) is

$$I = -|e| n_e \mu_e = -|e| \Gamma_e \quad (1\text{-}21),$$

One can easily understand the physical meaning through **(Fig. 1-13),**

The total electron flux on positive electrode $\Gamma_e(d)$ is the combination of $\Gamma_{e1} e^{\alpha d}$ and $\Gamma_{e2} e^{\alpha d}$, that is

$$\Gamma_e(d) = \Gamma_{e1}e^{\alpha d}+\Gamma_{e2}e^{\alpha d} \quad (1\text{-}22),$$

and

$$\Gamma_{e2}e^{\alpha d} = \gamma[(\Gamma_{e1}e^{\alpha d} - \Gamma_{e1}) + (\Gamma_{e2}e^{\alpha d} - \Gamma_{e2})] \quad (1\text{-}23),$$

Put (eq. 1-22) into (eq. 1-23), we have

$$\Gamma_{e2} = \frac{\gamma\Gamma_{e1}(e^{\alpha d}-1)}{[1-\gamma(e^{\alpha d}-1)]} \quad (1\text{-}24).$$

Substitute (eq. 1-24) back into (eq. 1-22),

$$\Gamma_e(d) = \frac{\Gamma_{e1}e^{\alpha d}}{[1-\gamma(e^{\alpha d}-1)]} \quad (1\text{-}25),$$

Thus, the current at x=d is

$$i_d = \frac{I_0 e^{\alpha d}}{[1-\gamma(e^{\alpha d}-1)]} \quad (1\text{-}26),$$

it implies that i_d will approach infinity and the electrical breakdown occurs when $[1-\gamma(e^{\alpha d}-1)] = 0$.

$$\gamma(e^{\alpha d}-1) \approx 1 \text{ in that } e^{\alpha d} \gg 1 \quad (1\text{-}27),$$

so

$$e^{\alpha d} = \frac{1}{\gamma} + 1 \quad (1\text{-}28),$$

which means

$$\alpha d = \ln(\frac{1}{\gamma} + 1).$$

For

$$\alpha = Ap \exp(\frac{-Bp}{E}) \quad (1\text{-}18),$$

we have

$$\ln\left(\frac{1}{\gamma} + 1\right) = pdA\exp(\frac{-Bp}{E}).$$

After rearrangement

$$\ln\left[\ln\left(\frac{1}{\gamma} + 1\right)\right] = \ln(pdA) - \frac{Bp}{E}.$$

If $E=\frac{V}{d}$, then

$$\ln\left[\ln\left(\frac{1}{\gamma}+1\right)\right] = \ln(\mathrm{pdA}) - \frac{\mathrm{Bpd}}{\mathrm{V}}.$$

The breakdown voltage is therefore

$$\mathrm{V_{br}} = \frac{\mathrm{Bpd}}{\ln(\mathrm{pdA}) - \ln\left[\ln\left(\frac{1}{\gamma}+1\right)\right]} \quad (1\text{-}29),$$

which can be simplified to

$$\mathrm{V_{br}} = \frac{\mathrm{Bpd}}{[\ln(\mathrm{pd}) + \mathrm{C}]} \quad (1\text{-}30),$$

with $C=\ln\left[\frac{A}{\ln\left(\frac{1}{\gamma}+1\right)}\right]$.

This is the Paschen's law which was first stated in 1889, named after Friedrich Paschen. It depicts the breakdown characteristics of a gap are a function (generally not linear) of the product of the gas pressure and the gap length, usually written as V= f(pd). As we plot (eq. 1-30) with x axis being the breakdown voltages versus the products of pressure and distance as y axis, one can obtain graphs like **(Fig. 1-14)**, which is the so-called Paschen's curve.

1-4 Motivation

1-4-1 Stability issue

Gas sensors operate on a variety of different fundamental mechanisms [42], and they play an important part in monitoring the environmental changes, controlling chemical processes, preventing from terrorism, and in the application of medical and agricultural behaviors. Gas sensors can be classified into two types, a chemical type operated by gas absorption and a physical type operated by ionization [43-44,27].

Since the electrical conductance of CNTs is highly sensitive to certain gas molecules, they have been used to fabricate the chemical sensors with a fast response

time than conventional materials like metal-oxide, polymer, porous silicon, etc. [45-48]. The sensing mechanism involves detecting conductance change of CNTs induced by charge transfer from gas molecules adsorbed on their surfaces. However, all gas-adsorptive types of sensors have several limitations. For instance, they are unable to detect gases with low adsorption energy, and also challenging to use electrical conductance measurement to distinguish between gases in a mixture, i.e., gases with different concentrations can produce the same output signal as that for a single pure gas. Also, gas sensors of chemical type are sensitive to environmental conditions like moisture, temperature, and gas flow velocity. Besides, chemisorptions can cause irreversible changes in nanotube conductivity [26]. Thus, CNT-based gas ionization sensors are expected to overcome these disadvantages.

Gas ionization sensors are physical mechanisms that work by fingerprinting the ionization characteristics of distinct gases. However, conventional ionization sensors are limited by the huge and bulky architecture, risky high-voltage operation and high power consumption. Many investigations have studied on the improvement of these issues. Carbon nanotubes with relatively low work function, very sharp nanotips, and structural and chemical stability under high electrical field, were known to be the best field emitters over many conventional field emitting metals like Mo and W. The usage of CNTs for the improvement of the characteristic of gas ionization sensors has been addressed in recent years [49-52]. Modi et al. [4] proposed the fabrication and successful testing of ionization micro-sensors **(Fig. 1-15)** featuring the electrical breakdown of a range of gases and gas mixtures at carbon nanotube tips. The sharp tips of nanotubes generate very high electric fields at relatively low voltages, lowering breakdown voltages several-fold in comparison with traditional electrodes. Moreover, S J Kim et al. [50] fabricated a physical type gas sensor **(Fig. 1-16)** based on an electrical discharge theory known as Paschen's law. The gas sensor works by figuring

changes of the discharge current depending on the concentration of gases which can be ionized through collisions with electrons emitted from CNT emitters.

Therefore, the field emission electrons play an important role in the operational mechanism of gas ionization sensors. As shown in **(Fig. 1-11)**[40], when CNTs were used as the negative electrode, the mechanism can be classified into three processes, electron emission via nanotips, impact ionization, and recombination of electron along with γ process. Process II and Process III were associated with the characteristics of target gas molecules such as the diameter of molecules and the ionization energy of gases. However, few studies emphasized on the mechanism of Process I which indicates that the material, surface morphology and crystallinity of the electrode are the most critical factors in the breakdown characteristics of gas ionization sensors.

In the beginning of this thesis, the effect of different surface morphology of CNTs film on the gas breakdown characteristics is presented. In first, a random oriented and a uniform CNTs film are fabricated individually by sputtering catalyst on the substrate and thermal chemical vapor deposition (TCVD) method to grow the CNTs. The effect of protrusions on the breakdown characteristics is investigated. Then, the synthesis of CNT-based film with co-deposition catalyst is obtained to improve the stability issues.

1-4-2 The reduction of breakdown voltage

Moreover, several researchers [53-55] have suggested that the field emission properties of CNT films have a strong dependence on the density and morphology of the CNT deposit. Electrostatic screening effect provoked by the proximity of neighboring tubes is a crucial factor that might reduce the field enhancement and thus the number of emitted electrons. Therefore, another aim of this thesis is to find out an optimal morphology of pillar array of aligned CNT bundles to the application of gas

ionization sensors. To explore the effect of the pillar arrangement on its breakdown characteristic of gas ionization sensors, different spacer height ratio (R/H) as a function of H is investigated by changing H while maintaining R. An optimal R/H ratio that has a lowest breakdown voltage would lessen the high operating-voltage and high power consumption issues of the ionization sensors.

Finally, the pillar array of aligned CNT bundles with optimal R/H ratio is utilized to explore its gas ionization characteristics under different gas environment. Paschen's curve for distinct gases was obtained by experiments to approach a wide and appropriate breakdown voltage window that provide enough space to distinguish different gases.

1-3 Thesis organization

In chapter 1, the overview of gas sensors, the properties of carbon nanotubes gas ionization sensors, the research theory background and our motivation are described.

In chapter 2, the experimental procedures were illustrated. We utilize the Co-Ti/Ti/Al (4nm/1nm/10nm) co-sputtered catalyst sample to compare with pure Cobalt (4nm) sample and Ti/Co (1nm/4nm) sample in the synthesis of CNTs, the application of gas breakdown characteristics and the improvement of stability issue. Then, the reduction of the breakdown voltages of a CNT films using patterned method was discussed, and their gas sensing characteristics under different gases environment were also investigated. These experimental results and discussions were presented in chapter 3.

Finally, the summary and future prospects are provided in chapter 4.

Chapter 2

Experiment

Carbon nanotubes (CNTs) have attracted great interest due to their unique electronic properties and nanometer size. Because of these unique properties, they are candidates of great potential in many important applications like nano-scale electronic devices, chemical sensors and field emitters. Especially, for the application of field emitters, CNTs possess a small diameter and a great achievable aspect ratio as well as high chemical stability and excellent mechanical strength, whose potential advantages to be an ideal material for electrodes are implied [56-57]. As mentioned above, using chemical vapor deposition (CVD) method for carbon nanotubes growth has many features such as availability of high purity carbon nanotubes, selectivity in growing only for catalyst metals, good controllability for growth direction, and high suitability to the semiconductor fabrication procedure [58-60]. In practice, however, it is still difficult to control the length, diameter, and the morphologies of the CNTs to be uniform due to the variation of the size of the catalytic nanoparticles. The non-uniformity in length, diameter, and location distributions of the CNTs can greatly affect the uniformity of the intensity in the field emission and the number of field-emission electrons [61].

In the first step (chapter 2-2-1), carbon nanotubes were synthesized by thermal chemical vapor deposition (T-CVD) from different catalyst structures to investigate their effects on the gas breakdown characteristics. Initially, we compared the gas breakdown characteristics between the Random oriented CNTs film and the Uniform CNTs film. One could find that the Uniform CNTs film had a better reliability and stability in the applications of gas ionization sensor. However, the shift-up of

breakdown voltages owing to the pull-off and evaporation of CNTs among these two conventional samples after stability tests forced us to reconsider an alternative method to improve the adhesion and contact resistance between CNTs and the substrate.

Therefore, in the second experiment (chapter 2-2-2), a partially immersed structure of the CNTs was achieved by using co-deposited catalyst which enlarged the contact area to enhance the adhesion and reduce the contact resistance. With this proposed CNTs film synthesized from co-deposited catalyst structure, the improvement of the stability could be seen from the gas breakdown characteristics. Besides, one could find from SEM images of the proposed sample before and after the stability test that the pull-off and evaporation of CNTs were successfully reduced.

Moreover, with the purpose of improving the power consumption of the gas ionization sensor, the third experiment (chapter 2-2-3) was thus designed. The pattern technology was utilized to modify the local electrical field. And the gas breakdown characteristics of the pillar array of vertical aligned CNT bundles with different spacer height ratio (R/H) as a function of H was explored by changing H whilst maintaining R. Eventually, an optimal R/H ratio around 2.91 that has a lowest breakdown voltage was approached. One could use the co-deposited catalyst structure which proposed in the Experiment B to improve the stability of gas breakdown characteristics and use the optimal R/H ratio of pillar array of aligned CNT bundles proposed in this experiment to lessen the high operating-voltage and high power consumption of the gas ionization sensors. The optimal film sample and patterned sample would be preceded to the gas ionization measurement in different gases environment in the next experiment.

In our last experiment (chapter 2-2-4), optimized film sample and patterned sample was exploited to measure their breakdown characteristics under different gases environment. Then distinct Paschen's curve can be used to choose a proper p×d

product region to fabricate the gas ionization sensor. Finally, we investigated their changes of the breakdown voltages of Ar and CO_2 gases in mixture with air as a function of concentration.

2-1 Experimental Procedures

2-1-1 Sample fabrication and CNTs synthesis

In the beginning, the process procedure of the conventional two samples was depicted in **(Fig. 2-1)**. P-type silicon wafers (100) with low resistance (1~10 Ω/cm^2) were utilized as the substrates in our experiment. To distinguish these two samples with different surface morphology for the sake of convenience, they were referred to as sample (A) and sample (B), respectively. So as to ensure the cleanness of the silicon substrate and to prevent the effect of particle contamination at the beginning of our experiment, the two conventional samples were both carried out with the RCA clean process **(Fig. 2-1 (a))**.

After the RCA clean process, a 4-nm-thick Cobalt layer was deposited on both sample (A) and sample (B) by magnetron sputtering (Ion Tech Microvac 450CB) at the pressure of 7.6×10^{-2} torr at room temperature. This Cobalt layer would transform into the catalyst nanoparticles which are the growth site of CNTs afterwards. Moreover, sample (B) would deposit an extra 1-nm-thick Ti capping layer to generate the different surface morphology from sample (A) after the CNTs growth. After the metal deposition, both the conventional samples were loaded into the chamber of thermal-CVD. The atmospheric pressure thermal CVD system we used here was consisted of a 2-in.-diameter horizontal quartz tube, an electric heating system, a reaction gas supply and several related mass flow controllers as shown in (**Fig. 2-2**).

Samples loaded into the quartz tube would pass through some high temperature process in different gases environment to grow CNTs. The parameters of thermal CVD to grow the CNTs were illustrated in **(Fig. 2-3)** and **(Table 2-X)**. At the start, samples would be heated to the predetermined temperature of 600℃ in a nitrogen flow rate of 1000 standard cubic centimeter per minute (sccm) for an oxygen-free ambience. Prior to the CNTs growth, hydrogen gas with a flow rate of 300 sccm was fed into the reaction tube for 10 min to reduce the catalyst metal to the metallic phase, meanwhile transform into nanoparticles. It is worth noting that the size and uniformity of the nanoparticles are related to the temperature, the flow rate of reducing gas and the characteristics of catalyst metal. After the pretreatment step, the chamber would be heated again under nitrogen flow rate of 1000 sccm to 700℃. Then, CNTs were grown at this temperature with hydrogen, nitrogen and ethylene at a flow rate of 300 sccm, 500 sccm and 100 sccm for designated growth time. After that, samples were furnace-cooled to room temperature in nitrogen flow rate of 5000 sccm to fully exhaust the reaction and byproduct gases.

What's more, after the investigation of the gas breakdown characteristics of sample (A) and sample (B), a CNTs-based film synthesized from the co-deposited catalyst structure was proposed to improve the gas breakdown stability, and this sample was referred to as sample (C). Its schematic flowchart for the fabrication was depicted in **(Fig. 2-4)**. At first, a 10-nm-thick aluminum supporting layer was deposited on the substrate. Then a 1-nm-thick titanium interlayer and a 4-nm-thick Co-Ti co-deposited layer were deposited sequentially. The effect of Al supporting layer and Ti interlayer to the grown CNTs would be discussed in chapter 3. All of these metal layer were deposited also by magnetron sputtering (Ion Tech Microvac 450CB) at the pressure of 7.6×10^{-2} torr at room temperature. Because the sputtering system consisted of three sputtering sources, the three components of multi-metal

layers could be sequentially prepared without breaking the vacuum environment. After the catalyst structure was prepared, sample (C) would be loaded into the furnace and go through the same thermal CVD processes like sample (A) and sample (B) to grow the CNTs. After that, its gas breakdown characteristics and surface morphology before and after the stability test would be compared with the conventional two samples as well.

Moreover, in order to ameliorate the issue of high-voltage operation, the pattern technology was used to redistribute the local electrical filed. To compare the difference, we fabricate two types of samples just like the method utilized above. One is the CNTs film sample synthesized from the co-deposited catalyst structure mentioned above. The other is pillar arrays of vertical aligned CNTs bundles synthesized also from the co-deposited catalyst structure. With the purpose of the convenience in their comparison, we referred the former to film sample and the latter to pattern sample. Their detailed fabrication processes were depicted in **(Fig. 2-4) and (Fig. 2-5)**, firstly, a lithography processes was used to define circle patterns **(Fig. 2-6)** for CNTs pillar arrays with 50 μm in diameter, and the spacing of the center of each circle was 80 μm , that is, the pillar-to-pillar spacing was 30 μm. After the lithography processes, Co-Ti (40 Å)/Ti(10 Å) /Al (100 Å) as catalyst structure were deposited on the silicon substrate by magnetron sputtering, and the lift-off technique using acetone was utilized to transfer the circle patterns onto the substrate. Finally, both of the film sample and the patterned sample were loaded into the chamber of thermal CVD to undergo the same processes **(Fig. 2-3)** to grow the CNTs. However, in this time, the parameter of CNTs growth time was adjusted to control the height of CNTs. Therefore, pillar array of vertical aligned CNTs bundles with different R/H ratio were obtained in our experiment.

2-1-2 Material analysis and Breakdown characteristics measurement

The micrographs of samples were taken by Scanning electron microscope (SEM) to see the surface morphologies **(Fig. 2-7)**. Besides, the high resolution transmission electron microscope (HRTEM; JEOL JEM-2000EX) **(Fig. 2-8)** and Raman spectra **(Fig. 2-9)** were also applied to analyze the structure and crystallinity of the CNTs.

To obtain the gas breakdown characteristics, all the samples with different catalyst structures were loaded into a vacuum chamber to measure the discharge current. The gas ionization measurement setups were depicted in **(Fig. 2-10)**. In the chamber, an Indium Tin Oxide (ITO) was utilized as the anode electrode and CNTs as the cathode electrode with a distance (d) of 160~170μm. Besides, the vacuum degree of the whole chamber was controlled by a turbo pump and a rotary pump. In the application of gas ionization sensor measurement, the chamber would be firstly evacuated to high vacuum (10^{-6} torr) and then it switched to the rotary pump to control the vacuum degree. Then, the target gas was fed into the chamber and the measurement was conducted under different gas pressures.

At the first step, we mainly discussed the gas breakdown characteristics between different surface morphology and catalyst structure. Therefore, the measurements were conducted only in the nitrogen environment and the discussion would focus on their gas breakdown characteristics under different gas pressure.

Moreover, a high-voltage source measurement unit, Keithley 237, was applied on the anode and a high-current source measurement unit, Keithley 238, was applied to the cathode (sample substrate). The samples were measured from 0V to several hundreds of volts until the gas breakdown occured and a high discharge current appeared (the discharge current is limited at 10mA for equipment protection).

2-1-3 Stability test

In the stability test, the samples were measured for 1000 cycle times where one cycle was defined as applying voltages from 0V to1000V with 10V as a unit, and the discharge current was limited at 10mA when gas breakdown occurs for the sake of preventing damages to equipments. All the experimental data were record and analysis by computers. After the stability tests, the micrographs of samples were taken by SEM to see their surface morphologies.

2-1-4 Gas sensing measurement

The same setups like **(Fig. 2-10)** were used in the gas sensing measurement. However, different gases like carbon dioxide, oxygen, air and argon were fed into the chamber in replace of nitrogen we used in above, and their Paschen's curve would be depicted, correspondingly. Finally, the change of breakdown voltages was measured in different concentration of mixed gas environment of air and target gas.

2-2 Experimental Design

2-2-1 The comparison between the Uniform CNTs film and the Random Oriented CNTs film

In the this experiment, in order to discuss the effect of surface morphology and protrusion of CNTs to their gas breakdown characteristics, two CNTs film with different surface morphology were demonstrated, which is referred to as the Random oriented CNTs film and the Uniform CNTs film. For the purpose of preventing the addition of variable factors in our experiment, the difference of crystallinity of the two demonstrated samples must be reduced. Traditional methods such as post plasma

treatment [62], post laser treatment [63], post acid treatment [64] had been prohibited to avoid the CNTs from structural damages. In replace, a thin Ti capping layer was utilized to generate the rough surface morphology of the CNTs film.

After the comparison of the gas breakdown characteristics of Random oriented CNTs film and the Uniform CNTs film, the stability tests were carried out to both of them.

2-2-2 Effects of the utilization of co-deposition catalyst structure

After examining the results in the last experiment, a co-deposited catalyst structure was proposed to improve the poor stability of the two conventional samples. The enhancement of the adhesion and the reduction of the contact resistance between CNTs and substrate could be realized with the CNTs film synthesized from Co-Ti co-deposited catalyst structure. As a result, the more optimal gas breakdown characteristics of this catalyst structure would be exploited into the application of our gas ionization sensor.

2-2-3 Finding optimum spacer / height ratio of the pillar array of vertical aligned CNTs bundles

In the last experiment, a CNTs-based film synthesized from the co-deposited catalyst method had been used to stabilize the gas breakdown characteristics of gas ionization sensors. However, the issue of risky high-voltage operation and high power consumption was still not improved. In this experiment, the gas breakdown characteristics of pillar array of aligned CNTs bundles under different spacer height ratio (R/H ratio) **(Fig. 2-11)** were discussed, and the comparison between the film sample and the patterned sample with different R/H ratio were summarized, one could obtain the optimization of the gas breakdown voltages which was useful to improve

the high-voltage issue of the gas ionization sensors. Finally, we would discuss the factors that originate these differences of the gas breakdown characteristics of samples.

2-2-3 Gas sensing measurement under different gases environment

After finding the optimal film sample and patterned sample in above, their gas sensing characteristics would be quantified here. It's worth noting that all the gas breakdown characteristics we measured above were in the nitrogen environment. Therefore, different gases like carbon dioxide, oxygen, air and argon were fed into the chamber to obtain their gas sensing properties. The same measurement setups and processes were utilized and their gas breakdown characteristics would be recorded to access their own Paschen's curve, correspondingly. With these Paschen's curve, one can choose the proper area to fabricate the gas ionization sensor with low power consumption and wide breakdown window. Finally, the carbon dioxide and argon were fed into the chamber which is full of air, and their changes of gas breakdown voltage versus the concentration of target gas in air were illustrated.

Chapter 3

Results and Discussions

3-1 The comparison of breakdown characteristics between the Uniform CNTs film and the Random Oriented CNTs film

3-1-1 The Gas breakdown characteristics of the Random oriented CNTs film and the uniform CNTs film

The SEM micrographs of the CNTs of sample (A) were shown in **(Fig. 3-1)** and **(Fig. 3-2)**. From the tilted images (about 45°) taken by scanning electron microscope (SEM) for the Uniform CNTs film grown by thermal CVD, one could find that the vertical aligned CNTs film was grown on sample (A) through the thermal CVD. This is the vapor-liquid-solid (VLS) mechanism [65-67] and crowing effect [68-70] which many researchers have investigated on. At first, the hydrocarbon molecules decomposed and then carbon incorporation into and precipitation out of the metal particle. Graphite structured CNT would format out of the metal catalyst nanoparticles. Then the confinement of growth direction due to neighboring CNTs forces the CNTs to grow upward and their vertical alignment. Therefore, after the process of thermal CVD, a uniform CNTs film was successfully grown on sample (A). On the other hand, the surface morphology of CNTs grown from the same process of thermal CVD on sample (B) was quite different from sample (A). As seen from the tiled angle of **(Fig. 3-3)**, the surface morphology was ups and downs with no uniformity. And from the magnified **(Fig. 3-4)** one could found that the degree of CNTs' bending and tangling

was severe and the length of the CNTs was fairly different. The cross-section view of sample (B) was shown in **(Fig. 3-5)**, which indicates the nonuniformity of the height of the Random oriented CNTs film. The main reason for the rough surface morphology of the sample (B) was from the additional Ti capping layer on the Co catalyst layer. Because the melting point of Ti is higher than Co, it would put a ceiling on the catalyst when forming the nanoparticles in the pretreatment process. For the sizes of nanoparticles are quite dissimilar, the thickness of capping Ti are different everywhere. When growing the CNTs, these capping Ti might limit the growth direction and the length of the CNTs, part of them might lift up the Ti capping layer and part of them might penetrate it, which cause the nonuniformity of the surface morphology on sample (B). Since the different appearances of the CNTs of sample (A) and sample (B), they should have theoretically different gas breakdown characteristics in the application of gas ionization sensors. With the purpose of the convenient in comparison, we referred sample (A) as the Uniform CNTs film and sample (B) as the Random oriented CNTs film. However, for a fare baseline of comparison, Raman spectra were used to investigate the crystallinity of the two CNT films. **(Fig. 3-6)** and **(Fig. 3-7)** are the Raman spectra analysis of the Uniform CNTs film and the Random oriented CNTs film, respectively. The effects the qualities of CNTs could be analysis by the Raman spectroscopy [71-72]. The D peak is indicative of defects in CNTs, i.e., carbonaceous impurities with sp^3 bonding and broken sp^2 bonds in sidewalls. It serves as a measure of structural disorder in CNTs, usually at the closed ends and nanosized particulate carbon on top or near the walls. The G peak results from the graphitic nature of CNT, i.e., crystallinity: pristine arrangement of atoms. It originates from intravibration between carbon atoms and the in-plane tangential stretching of carbon–carbon bonds in the graphene sheets. Therefore, the intensity ratios of the D peak and the G peak were widely used as an index of purity and perfectness of the

grown CNTs. In our experiment, the I_G/I_D ratio indicates the graphite crystallinity of the two samples is quite similar. Traditionally, the nonuniform surface morphology was fabricated by post-treatments such as plasma, laser, acid…etc. However, these post-treatment might produce structural damages of CNTs, which reduce the crystallinity and the electron emission efficiency of the CNTs. In our experiment, these structural damages were avoided by only adding a thin Ti capping layer, and their gas breakdown characteristics were compared under fare baseline.

Besides, as shown in the micrographs of *Transmission electron microscopy* (TEM), one could find that both of the Uniform CNTs film **(Fig. 3-8)** and the Random oriented CNTs film **(Fig. 3-9)** were multiwalled structure, their diameters were around 15 to 20 nm, and the crystallinity of the two samples were almost equivalent, which guarantee the same result acquire from the Raman spectra.

Next, the Random oriented CNTs film and the Uniform CNTs film would be put into our measurement setups **(Fig. 2-10)** to examine their gas breakdown characteristics. Firstly, the chamber was evacuated to high vacuum (10^{-6} torr) and switch to the rotary pump to control the vacuum degree. Then the target gas was fed into the chamber. In this chapter, we mainly discuss the gas breakdown characteristics between different surface morphology. Therefore, the measurements were conducted only in the nitrogen environment and the discussion would focus on their gas breakdown characteristics under different gas pressure. Graphs was plotted with x axis being the breakdown voltages versus the products of pressure and distance as y axis, and the curves of alteration of breakdown voltages with gas pressures was depicted (constant distance about 160μm was used here).

The measurement results of the Random oriented CNTs film were shows in **(Fig. 3-10)** and **(Fig. 3-11)**. One can find that the breakdown voltage is relatively high at low gas pressures and decreases to a minimum value as the pressure rising up.

However, the breakdown voltage would increases linearly from the minimum value if the pressure keeps rising up. The trend of our experimental result was follow the expectation of Paschen's curve **(Table 3-1)**, which indicates the correspondence with the theoretical prediction. Besides, it's worth noting that the variations of the breakdown voltages are especially large at high voltage region. The error bars in the high voltage region are as high as 100 volts. These variations are associated to the nonuniformity of the CNTs' length. For those longer CNTs, the difference of local electrical field distribution is larger, which leads to higher electron emission efficiency. Therefore, their breakdown voltages are lower than that of shorter CNTs. Moreover, the difference of local electrical field distribution might cause the pull-off and evaporation of the CNTs, which could result in the unstable discharge current like **(Fig. 3-10-(a))**. This issue would be discussed lately.

On the other hand, the measurement results of the Uniform CNTs film were shows in **(Fig. 3-12)** and **(Fig. 3-13)**, and the same trend of Paschen's curve was found. However, it has a relatively stable gas breakdown characteristics and smaller error bars than that of the Random oriented CNTs film. It was related to the uniformity of the CNTs' length of the Uniform CNTs film.

3-1-2 The stability test of the Random oriented CNTs film and the uniform CNTs film

In order to compare their reliability of the two conventional samples, the stability tests of gas breakdown characteristics under nitrogen environment with the Random oriented CNTs film and the Uniform CNTs film were demonstrated. 1000 cycle times of high voltage were applied on both of the samples. Here one cycle was defined as an voltages was applied between cathode and anode from 0V to1000V, and the discharge current is limited at 10mA when gas breakdown occurs. After the stability tests, the

shift of breakdown voltages (V_{br}) could be seen from **(Fig. 3-14)**. One could found that the V_{br} of Random oriented CNTs film lift up from 365V to 605V after 1000 cycles, 68% in increase. And for uniform CNTs film, it lift up from 395V to 575V after 1000 cycles, 46% in increase. The SEM images were used to examine the reason of this lift up of the breakdown voltages. As shown in **(Fig. 3-15)**, both of the two samples were intact before the stability tests. Nevertheless, after 500 cycle times of the stability test, it appears that the CNTs on the Random oriented CNTs film were stretch upward and lot of CNTs were pulled off by the local electrical field in the high voltages test, and many particles could be seen in the backside of the SEM image **(Fig. 3-15-(c))**.The pull-off of CNTs was not so obviously in the SEM image of the Uniform CNTs film **(Fig. 3-15-(d))**, and they were pulled off with an island of CNTs bundles as a unit. After 1000 cycles times of stability tests, the CNTs could be barely seen on the substrate of the Random oriented CNTs film, which were replaced by many particles **(Fig. 3-15-(e))**. And the pull off of CNTs for the Uniform CNTs film was more severe than that of the samples after 500 cycles times **(Fig. 3-15-(f))**. The effects of these pull-off and evaporation of CNTs were related the high local electric field difference. The Random oriented CNTs film has a more nonuniform local electric field distribution, so the pull off of CNTs would be more severe than the Uniform CNTs film. It was also found that the CNTs broken or pulled off from the substrate would exhibit an abrupt drop in the discharge current. For the later one, a gradual degradation of the discharge current density was found which might result from the Joule heat generated from high current density. This is because the contact resistance between CNTs and substrate might become worse for those CNTs in the range of removal and not removal. The Joule heat was easy to be accumulated under these CNTs. As it at high temperature, the oxygen remained in the vacuum chamber tends to attack the defective regions in the CNTs. Additionally, the interface structure

between the CNTs and the substrates is also getting loose at high temperature that makes the CNTs more easily to be pulled off from the substrate. It causes a gradual degradation of the number of field emission sites [73].

In order to acquire a better stability in our CNTs gas ionization sensor, the improvement of the adhesion and the contact resistance between CNTs and substrate under high electric field is urgent needed.

3-2 The stability improvement of the gas breakdown characteristics using CNTs film with co-deposition catalyst structure

3-2-1 Enhancing the adhesion and contact resistance between CNTs and substrate using co-deposited catalyst structure

To improve the gas breakdown characteristics of the Random oriented CNTs film and the Uniform CNTs film, a new catalyst structure was proposed, which is depicted in **(Fig. 2-4)**. Here we have to explain the roles of the Ti interlayer and the Al supporting layer. Firstly, the Ti interlayer would transform into liquid phase and the Co-Ti co-deposited layer would transform into nanoparticles as well in the pretreatment step under high temperature, and the Co catalyst nanoparticles might be grabbed like the roots in the soil. However, we should scale down the size of nanoparticles as small as possible for enough density of CNTs. As shown in **(Fig. 3-16)**, the various surface energy of different metals were exhibited. One can find that the surface energy of cobalt is familiar with that of titanium. If the two elements with nearly same surface energy as Co and Ti were used, the particles of each element will dispread uniformly to the similar sized nano-particles after hydrogen pretreatment. Depending on the past researches in our group, we were experimentally success demonstrating the Ti is the best buffer-component when we utilized Co or Fe as the

catalyst element, the result was demonstrated our assumption, so we just used Ti as buffer-component in this study [74] **(Fig. 3-17)**. The empirical experimental results could be seen in the SEM images of **(Fig. 3-18)**, with regard to the conventional two samples, the CNTs-based film synthesized from the co-deposited catalyst structure demonstrates the CNTs seemed to partially immerse into the catalyst structure like the tree rooted into the soil. This rooted structure was expected to improve the adhesion and contact resistance of our CNTs. On the other hand, for the Al supporting layer, we knew that Al plays a role of providing an additional curvature for surface of catalyst and quite increasing roughness mean square (RMS) as it transform into alumina. The advantage of increasing RMS is raising the density of catalyst particle on the same top view area, as **(Fig. 3-19)**, and then we could obtain better density of CNTs. As well as some drawbacks of CNT growth at low temperature are poor density of CNTs and weak adhesion between CNTs and substrate. We estimated that increasing CNTs density will not only improve the dense of emission sites, but also solve problem of weak adhesion by increasing Van Der Waal force between CNTs. In the Transmission Electron Microscopy (TEM) images of **(Fig. 3-20)**, one could found that the diameters of CNTs of the samples with catalyst co-deposition were smaller and the density was higher. This catalyst structure was used in our gas ionization sensor measurement and was expected to improve the adhesion and contact resistance.

3-2-2 The improvement of stability and gas breakdown characteristics using CNTs-based film synthesized from the co-deposited catalyst structure

The gas breakdown measurement results were illustrated in **(Fig. 3-21)**, where the breakdown characteristics became more stable and the multi-step breakdown or variations of breakdown voltages were no more obviously. As well as the error bars of the high voltage region were also reduced in **(Fig. 3-22)**. These were related to the

improvement of adhesion and contact resistance via the catalyst co-deposition. Besides, for the stability tests of the proposed sample **(Fig. 3-23)**, we found that the V_{br} of the CNTs film synthesized from Co-Ti co-deposited catalyst lift up from 375V to 435V after 1000 cycles, 16% in increase, which is further improved than the first two conventional CNTs film. From the SEM images before and after the stability test **(Fig. 3-24)**, the pull off and evaporation of CNTs were fairly improved. This is related to the improvement of the adhesion and contact resistance by the Co-Ti co-deposition and Al supporting layer used between the CNTs film and the substrate in the proposed sample.

3-3 Reduction of the breakdown voltages using pillar array of vertical aligned CNTs bundles with optimal spacer height ratio

3-3-1 Finding the optimal R/H ratio of pillar arrays of vertical aligned CNTs bundles that has lowest gas breakdown voltages

From the theory background in chapter 1, one could find that increasing the number of field emission electrons is constructive to reduce the breakdown voltages of the gas ionization sensors. Many investigations have explored that it is important to control the length and the inter-tube distance of CNTs to reduce the screening effect in adjacent CNTs [75] shown in (**Fig. 3-25)**. When an external electrical field applied on the emitters, a local electrical field based on its shape and other body factor would be generated around the tip of the emitters. The absence of screening effect occurred when only one emitter was used, and the electron tunneling effect was more easily to be produced by the local electrical field. However, under the consideration of several million of emitters which with closely nearness, the local electrical field would interfere with each other and make it harder to emit electrons, which cause the

reduction of current density.

It has been reported that field emission can effectively enhanced for aligned CNTs as field emitters when the ratio of the inter-tube distance to the height of each CNT is about 2 [76-79]. That is to say, CNT films of low density yield low currents essentially because the emitter density and the field enhancement factor are low. For high density films, screening effects reduce the field enhancement and thus the emitted current. For films of medium density, there is an ideal compromise between the emitter density and the intertube distance, which is sufficiently large to avoid screening effects [76] **(Fig. 3-26)**.

In order to investigate the change of breakdown voltages under different surface electrical field, we have to invent dissimilar morphology of CNTs film. Therefore, pillar arrays of vertical aligned CNTs bundles with different spacer height ratio (R/H) were utilized **(Fig. 3-27)**. The method we used was to obtain it by changing H while maintaining R. and different growth time was utilized to control the height of CNTs bundles **(Table 3-3).**

Firstly, for a low R/H ratio comparison, we used long growth time to acquire enough high CNTs. As shown in **(Fig. 3-28)**, it was the cross-sectional view of CNTs film synthesized from Co-Ti co-deposited catalyst structure for 50.8 μm in CNTs height. In contrast, 48.8 μm high pillar-like CNTs synthesized from the Co-Ti co-deposited catalyst structure was shown in **(Fig. 3-29)**. Both of them were conducted to the gas breakdown measurement under nitrogen environment, and the results were demonstrated in **(Fig. 3-30)**. One could find that there is no much difference of breakdown voltages between the film sample and the pattern sample at this R/H ratio, which means the employment of the pattern method, was in vain in the improvement of reducing breakdown voltages. Besides, the breakdown voltages only fluctuate slightly at high voltage regime in our curves, so the error bars were ignored

in the graphs.

Next step, the height of CNTs was shortened for the purpose of increasing the R/H ratio. As shown in **(Fig. 3-31)**, it was the cross-sectional view of CNTs film synthesized from Co-Ti co-deposited catalyst structure for 11.3 μm in height. On the other hand, 12.5 μm high pillar-like CNTs synthesized from the Co-Ti co-deposited catalyst structure with R/H ratio of 2.40 was obtained to compare with it **(Fig. 3-32)**. Both of them were conducted to the gas breakdown measurement under nitrogen environment, and the results were demonstrated in **(Fig. 3-33)**. At this R/H ratio, the breakdown voltages of the patterned sample begin to lower than that of film sample, which means the pattern method starts to bringing constitution into the breakdown voltages.

Then, the height of CNTs was more shortened for higher R/H ratio. As shown in **(Fig. 3-34)**, CNTs film synthesized from Co-Ti co-deposited catalyst structure for 13.1 μm in height was obtained. In contrast, 10.3 μm high pillar-like CNTs synthesized from the Co-Ti co-deposited catalyst structure with R/H ratio of 2.91 was achieved to compare with it **(Fig. 3-35)**. Both of them were conducted to the gas breakdown measurement under nitrogen environment, and the results were demonstrated in **(Fig. 3-36)**. One could find that the breakdown voltages of patterned sample are greatly lower than film sample at this R/H ratio, which means the pattern method has significantly effect on promoting the emission of electrons by utilizing the local electrical field.

After that, for higher R/H ratio, the height of CNTs was further shortened. As shown in **(Fig. 3-37)**, it was the cross-sectional view of CNTs film synthesized from Co-Ti co-deposited catalyst structure for 5.95 μm in height. On the other hand, the 5.95 μm high pillar-like CNTs synthesized from the Co-Ti co-deposited catalyst structure was obtained to compare with it **(Fig. 3-38)**. Both of them were conducted to

the gas breakdown measurement under nitrogen environment, and the results were demonstrated in **(Fig. 3-39)**. One could find that, at this R/H ratio, the breakdown voltages of patterned sample is lower than film sample but not so much as that of R/H = 2.91. We also have another patterned sample with 2.63**μm** (R/H=11.45) in height of the CNTs. However, its breakdown voltages were worse than the one with R/H = 2.91. Therefore, an optimal gas breakdown characteristic with lowest breakdown voltages was approached via modified local electrical field distribution with the pattern method, and the optimized R/H ratio was around 2.91.

The comparison of the breakdown voltages characteristics of the film samples with different height was integrated in **(Fig. 3-40)**. The lowest breakdown voltages were obtained at the height of CNTs around 11.3 μm to 13.1 μm. The breakdown voltage would increase when the height of the CNTs was too long or too short. On the other hand, the comparison of the breakdown voltages characteristics of the pattern samples with different R/H ratio was integrated in **(Fig. 3-41)**. It's obviously that the lowest breakdown voltages were approached as the R/H ratio was around 2.91. If the R/H ratio increases to 5.04 and 11.4, the breakdown voltages will raise up gradually. Here are several issues needed to be discussed. Firstly, why there exists a lowest breakdown voltage in the Paschen's curve? Secondly, what's the mechanism leads to a generally lower breakdown voltages of patterned samples than film samples? Thirdly, why the lowest breakdown voltage was approached around R/H = 2.91?

3-3-2 Discussions of the gas breakdown characteristics of patterned sample

In first issue, for the existence of a lowest breakdown voltage in the Paschen's curve, the explanation could be given in two ways. For a constant gas pressure, the breakdown voltages decrease at left side of the curve because the distance between anode to cathode raises and the numbers of the effective collision for electrons

increase as well. However, at right side of the curve, as the distance become too long, the electrical field under the same applied voltage will decrease and electrons cannot receive enough kinetic energy to generate effective impact ionization, which causes the increase of breakdown voltages. On the other hand, for a constant anode-to-cathode distance, the breakdown voltages decrease at left side of the curve because more neutral molecules participate in the ionization reaction as the gas pressure raises up, and the electron mean free path declines. However, at right side of the curve, as the number of neutral molecules become too much, the ionized electrons might be scattered more easily before they arriving to the anode. Therefore, the breakdown voltages increase.

Secondly, to find a mechanism that leads the general lower breakdown voltages of patterned samples than film samples, a possible explanation was given in **(Fig. 3-42)**. **(Fig. 3-42-(a))** shows the local electrical field distribution of the film sample and the patterned sample for a constant anode-to-cathode distance and the same gas pressure. In this situation, if the modified local electrical field allows every pillar on the patterned sample to have emission site on both end of the corner, then one could find that the emission site of the patterned sample is more than that of the film sample **(Fig. 3-42-(b))**. The higher initial current was consequent on the additional emission sites of the patterned sample, which permit the arrival of gas breakdown at relatively low applied voltages.

In the last issue, the existence of an optimal R/H ratio could be elucidated by **(Fig. 3-43)**. When one only take the screening effect into account, the effect would become severe as the pillar-to-pillar distance shrinks. That is to say, the field enhancement might decline as the R/H ratio decreases. On the other hand, when one only considered the aspect ratio effect originated from body factors of the pillar-like CNTs, the difference of the local electrical field distribution might become no more

obviously as the height o the CNTs pillar was shortened. Specifically, the field enhancement might decline as the R/H ratio increases. Taking these two effects into consideration, the graph of field enhancement versus R/H ratio could be illustrated like **(Fig. 3-43-(c))**, which indicated there exist a specific R/H ratio that has the maximum value of the field enhancement, and at this R/H ratio comes the most efficient field-emission ability to possess the lowest breakdown voltage.

In summary, there exists a lowest breakdown voltage in the Paschen's curve for both of the film sample and the patterned sample. In our experiment, it reaches minimum at 11.3 μm to 13.1 μm in CNTs' height for the film sample. However, the patterned sample has lower breakdown voltages than the film sample when the former was under optimized local electrical distribution, and the optimal R/H ratio was experimental approached around 2.91. In the following experiment, these optimized CNTs sample would be led to the gas sensing measurement under different gases environment.

3-4 The gas breakdown characteristics of the optimized CNTs film gas ionization sensors under different gases environment

3-4-1 The Paschen's curve of different gases and its application to gas ionization sensors

Breakdown voltages optimized film sample and patterned sample were obtained in the experiments above. Here they were measured with the same setups of **(Fig. 2-10)** to acquire the breakdown characteristics in different gases environment. The experimental method and the anode-to-cathode distance were standardized as measuring that of nitrogen. These results were shown in **(Fig. 3-44)**, which describe

that argon displays the lowest breakdown voltages, carbon dioxide displays the highest ones, and the breakdown voltages of air is between nitrogen and oxygen as expected. Besides, it's intuitional recognized that different gases have their own distinct Paschen's curve. For different gases will have different diameters, that is, different mean free paths for their molecules and electrons. For instance, Noble gases like helium and argon are monoatomic and tend to have smaller diameters. This gives their molecules a greater mean free path length. Ionization potentials differ between molecules as well as the speed that they recapture electrons after they have been knocked out of orbit. All these three effects change the number of collisions needed to cause an exponential growth in free electrons. These free electrons are necessary to cause a gas breakdown in the experiment. Therefore, one could find distinct breakdown characteristics for different gases.

Moreover, on could find that after each gas pass through their lowest point in their Paschen's curve, the breakdown voltage would enter a linear regime and continue rising gradually. This is what we have predicted in chapter 1, and generally the gas ionization sensor was fabricated by utilizing this regime.

However, choose a proper p×d area is extremely important in fabricating the gas ionization sensor. For example, to the film sample with 11.3 μm in CNTs' height whose discharge current versus breakdown voltage curves for Ar, N_2, Air, O_2 and CO_2 were illustrated in **(Fig. 3-45)**. If the sensor was operated at the p×d product value around 8×10^{-4} torr cm, then a low-voltage-operating Ar was available while at the cost of the residual gases was operated at high voltages and have narrow breakdown voltage windows between each other. Through the revelation from previous experiment, one acknowledged that high voltage operation was easy to cause damages on the sample and variation in the breakdown characteristics. And in the critical situation, there might be misdetection for gases with small difference in their

breakdown voltage. On the other hand, if the sensor was operated at the p×d product value around 8×10^{-3} torr cm **(Fig. 3-45-(b))**, then the advantages like low voltage operation and wide windows between gases was both achieved, and one could reduce the power consumption and lessen the probability of misdetection.

To the patterned sample with R/H = 2.91, the similar characteristics was found in **(Fig. 3-46)**. Though, it was demonstrated above that the optimized patterned sample has relatively low breakdown voltages than that of the film sample, and therefore more superiority in the issue of power consumption.

3-4-2 Breakdown characteristics of carbon dioxide and argon in a mixture with air

The experimental results of measuring the breakdown voltages of Ar and CO_2 gases in mixture with air as a function of concentration were shown **(Fig. 3-47)**. It's obviously that for both of the film sample and the patterned sample, their breakdown voltage increases with increasing CO_2 concentration in the mixture, and decreases with increasing Ar concentration. In term of the film sample, the breakdown voltage decreases 130V as the concentration of Ar in the air reaches 15 %, and decreases 190V as it reaches 34 %. The breakdown voltage increases 60V as the concentration of CO_2 in the air reaches 15 %, and increases 100V as it reaches 43 %. On the other hand, to the patterned sample, the breakdown voltage decreases 100V as the concentration of Ar in the air reaches 11 %, and decreases 180V as it reaches 34 %, As the concentration of CO_2 in the air reaches 15 %, the breakdown voltage increases 50V, as it reaches 42 %, the breakdown voltage increases 120V. When the concentration of Ar and CO_2 is more than 50%, the breakdown voltage is nearly the same as that of pure Ar or CO_2. This is because air has a higher breakdown voltage than Ar and lower breakdown voltage than CO_2, so the presence of air molecules

tends to impede the breakdown of Ar and assist that of CO_2. Below 10% concentration, the breakdown of Ar ceases and the breakdown voltage rises sharply to the value for pure air. Similar results were also obtained for detection of CO_2 in a mixture with air, but the breakdown voltage declines slowly to the value for pure air.

Besides, as mentioned above, the patterned sample has the superiority in power consumption than that of the film sample when the former was under optimized local electrical field distribution, that is, optimal R/H ratio.

Consequently, with the utilization of the pattern technology and proper operation at p×d product value around 8×10^{-3} torr cm, the CNT gas ionization sensor can reduce both of the power dissipation and the error analysis between different gases.

Chapter 4

Summary and Future prospects

4-1 Summary and conclusions

At the beginning of this thesis, the gas breakdown characteristics of the Random oriented CNTs film and the Uniform CNTs film were compared. It was found that the breakdown characteristics of the Random oriented CNTs film was less stable, whose soft breakdown and variation of breakdown voltages were more obvious. Moreover, after the stability tests, the breakdown voltages of the Random oriented CNTs sample shift upward 68%, and it shifts upward 46% for the Uniform CNTs film. Besides, CNTs pull-off could be evidently seen from both of the SEM images. And the evaporation of CNTs of the Random oriented CNTs film were more severe.

However, with the proposed CNTs film synthesized from co-deposited catalyst sample, the improvement of the stability of CNTs film was apparent as could be observed from the gas breakdown characteristics and the SEM images before and after 1000 cycle times of stability tests. With strong adhesion between the CNTs and the substrate, the CNTs films synthesized from co-deposited catalyst structure could sustain large electrostatic force induced by the applied electrical field and thus suppress the abrupt decrease in the discharge current. Moreover, the reduction of contact resistance also eased the Joule heat generated from high current density passing through the high resistive regions. The high temperature due to the Joule heat could make the remained oxygen molecules react with defective regions in the CNTs, causing the evaporation of the CNTs, or degrading the interfacial structure between

the CNTs and the substrate. Therefore, the abrupt decrease and gradual degradation of the discharge current were both suppressed by means of utilizing the catalyst co-deposited structure.

Another aim of this thesis is to shrink the screening effect provoked by the proximity of neighboring tubes. Hence, to find out an optimal morphology of pillar array of vertical aligned CNT bundles for the application of gas ionization sensors, different spacer/height ratio (R/H) as a function of H is investigated by changing H while maintaining R. After comparing the film samples with the patterned samples for many different heights, briefly speaking, there exists a lowest breakdown voltage in the Paschen's curve for both the film sample and the patterned sample. In our experiment, the breakdown voltage reaches its minimum at 11.3 μm to 13.1 μm in CNTs' height of the film sample. However, the patterned sample has lower breakdown voltages than the film sample when the former was under appropriate local electrical field, and the optimal R/H ratio was experimentally approached around 2.91. This optimal R/H ratio that has a lowest breakdown voltage would lessen the high operating-voltage and thus improve high power consumption issues of the ionization sensors.

Next, both of the optimized film sample and patterned sample were utilized to explore its gas ionization characteristics under different gases environment. For different gas molecules having different mean free path, ionization energy and recombination rate, different trends of Paschen's curve for distinct gases were obtained in this experiments. Besides, with the proper choice of the p×d product value, CNT gas ionization sensor could not only operates under low voltages but also provides enough space to distinguish different gases.

Finally, the breakdown voltages of Ar and CO_2 gases in mixture with air as a function of concentration were also investigated. It's obvious that for both of the

optimal film sample and the patterned sample, their breakdown voltage increases with increasing CO_2 concentration in the mixture, and decreases with increasing Ar concentration. For instance, for the optimal patterned sample, the breakdown voltage decreases 100V as the concentration of Ar in the air reaches 11 % and increases 50V as the concentration of CO_2 in the air reaches 15 %. These tests indicate that the CNT gas ionization sensor (with proper calibration) shows promise for room-temperature detection of gases at the percentage level in mixtures with air.

In conclusion, we demonstrate a gas sensor using carbon nanotubes as the field ionization cathode. The sensor has the merits of low cost, low breakdown voltage and wide breakdown voltage window because the sharp tips of the nanotubes can generate very high electric fields at relatively low voltages. Sensors with carbon nanotubes as the cathode material also show good sensitivity and selectivity; in our experiment, the detection limitation of the field ionization based CNT gas sensors is about percentage level. More outstandingly, the stability was significantly improved by co-deposited catalyst structure. Therefore, the simple, low-cost, sensors described here could be deployed for a variety of applications, such as environmental monitoring and sensing in chemical process.

4-2 Future prospects

Operating under atmospheric pressure (760 torr) is a milestone to marketwise the gas sensor. For our CNT gas ionization sensor, which works with remarkable characteristics, it is still challenging to realize the operation under atmospheric pressure. For example, as we have mentioned in the experiment of sensing different gases, if the sensor was operated at the p×d product value around 8×10^{-3} torr cm [Fig. 3-r-b], then the advantages such as low voltage operation and wide windows between gases were both achieved, and one could reduce the power consumption and lower

down the probability of misdetection. However, under this p×d product value, operation under 760 torr means one have only 0.1μm for the anode-to-cathode distance. What's more, CNTs tend to be straightened along the direction of the electrical field as one applies high voltages. Therefore, the straightened CNTs might have chance to short with the anode electrode directly in such a narrow gap. In order to realize the prospect of practical operation, we extend the linear region in the right side of the Paschen's curve to locate a suitable p×d product value to fabricate the atmospheric operating CNT gas ionization sensor. As shown in **(Fig. 4-1)**, if one locates at p×d product value around 0.1 torr cm, the corresponding anode-to-cathode distance under 760 torr is 1.3μm. If one chooses p×d product value around 1 torr cm, the equivalent anode-to-cathode distance under 760 torr is 13.2μm. It's evident that the later ought to reduce the short phenomenon successfully. However, it needs several tens of volts higher in operation voltages, which implies a trade off event.

On the other hand, to attain the precise requests of spacing under atmospheric pressure, one can also use ZnO nanowires whose length are better controlled. Although the breakdown voltages of ZnO nanowires are appreciably higher in comparison to that of CNT electrodes, their stability and anti-oxidation are significantly better than CNTs as electrodes.

Tables

	Analytical instrument	Gas sensor
Data precision	excellent (absolute value)	excellent (fair enough)
Data acquisition time	long	short (real time)
Size	large	compact
Cost	high	low
Application	Environmental monitoring stationary site	Precise control, monitoring stationary site or mobile site

Table 1-1 Comparison between analytical instruments and gas sensors.

CNT growth	Time (min)	H_2 (sccm)	C_2H_4 (sccm)	N_2 (sccm)
heating	9	0	0	1000
Pre-treatment	10	300	0	0
Heating	4	0	0	1000
Growth	10	300	100	500
cooling	120	0	0	5000

Table 2-1 The parameters of thermal CVD to grow the Uniform CNTs film and the Random oriented CNTs film.

Chamber pressure	Breakdown voltage
0.023 torr	725V
0.052 torr	505V
0.079 torr	485V
0.1 torr	465V
0.2 torr	405V
0.51 torr	415V
0.8 torr	365V
1.0 torr	375V
2.1 torr	435V
5.1 torr	445V

Table 3-1 Gas breakdown voltages of the Random oriented CNTs film

Chamber pressure	Breakdown voltage
0.024 torr	605V
0.049 torr	445V
0.078 torr	425V
0.1 torr	425V
0.21 torr	415V
0.51 torr	385V
0.82 torr	375V
1.0 torr	385V
2.0 torr	425V
4.9 torr	465V

Table 3-2 Gas breakdown voltages of the Uniform CNTs film

CNT growth	Time (min)	H_2 (sccm)	C_2H_4 (sccm)	N_2 (sccm)
heating	9	0	0	1000
Pre-treatment	10	300	0	0
Heating	4	0	0	1000
Growth	It depends	300	100	500
cooling	120	0	0	5000

Table 3-3 The parameters of thermal CVD to grow pillar arrays of vertical aligned CNTs bundles with different spacer height ratio (R/H).

Figures

Chapter 1

==========

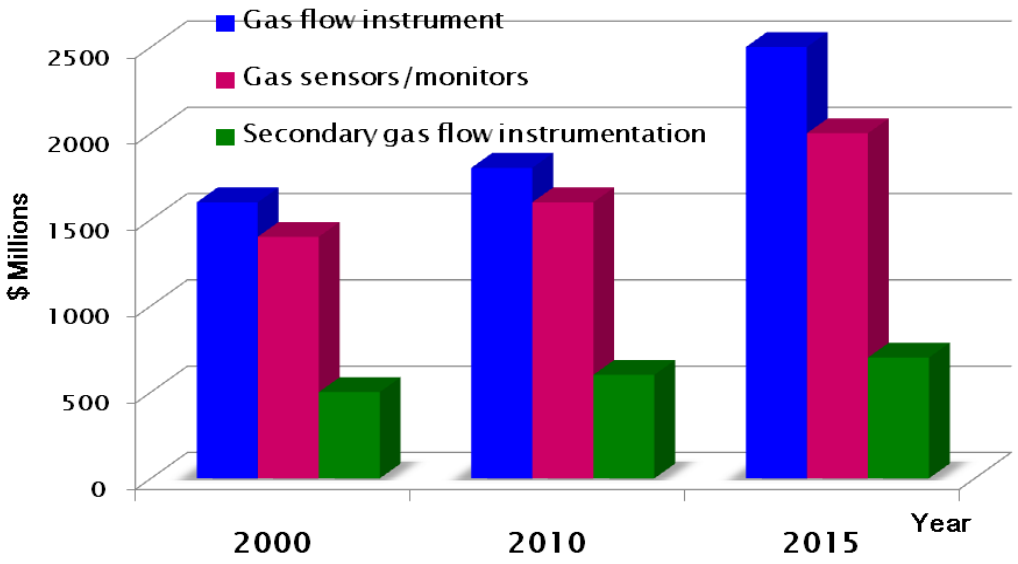

Figure 1-1 Trends in global markets for gas sensors [Frost and Sullivan & BCC Research].

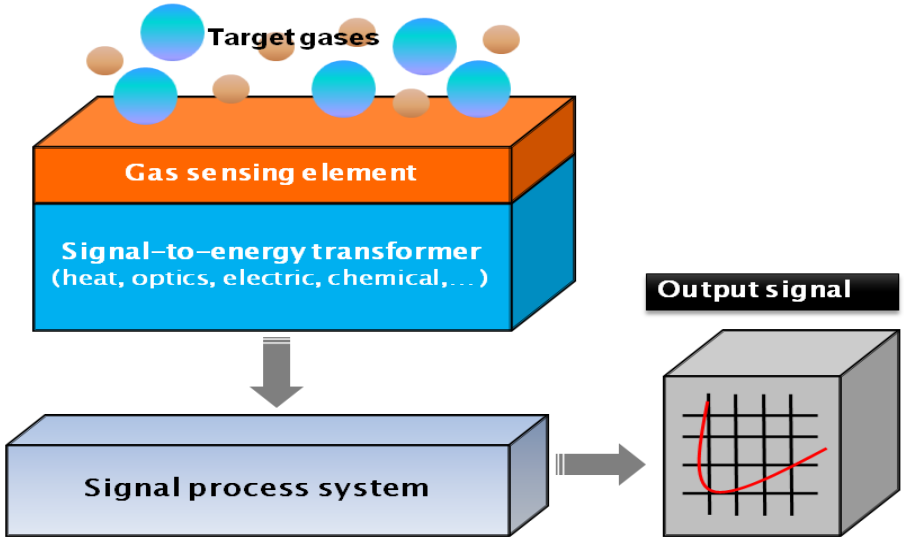

Figure 1-2 A gas sensor is a device which outputs the appropriate signals for detection and measurement when specific gas was released.

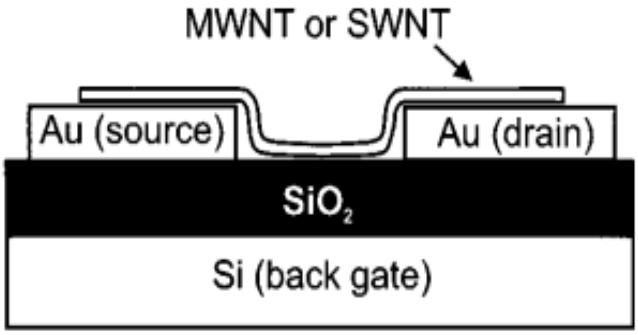

Figure 1-3 Schematic cross section of the FET devices. A single nanotube of either multi-wall or single-wall type bridges the gap between two gold electrodes. The silicon substrate is used as back gate [2].

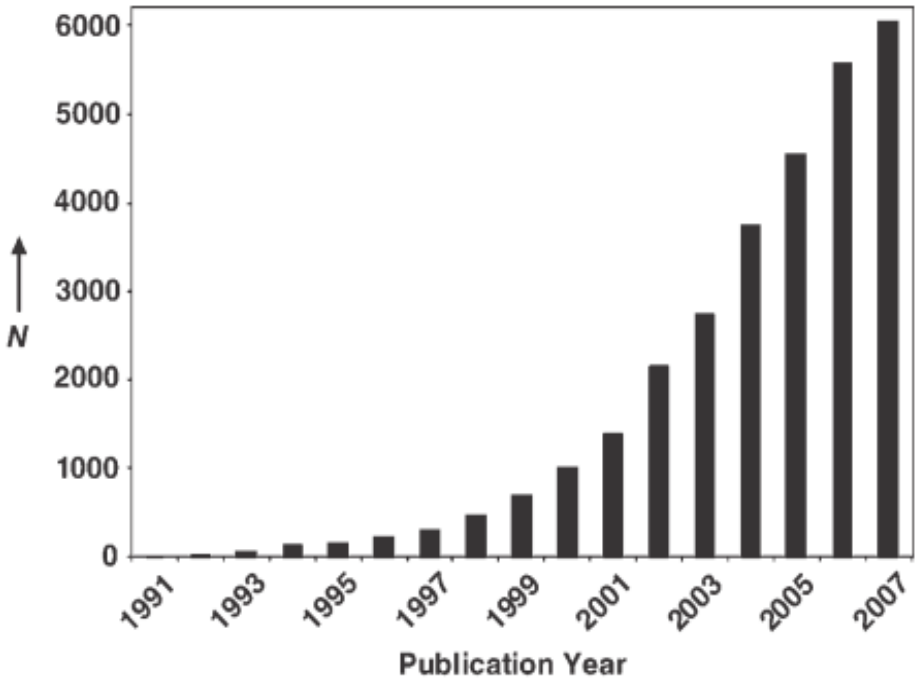

Figure 1-4 Histogram detailing the number of CNT publications per year between 1991 and 2007 (data obtained from ISI Web of Knowledge) [7].

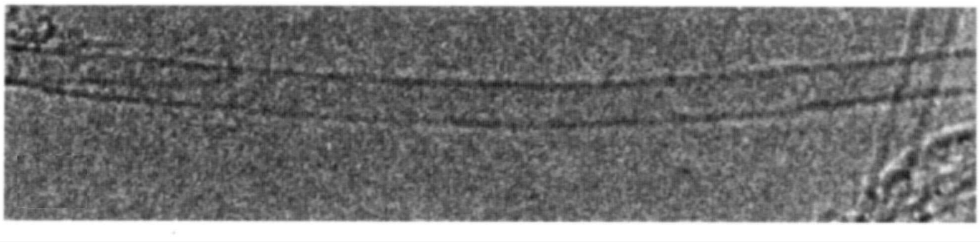

(a)

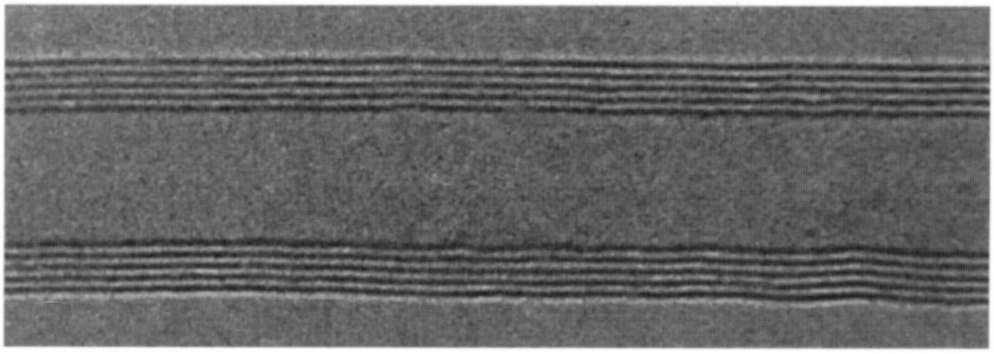

(b)

Figure 1- 5 High-resolution transmission electron microscopy images of (a) SWNTs, and (b) MWNTs. Every layer in the image (fringe) corresponds to the edges of each cylinder in the nanotube assembly [9].

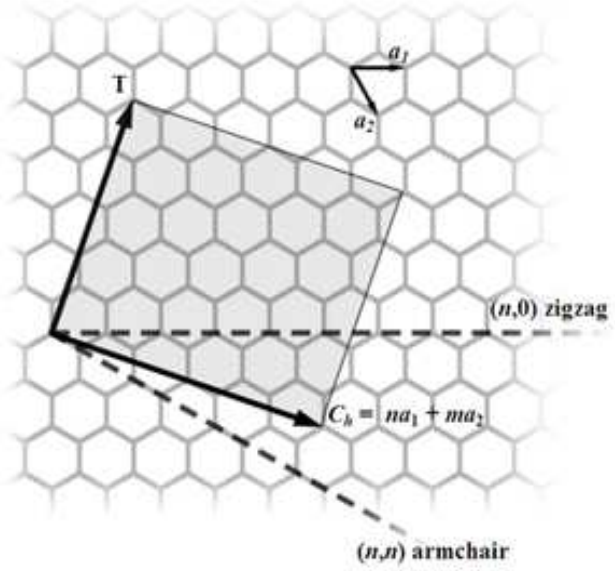

(a)

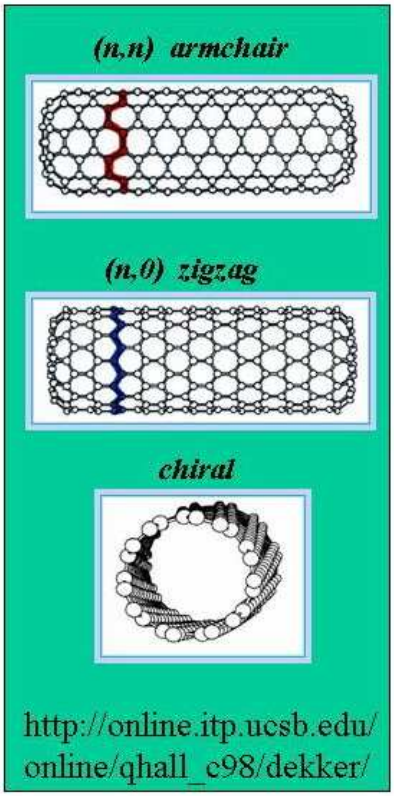

(b)

Figure 1- 6 Molecular models of SWNTs with (a) chiral vector (b) the categories of the configuration [12][13].

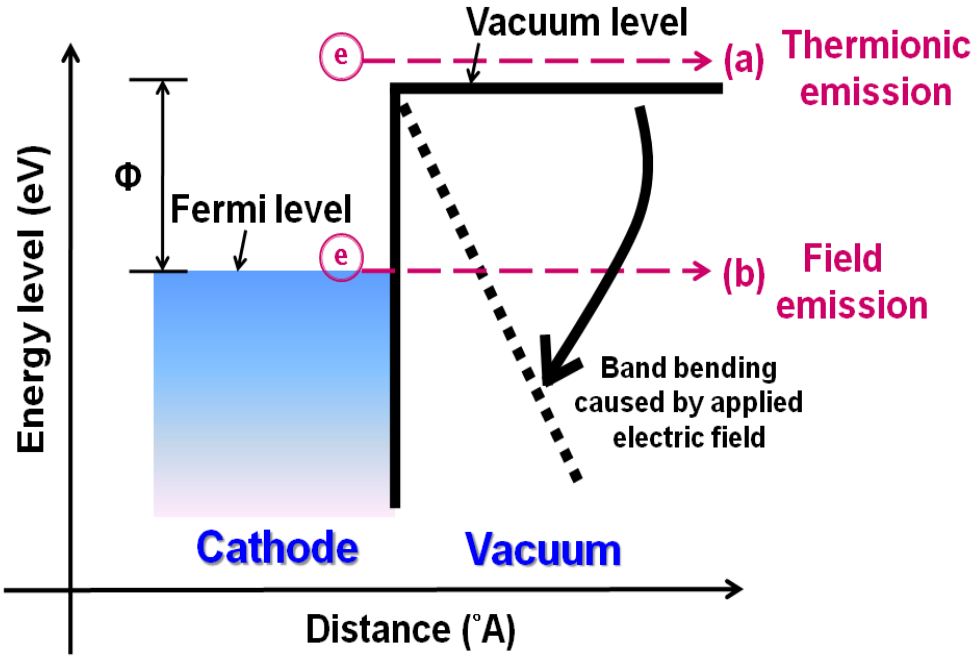

Figure 1-7 Energy band diagrams of vacuum-metal boundary (a) electron tunneling via thermionic emission and (b) electron tunneling via field emission.

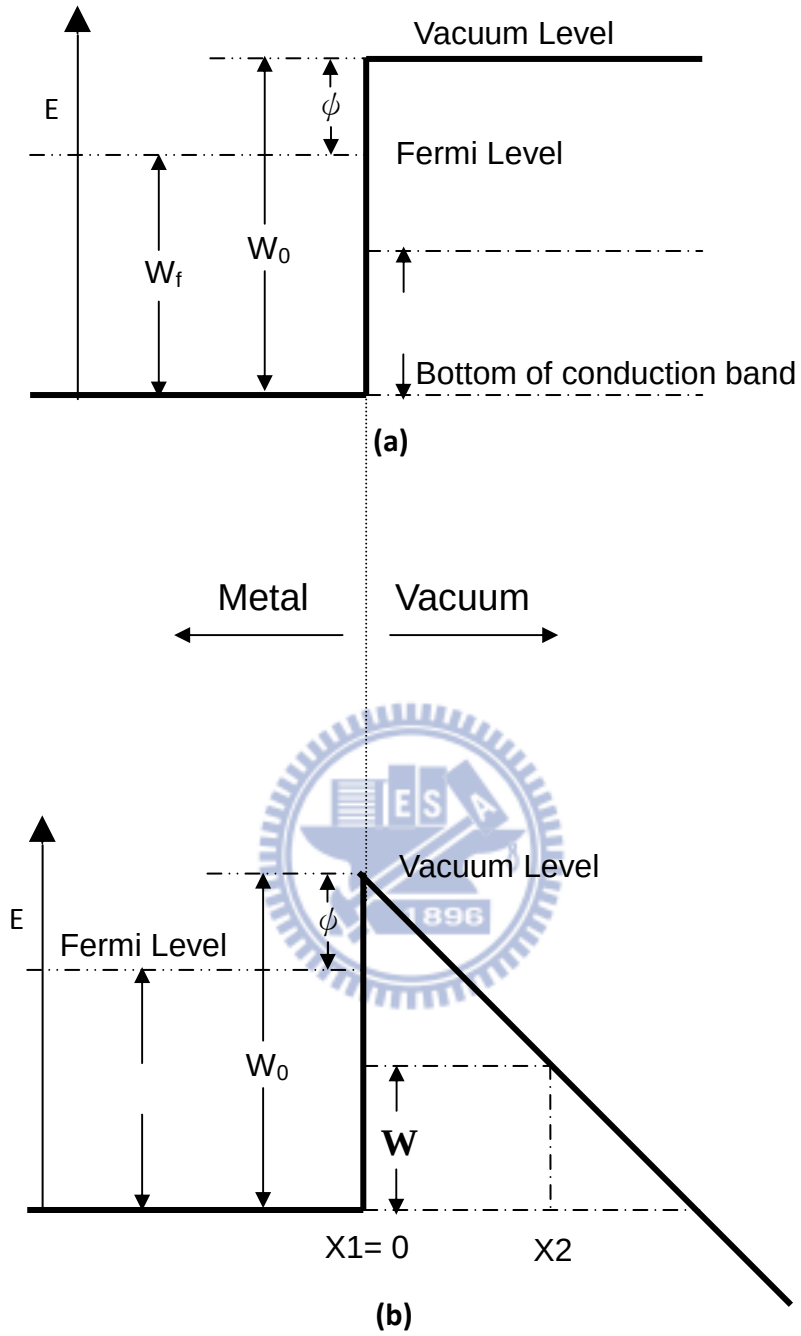

Figure 1-8 Energy diagrams of vacuum-metal boundary: (a) without external electric field; and (b) with an external electric field.

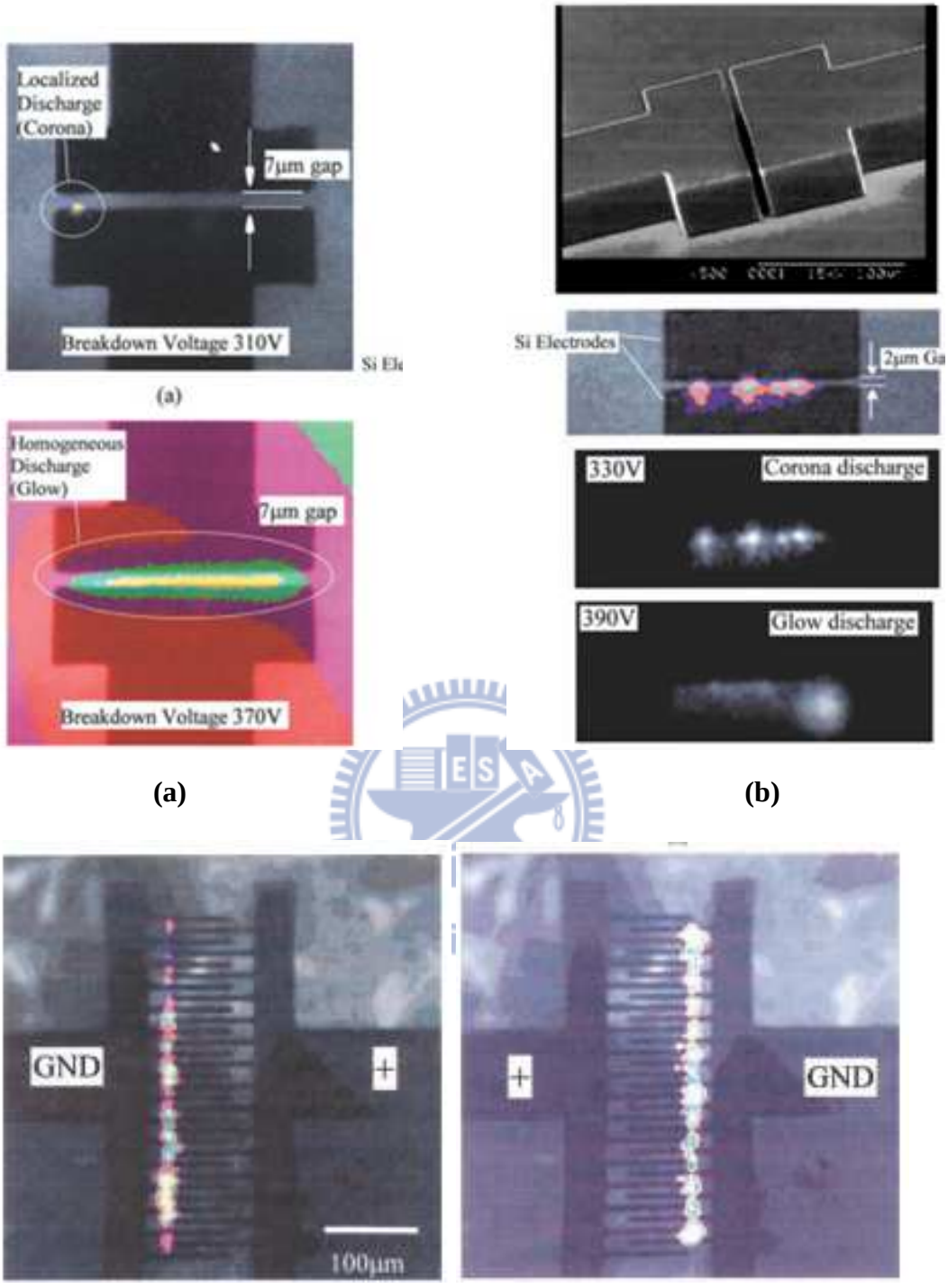

Figure 1-9 (a) Localized discharge spot can be seen at the gap with applying low voltage, (b) plane-to-plane silicon electrodes with narrow gap. (c) micro-discharge in the gap of a comb actuator [39].

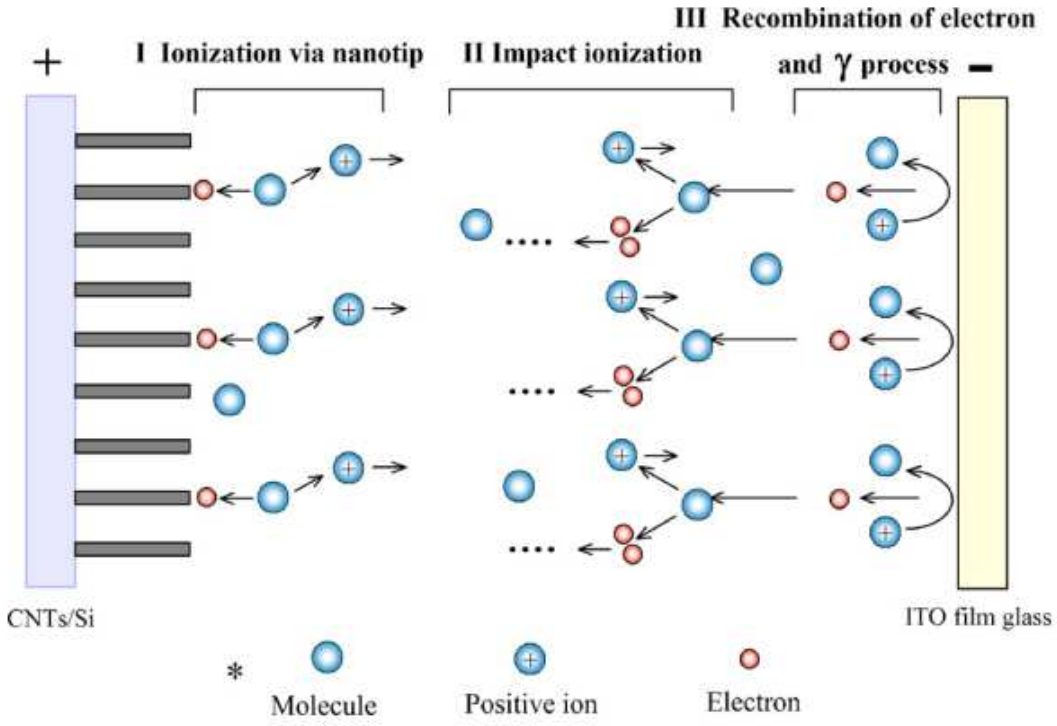

Figure 1-10 The breakdown discharge process of gas ionization sensor with CNTs as positive electrode [40].

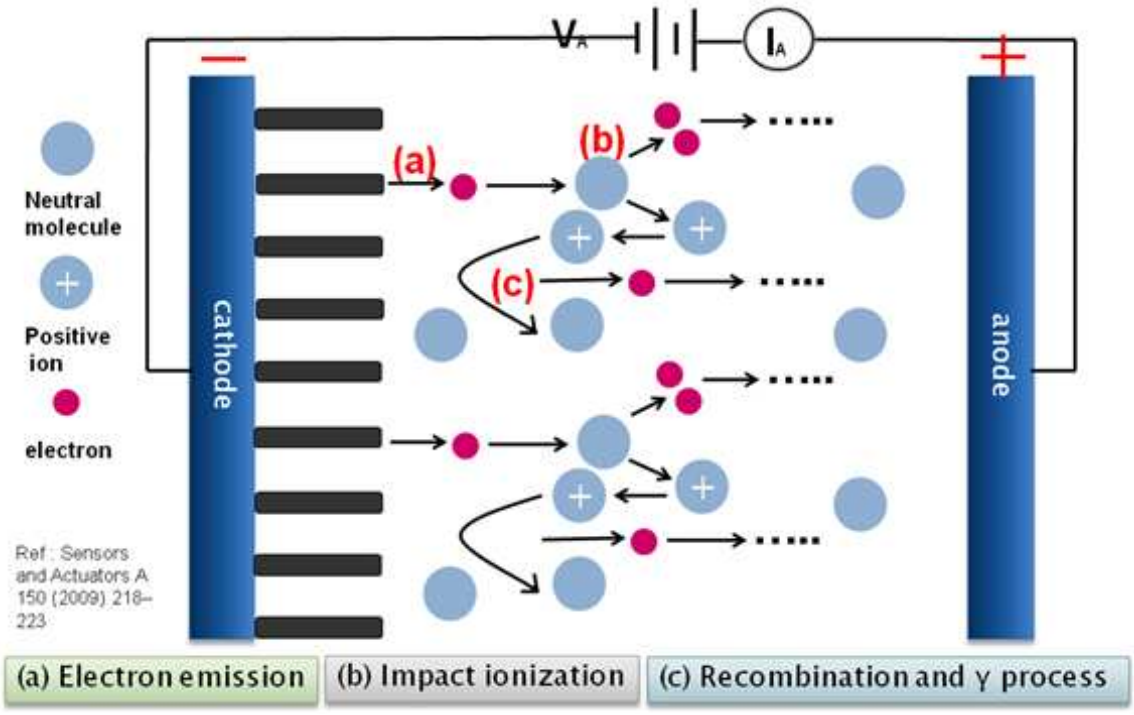

Figure 1-11 The breakdown discharge process of gas ionization sensor with CNTs as negative electrode.

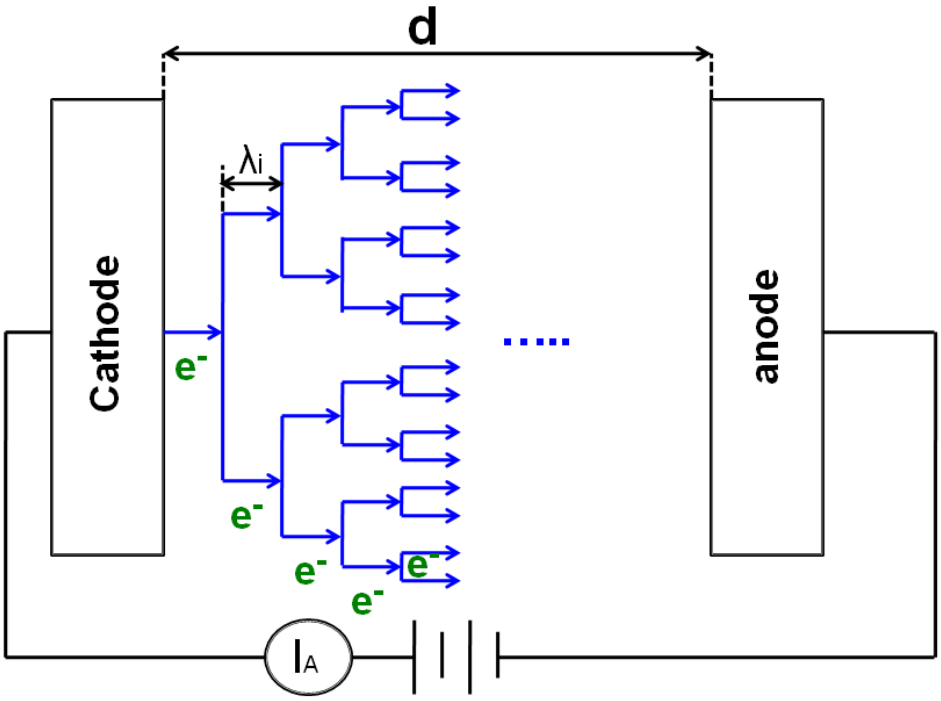

Figure 1-12 Schematic initially very small amount of free electrons, accelerated by a sufficiently strong electric field, give rise to electrical conduction through a gas by avalanche multiplication.

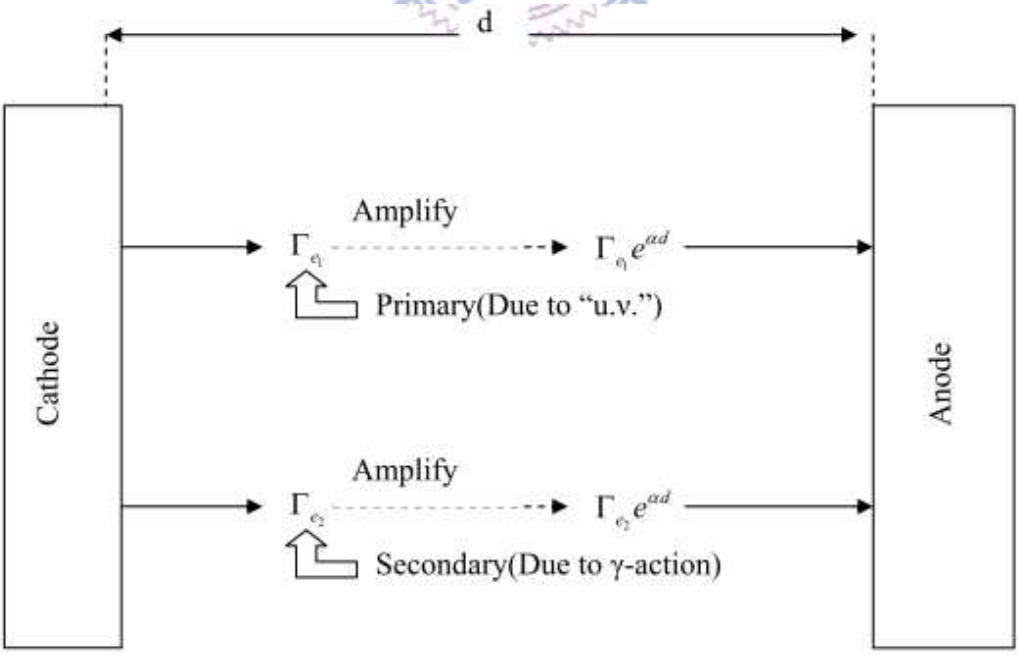

Figure 1-13 The Amplified mechanism of the electron flux in Townsend's discharge [80].

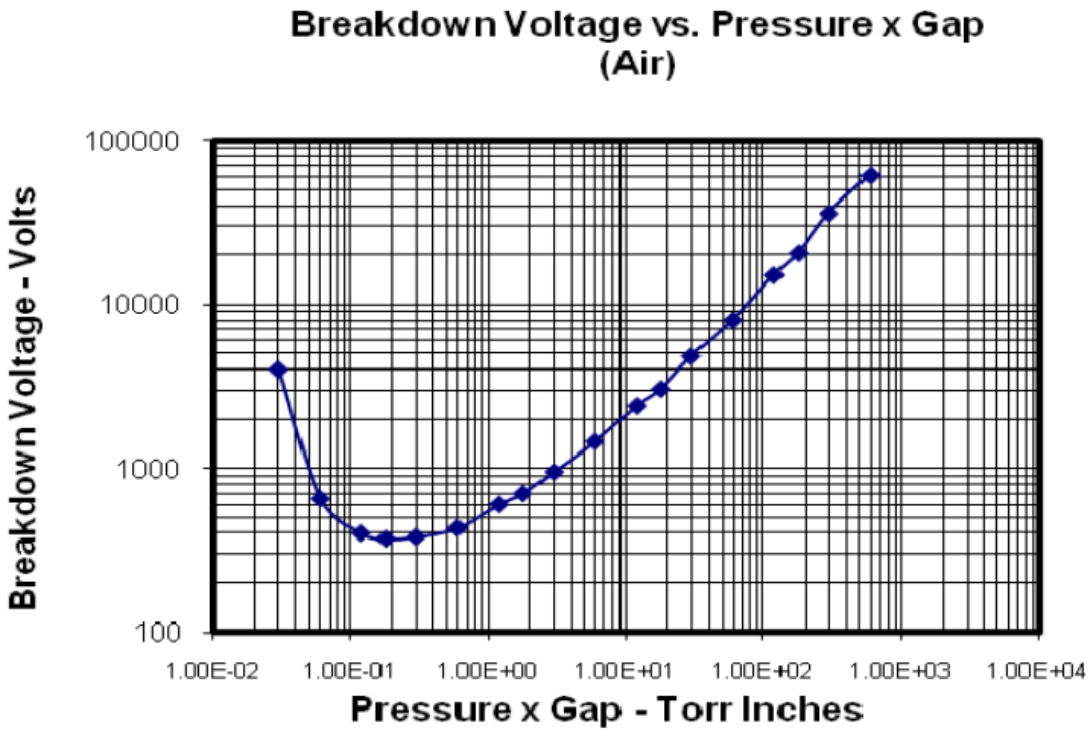

Figure 1-14 The Paschen's curve for air, two flat parallel copper electrodes, separated by 1 inch, for pressure between 3×10^{-2} torr and 760 torr. As the pressure is reduced below a torr (as shown in the diagram below) the curve of breakdown voltage versus pressure reaches a minimum, and then, as pressure is further reduced, rises steeply again.

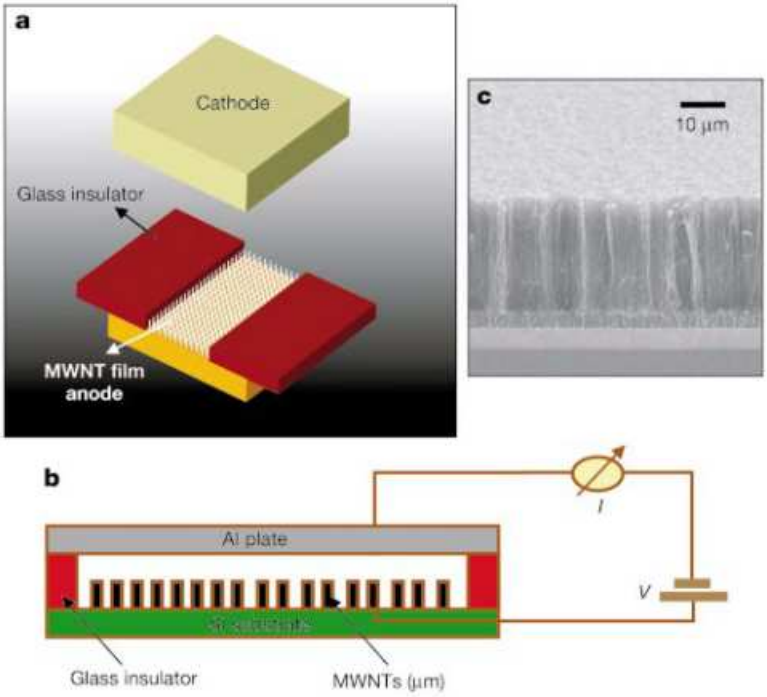

Figure 1-15 The carbon nanotubes gas ionization sensor proposed by Modi et al [4].

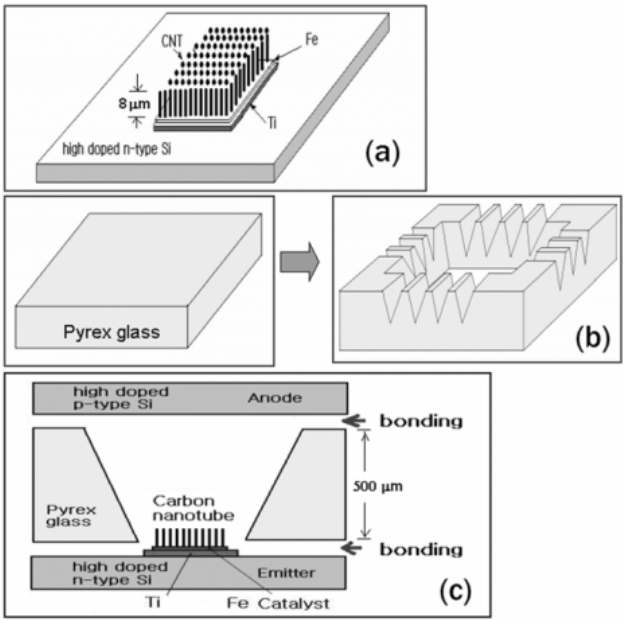

Figure 1-16 The carbon nanotubes gas ionization sensor proposed by S J Kim et al [50].

Chapter 2

==========

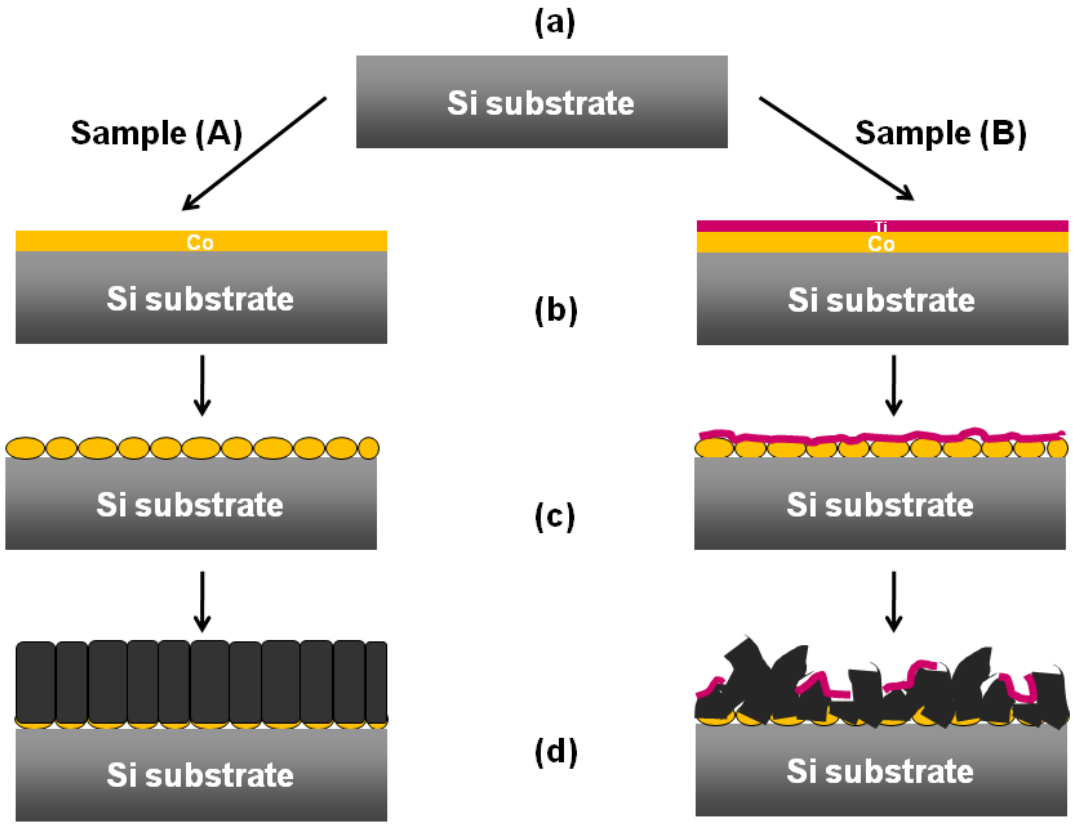

Figure 2-1 The schematic flowchart for the fabrication of the Uniform CNTs film and Random oriented CNTs film: (a) RCA clean process to remove contamination particles on the silicon substrate. (b)Deposition of a 4-nm-thick Co catalyst layer for sample (A) and 4-nm-thick Co catalyst layer along with 1-nm-thick Ti capping layer for sample (B). (c)Loading the samples into thermal CVD to be pretreated in hydrogen environment and forming Co nanoparticles, and (d) synthesizing CNTs in the thermal CVD. It's worth noting that the nonuniformity of Ti capping layer on the Co catalyst of sample (B) would limit the growth direction of CNTs and forming the random oriented CNTs film.

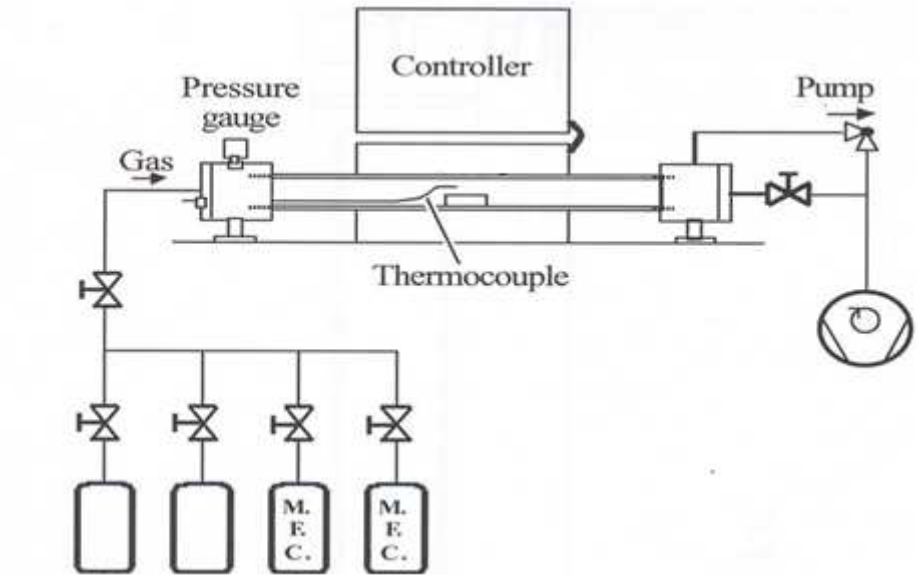

(a)

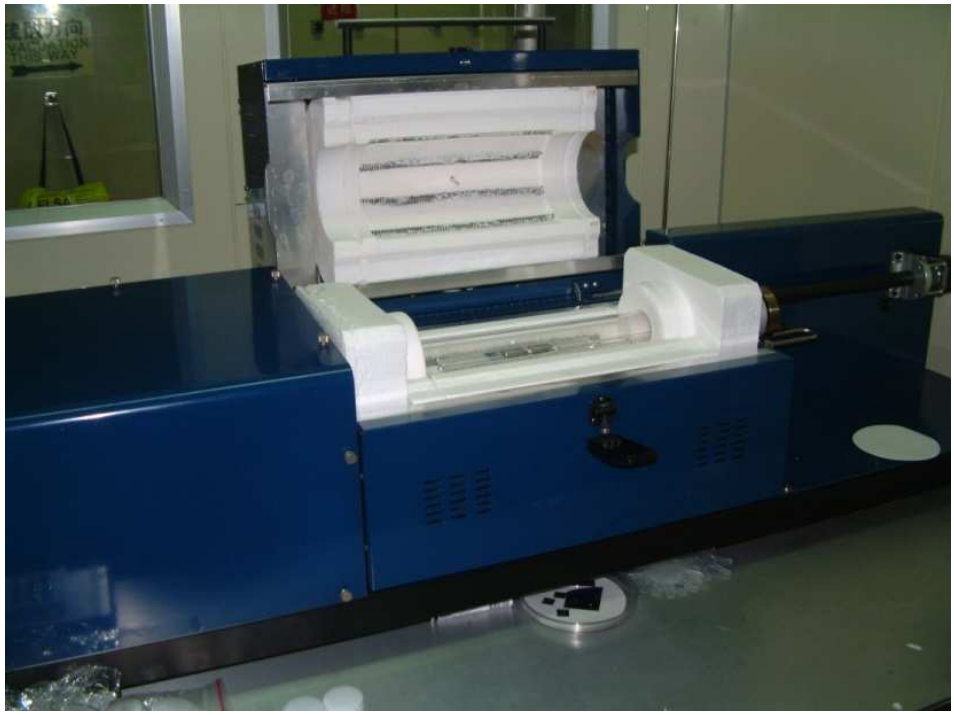

(b)

Figure 2-2 (a) Schematic picture and (b) photograph of thermal CVD. The process gases used here is hydrogen, nitrogen and ethylene.

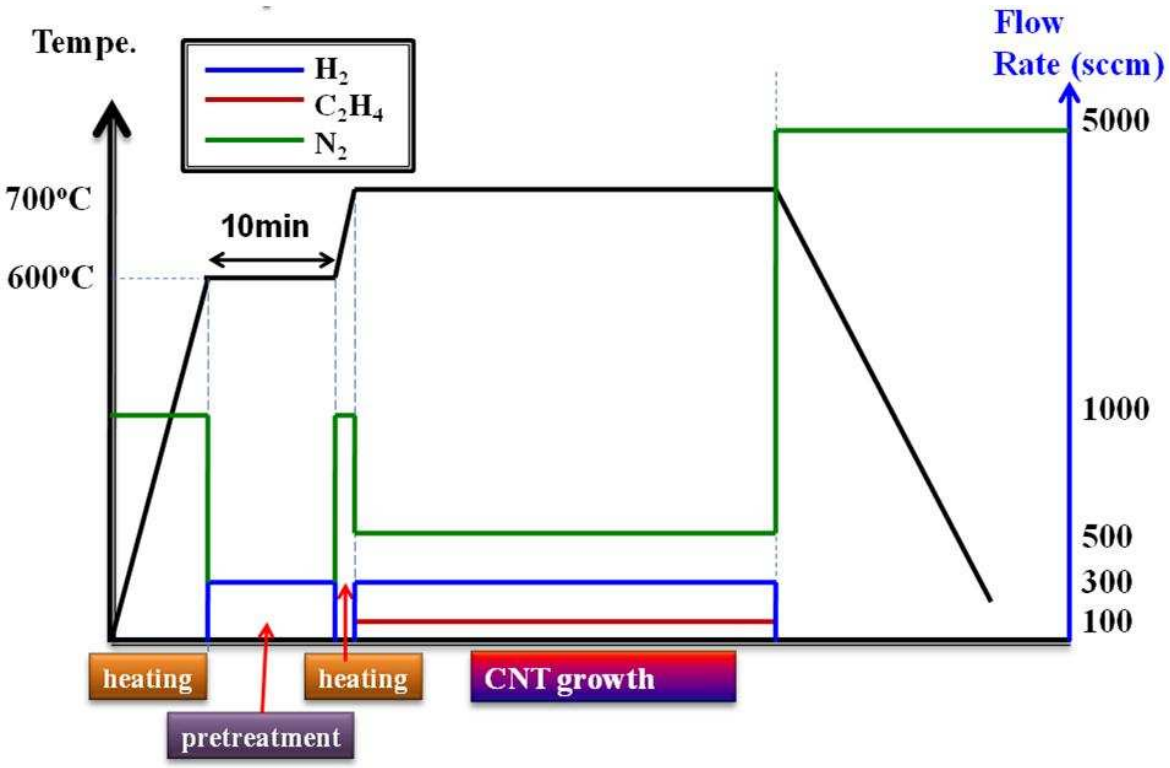

Figure 2-3 The process parameters to synthesize CNTs. At the start, samples would be heated to the predetermined temperature of 600℃ in a nitrogen flow rate of 1000 standard cubic centimeter per minute (sccm) for an oxygen-free ambience. Prior to the CNTs growth, hydrogen gas with a flow rate of 300 sccm was fed into the reaction tube for 10 min to reduce the catalyst metal to the metallic phase, meanwhile transforming into nanoparticles. After the pretreatment step, the chamber would be heated again under nitrogen flow rate of 1000sccm to 700℃. Then, CNTs were grown at this temperature with hydrogen, nitrogen and ethylene, at a flow rate of 300 sccm, 500 sccm and 100 sccm for designated growth time. After that, samples were furnace-cooled to room temperature in nitrogen flow rate of 5000 sccm to fully exhaust the reaction and byproduct gases.

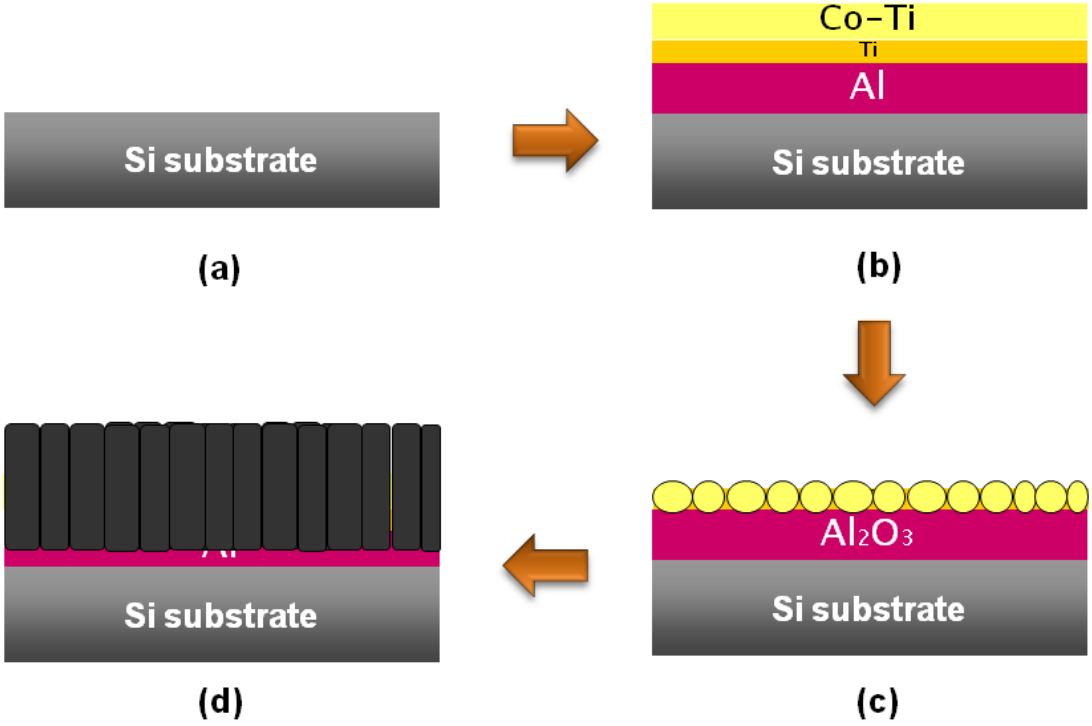

Figure 2-4 The schematic flowchart for the fabrication of CNTs-based film synthesized from the co-deposited catalyst. (a) At first, RCA clean process is used to remove contamination particles on the silicon substrate, and then (b) a 10-nm-thick aluminum supporting layer, a 1-nm-thick Titanium interlayer and a 4-nm-thick Co-Ti co-deposition layer were deposited sequentially. (c) Loading the samples into thermal CVD to be pretreated in hydrogen environment and forming nanoparticles, and (d) synthesizing CNTs in the thermal CVD.

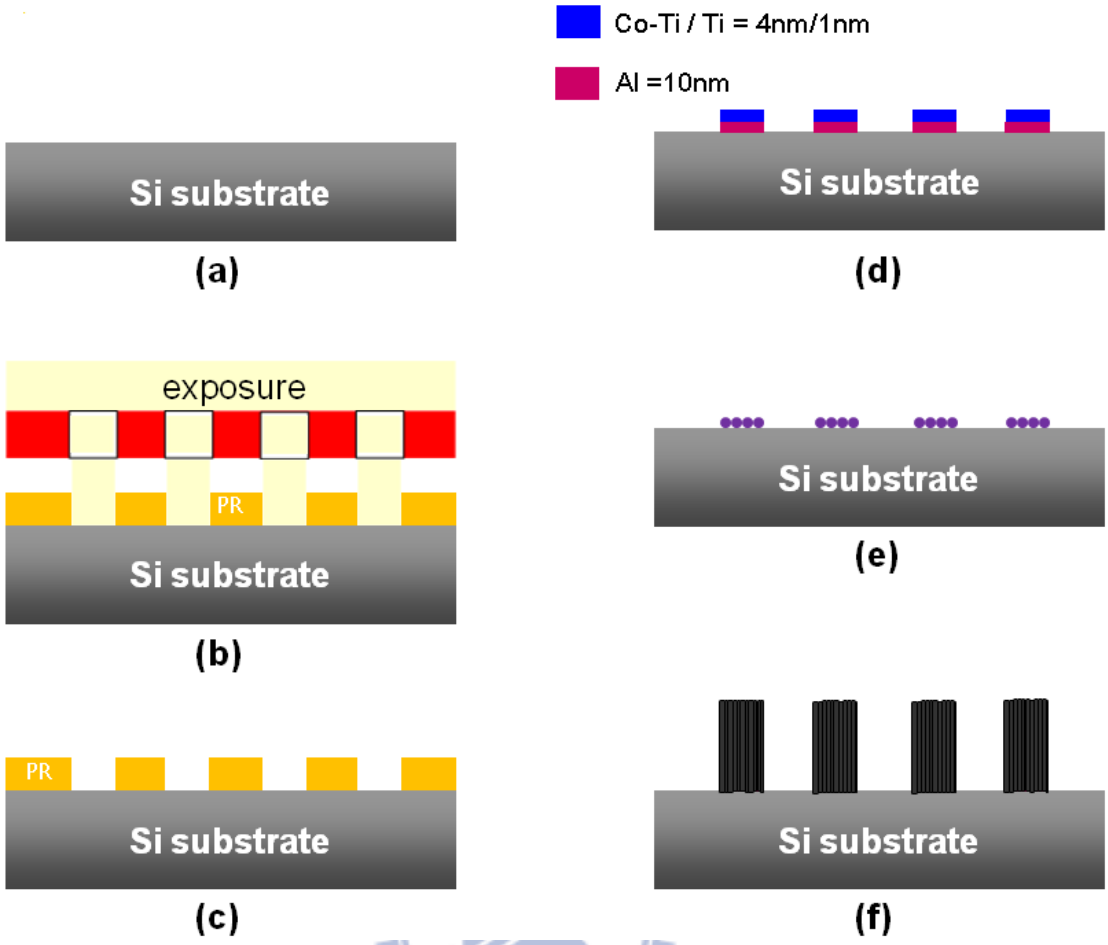

Figure 2-5 The schematic flowchart for the fabrication of pillar array of vertical aligned CNTs bundles using co-deposited catalyst structure. (a) Firstly, the RCA clean process is used to remove contamination particles on the silicon substrate. (b) Secondly, the substrate was coated with photoresist and then the exposure was executed under the mask, and immediately (c) the development of the patterns was followed. (d)Co-Ti (40 Å)/Ti(10 Å) /Al (100 Å) as catalyst structure were deposited by magnetron sputtering and the lift-off process was used to define our circle patterns. (e) Loading the samples into chamber to be pretreated in hydrogen environment and forming the nanoparticles, and (f) synthesizing CNTs in the thermal CVD processes.

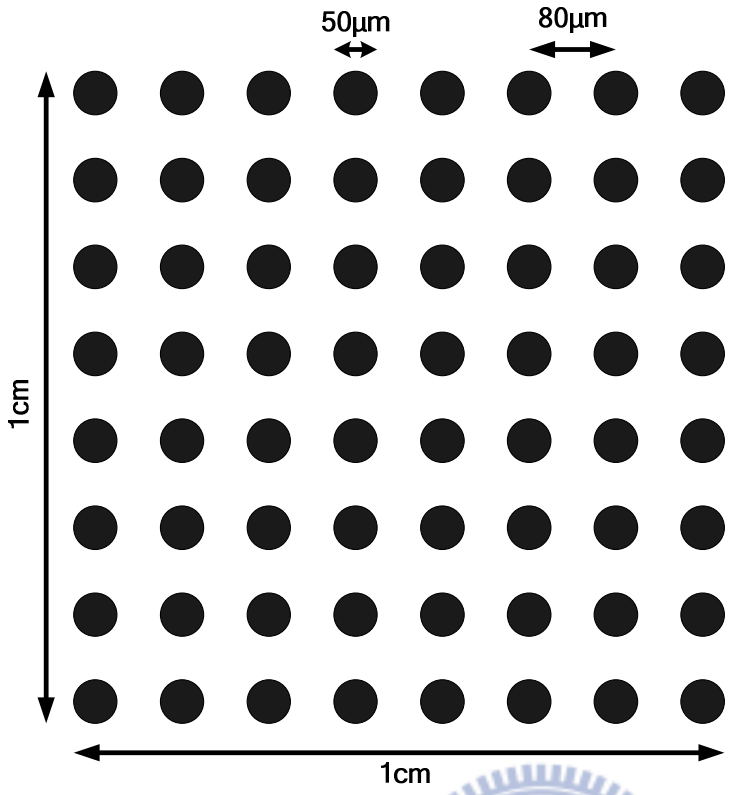

Figure 2-6 Mask design shows the array of 80μm in inter-pillar distance and 50μm in circle diameter defined in 1cm × 1 cm area.

Figure 2-7 The micrographs of samples were taken by scanning electron microscope (SEM, Hitachi S-4700I).

Figure 2-8 The high resolution transmission electron microscope (HRTEM; JEOL JEM-2000EX) was used to examine the structure of CNTs.

Figure 2-9 High resolution confocal Raman microscope (HOROBA, Lab RAM HR) was also applied to analyze the crystallinity of the CNTs.

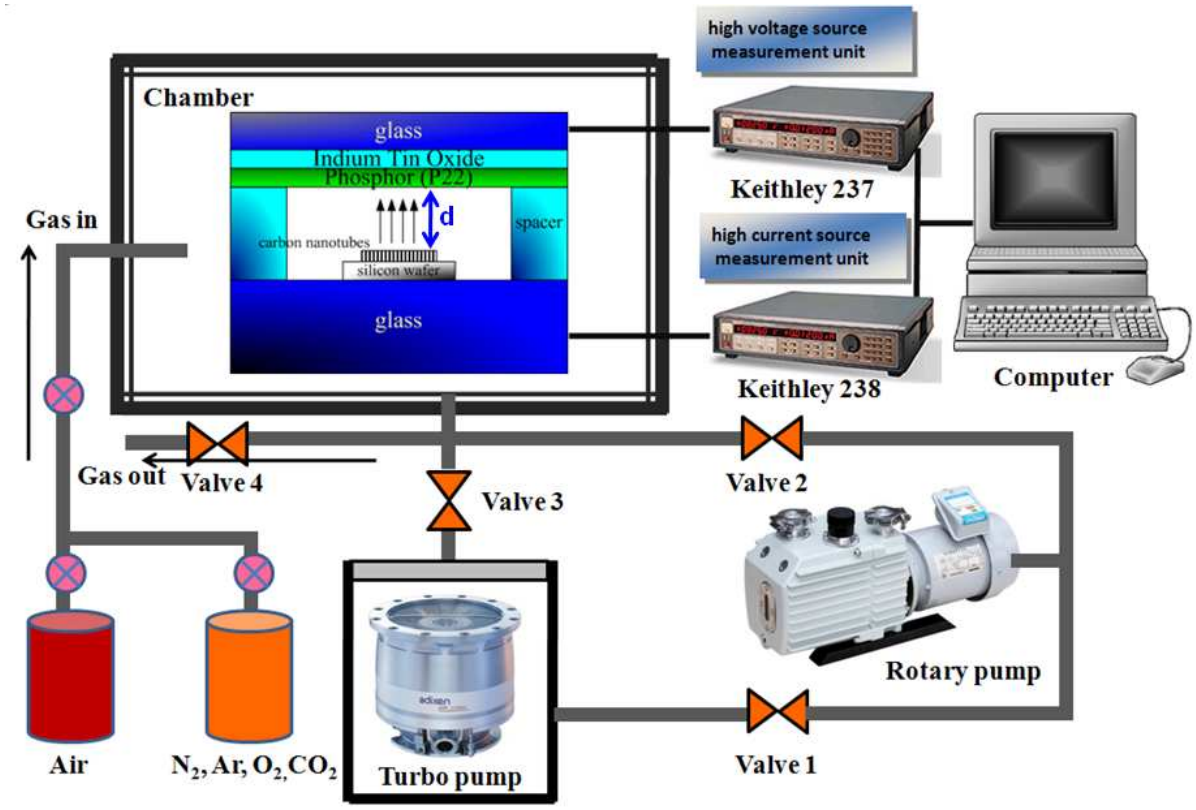

Figure 2-10 The gas ionization sensor measurement setups. The samples were put on a glass substrate with a spacer to control the distance between CNTs nanotips to the anode, and the anode was a glass coated with a indium-tin-oxide (ITO) film and green phosphor (P22). The samples were loaded into a vacuum chamber with anode applied to the high-voltage source measurement unit, Keithley 237, and the cathode applied to the high-current source measurement unit, Keithley 238, to measure the discharge current and the breakdown voltages of the samples.

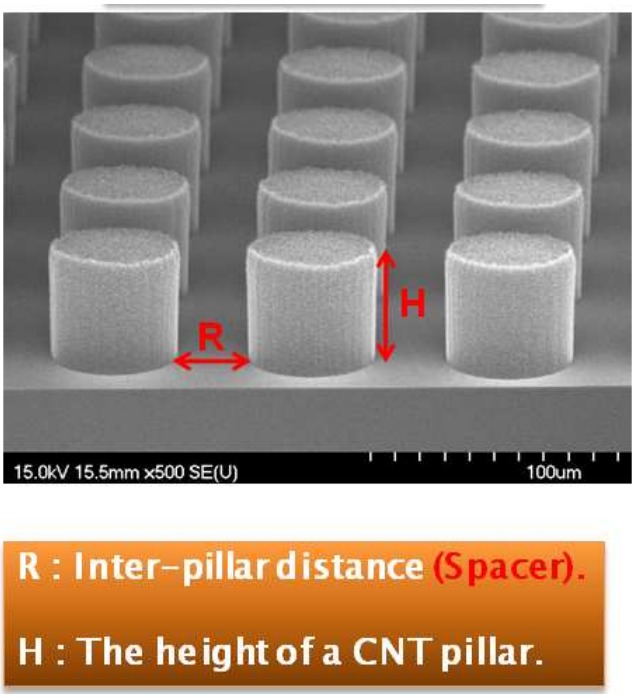

Figure 2-11 Definition of the R/H ratio, where R is the inter-pillar distance (spacer) and H is the height of a CNT pillar.

Chapter 3

==========

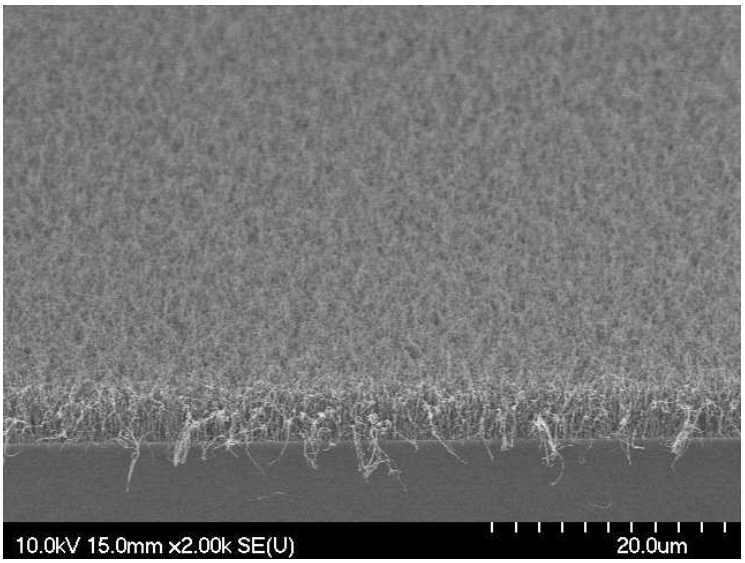

Figure 3-1 The pictures shown here was the tilted images (about 45°) taken by scanning electron microscope (SEM) for the Uniform CNTs film grown by thermal CVD.

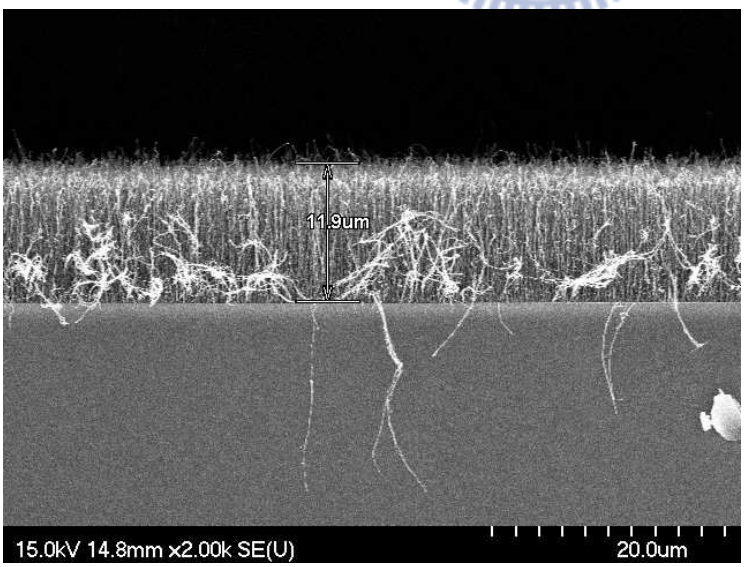

Figure 3-2 The pictures shown here was the cross-sectional image taken by SEM for the Uniform CNTs film grown by thermal CVD. The height of the vertical aligned CNTs is about 11.9μm.

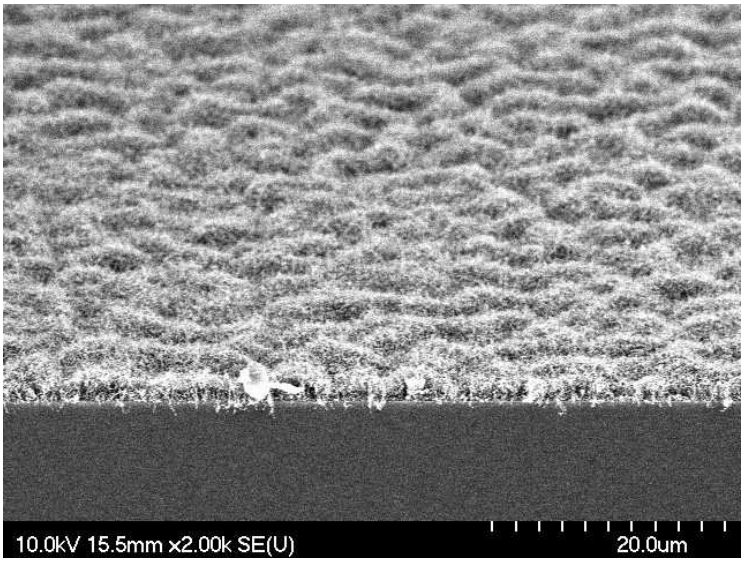

Figure 3-3 The pictures shown here was the tilted images (about 45°) taken by SEM for the Random oriented CNTs film grown by thermal CVD.

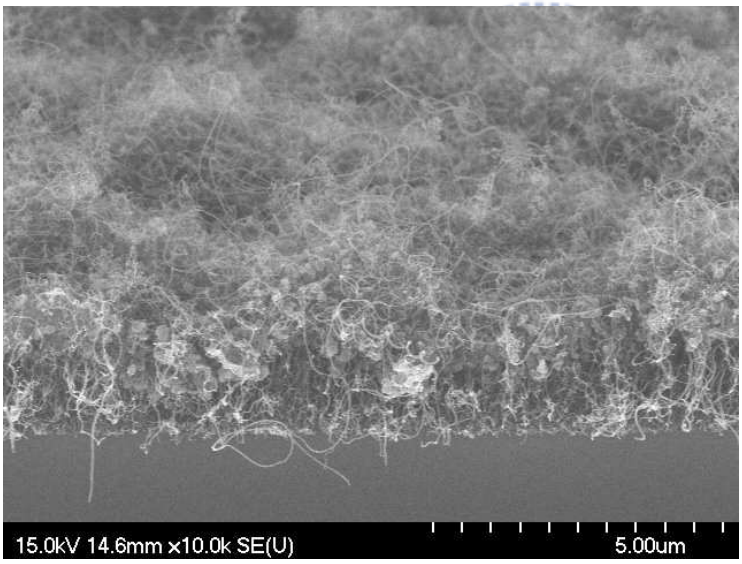

Figure 3-4 The pictures shown here was the magnified (10000 times) tilted images (about 45°) taken by SEM for the Random oriented CNTs film grown by thermal CVD. It could be seen obviously that the CNTs tangled together and the growth direction is rarely vertical.

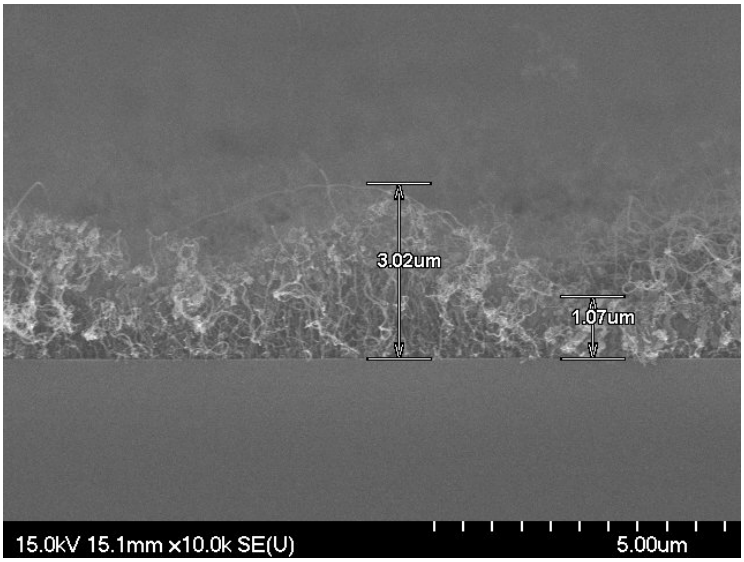

Figure 3-5 The pictures shown here was the cross-sectional image taken by SEM for the Random oriented CNTs film grown by thermal CVD. The height of the CNTs is quite nonuniform.

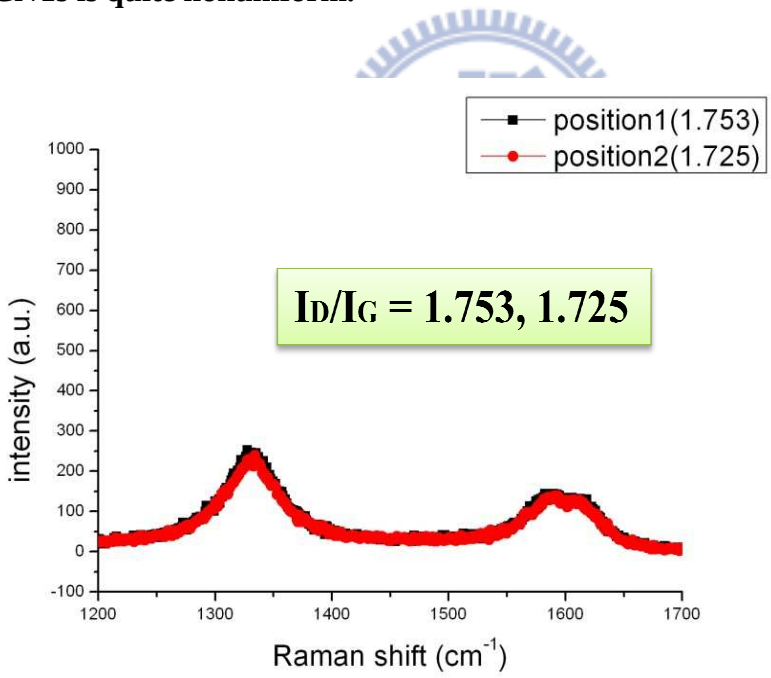

Figure 3-6 The Raman spectra analysis of the Uniform CNTs film and the *ID/IG* ratio which indicates the graphite crystallinity of the samples are 1.753 and 1.725.

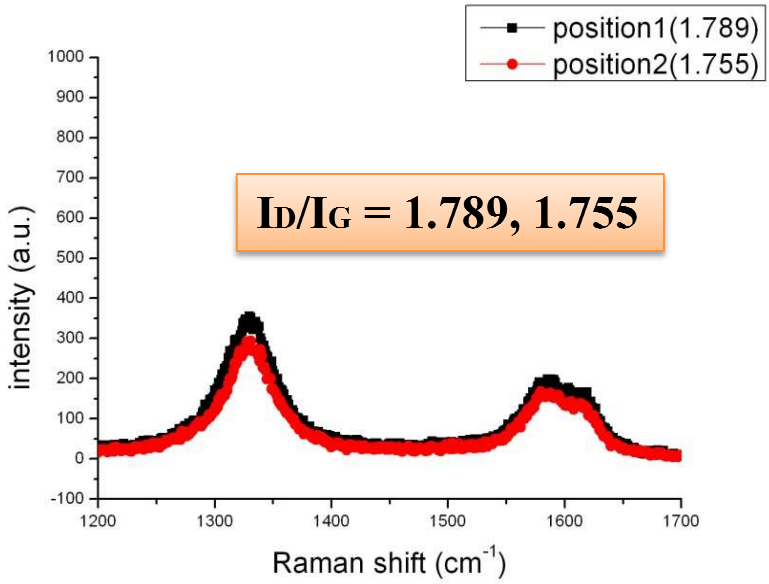

Figure 3-7 The Raman spectra analysis of the Random oriented CNTs film and the *ID/IG* ratio which indicates the graphite crystallinity of the samples are 1.789 and 1.755.

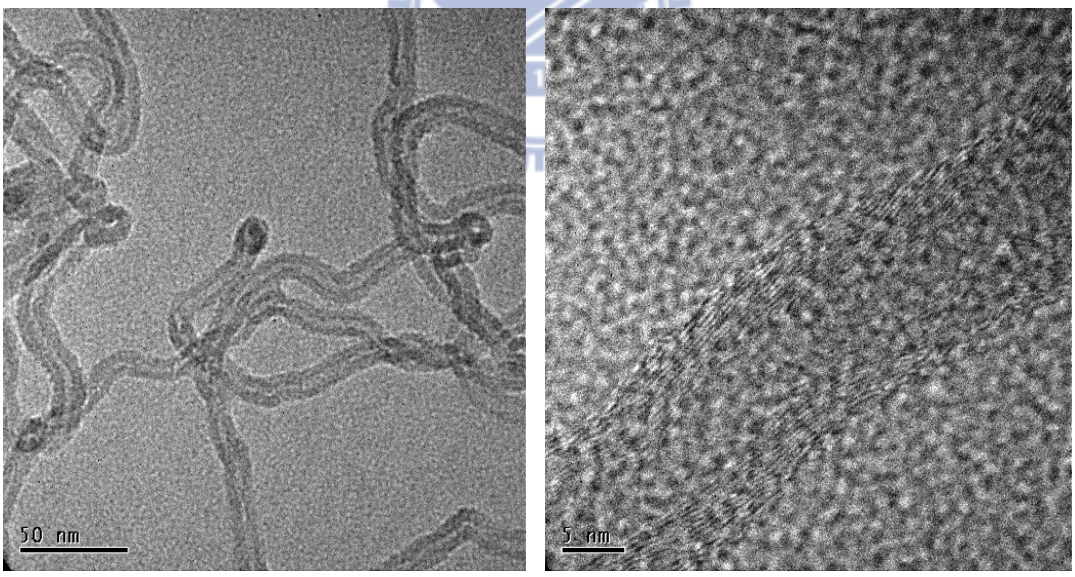

(a) **(b)**

Figure 3-8 (a)The micrographs of CNTs taken by transmission electron microscopy (TEM) obtained from the Uniform CNTs film and (b) their multiwalled structure can be found with higher resolution.

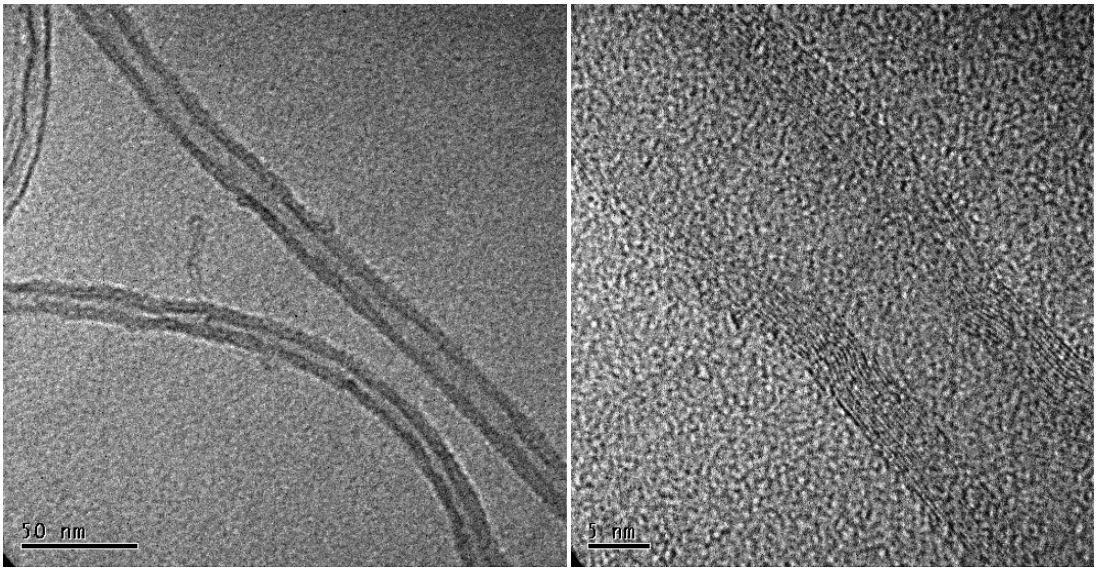

(a) **(b)**

Figure 3-9 (a)The micrographs of CNTs taken by TEM obtained from the Random oriented CNTs film and (b) their multiwalled structure can also be found with higher resolution.

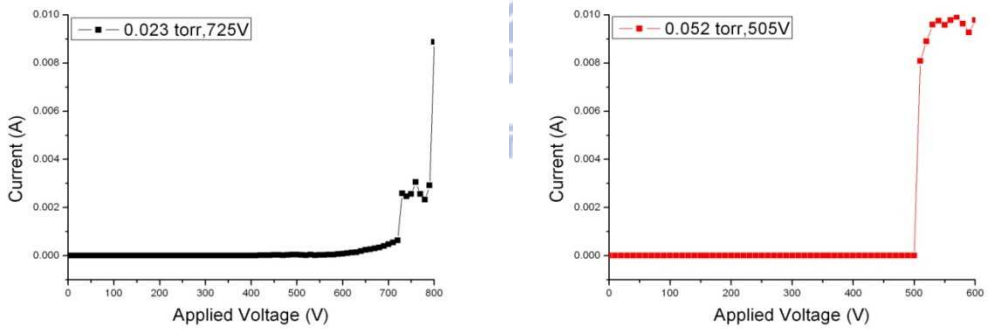

(a) **(b)**

Figure 3-10 The gas breakdown characteristics of the Radom oriented CNTs film under different gas pressures in the nitrogen environment. The pressures are (a) 0.0023 torr, (b) 0.0052 torr, (c) 0.079 torr, (d) 0.1 torr, (e) 0.2 torr, (f) 0.51 torr, (g) 0.8 torr, (h) 1.0 torr, (i) 2.1 torr and (j) 5.1 torr. They are integrated into (k).

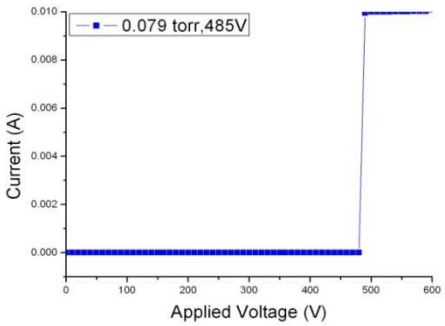

(b)

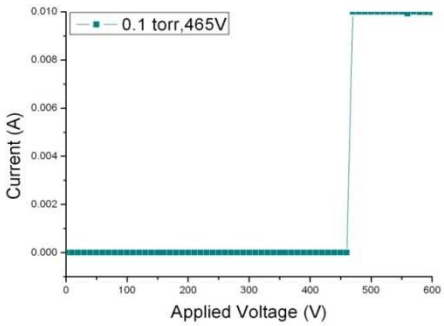

(d)

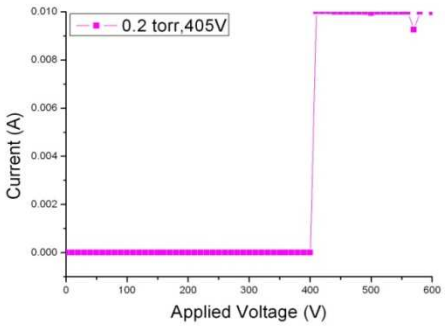

(e)

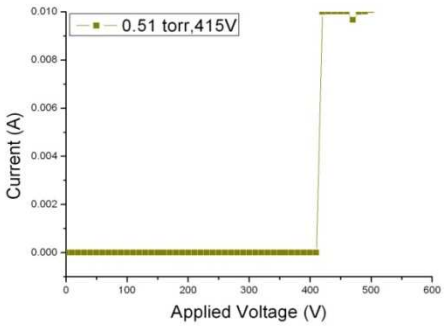

(f)

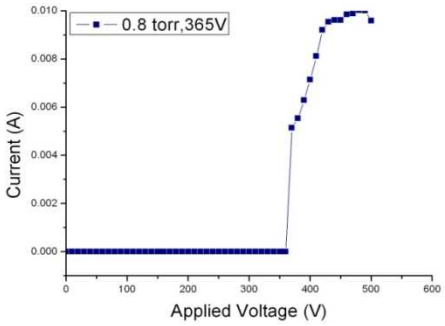

(g)

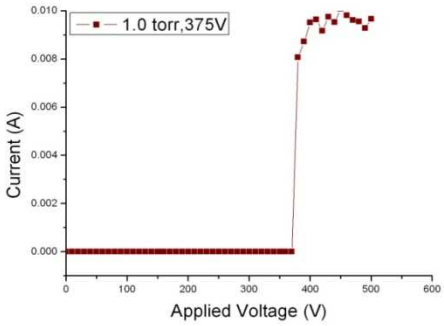

(h)

Figure 3-10 (cont.).

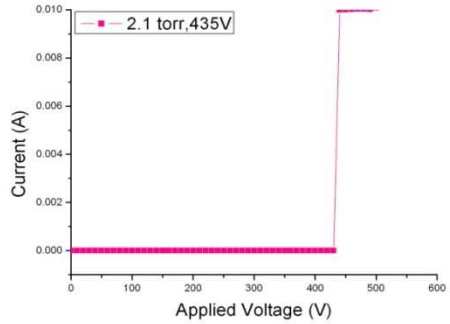

(i)

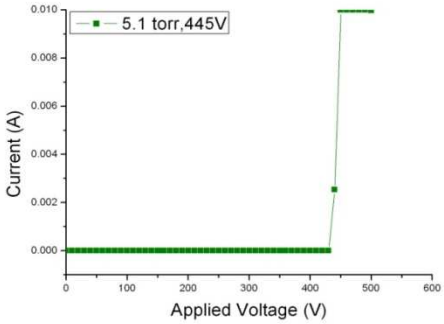

(j)

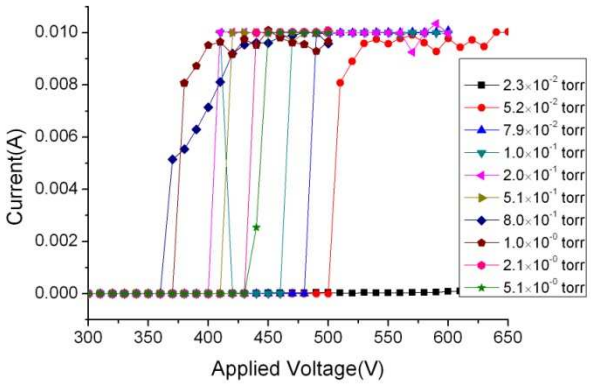

(k)

Figure 3-10 (cont.).

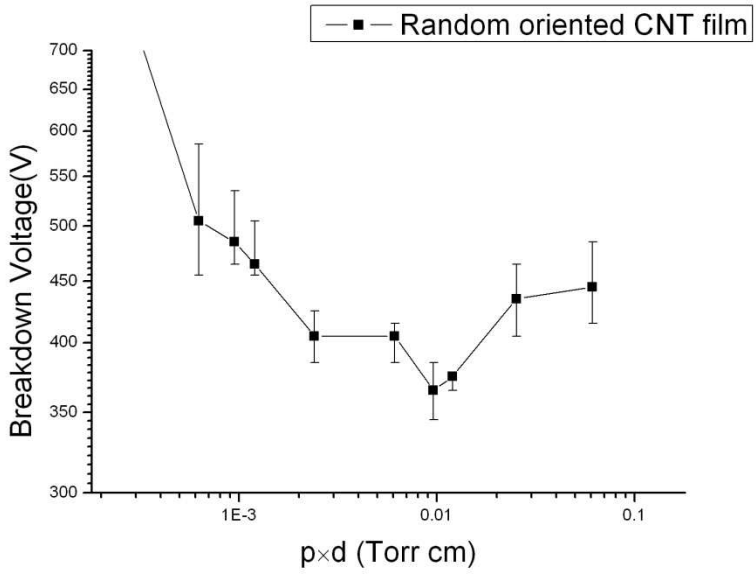

Figure 3-11 Breakdown voltages vs. p×d characteristics of the Random oriented CNTs film under nitrogen environment (Paschen's curve). It's apparently that the variations of the breakdown voltages are especially large at high voltage region and these variations are referred to the nonuniformity of the CNTs' length. For those longer CNT, the difference of electrical field is larger, which leads to higher electron emission efficiency. Therefore, their breakdown voltages are lower.

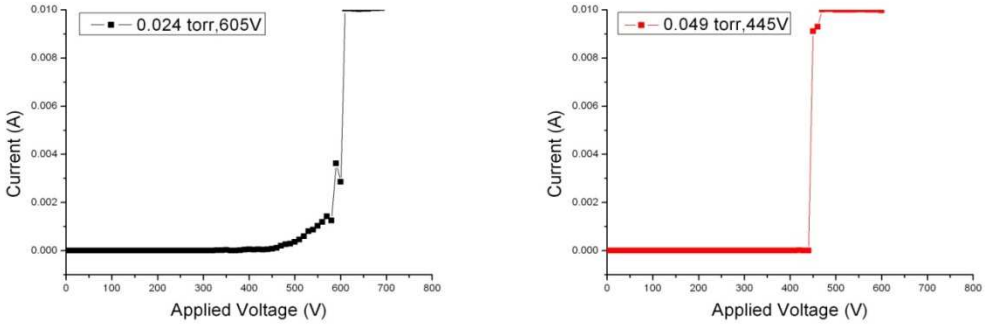

(a) **(b)**

Figure 3-12 The gas breakdown characteristics of the Uniform CNTs film under different gas pressures in the nitrogen environment. The pressures are (a) 0.0024torr, (b) 0.0049torr, (c) 0.078torr, (d) 0.1 torr, (e) 0.21torr, (f) 0.51 torr, (g) 0.82torr, (h) 1.0 torr, (i) 2.0torr and (j) 4.9torr. They are integrated into (k).

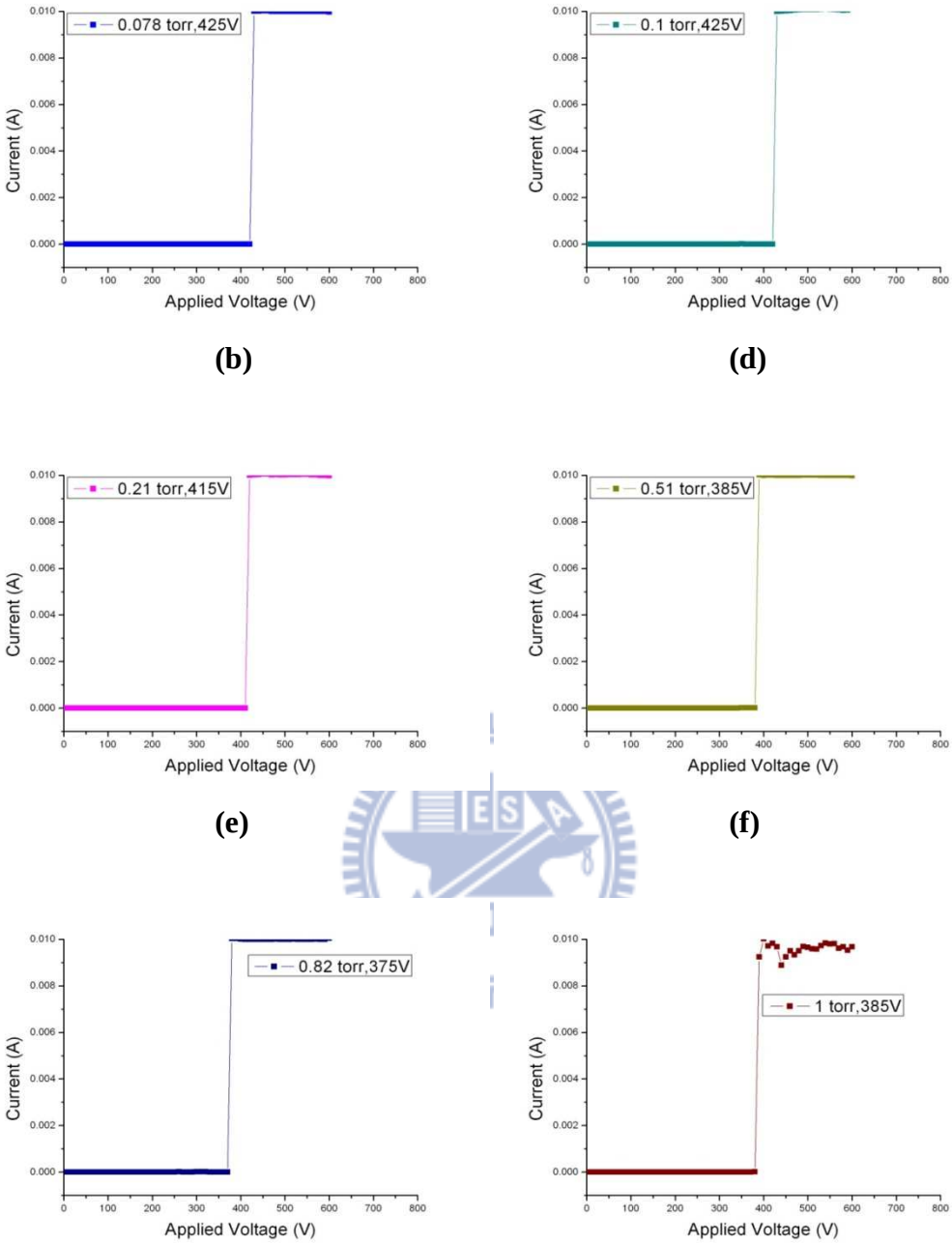

Figure 3-12 (cont.).

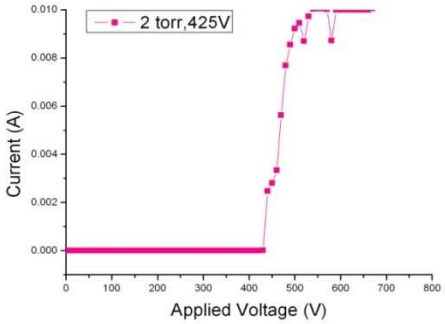

(i)

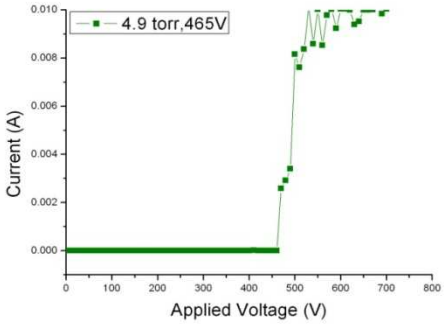

(j)

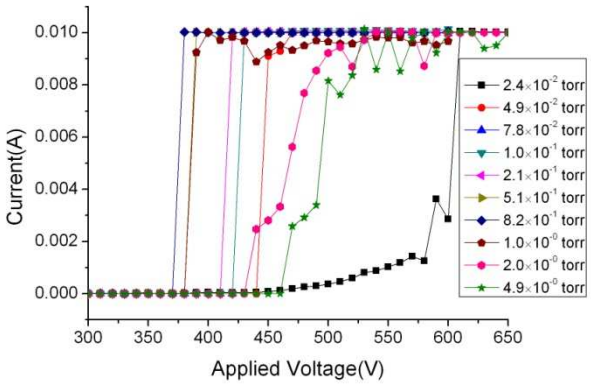

(k)

Figure 3-12 (cont.).

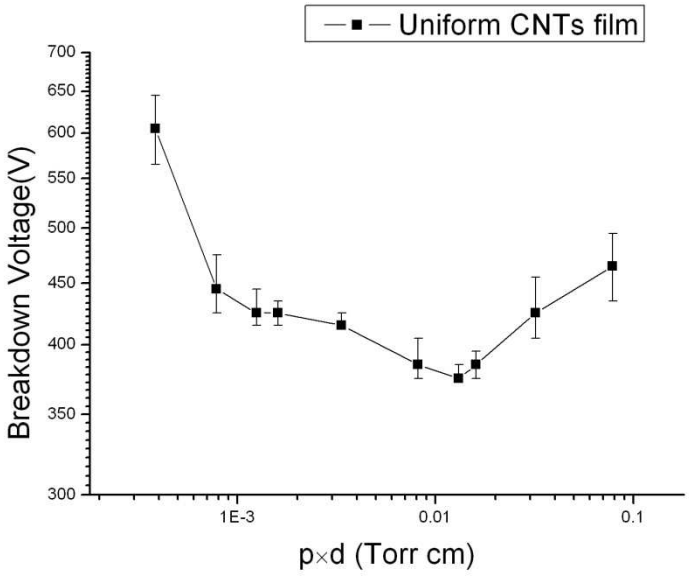

Figure 3-13 Breakdown voltages vs. p×d characteristics of the Uniform CNTs film under nitrogen environment (Paschen's curve). It's apparently that the variations of the breakdown voltages are smaller than the Random oriented CNTs film. It was referred to the uniformity of the CNTs' length of the Uniform CNTs film.

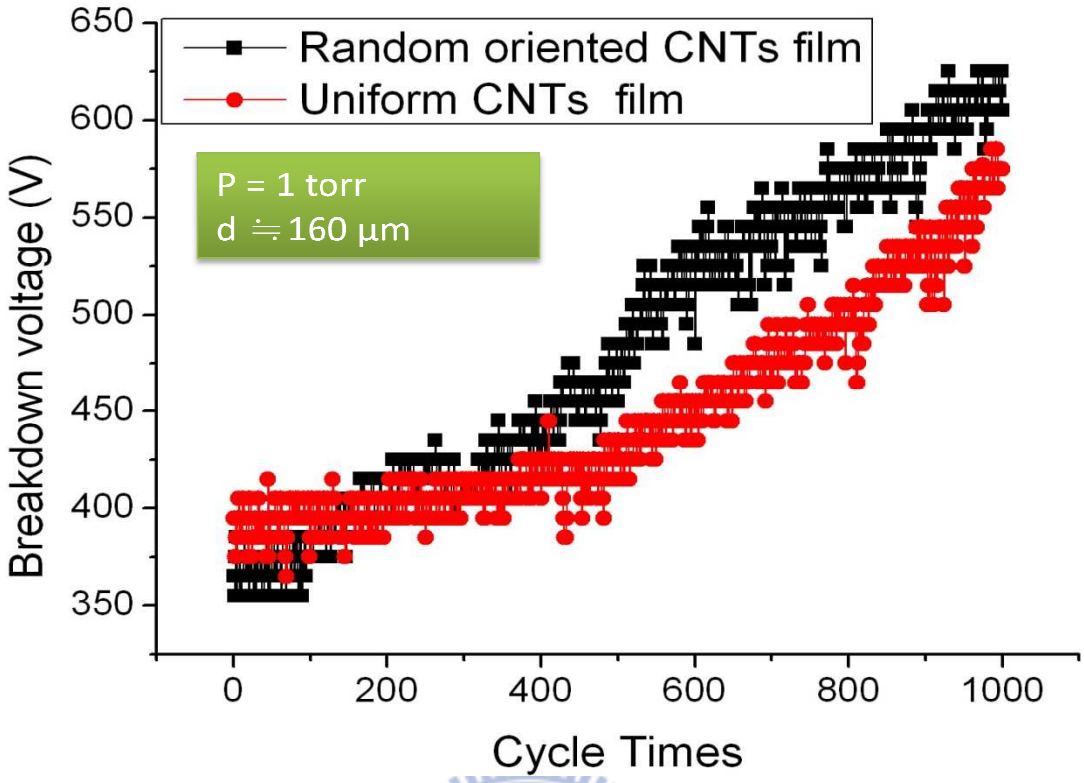

Figure 3-14 The stability test of gas breakdown characteristics under nitrogen environment with the Random oriented CNTs film and the Uniform CNTs film. The V_{br} of the Random oriented CNTs film lifts up from 365V to 605V after 1000 cycles, 68% in increase. And for the Uniform CNTs film, it lifts up from 395V to 575V after 1000 cycles, 46% in increase.

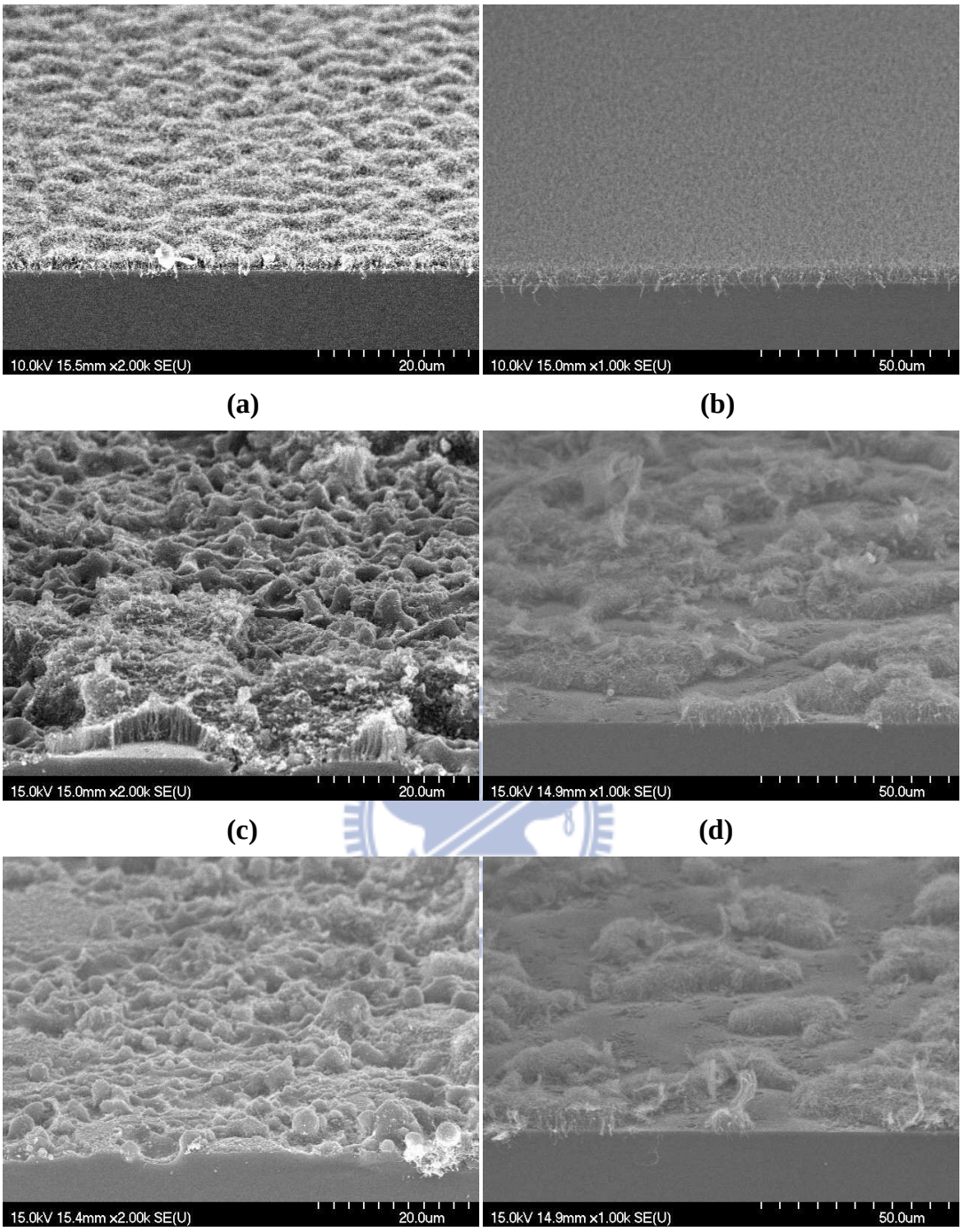

Figure 3-15 The SEM images before and after stability tests: (a), (c) and (d) are the images of the Random oriented CNTs film before stability test, after 500 cycles stability tests and after 1000 cycles stability tests. And (b), (d) and (f) are the images of the Uniform CNTs film before stability test, after 500 cycles stability tests and after 1000 cycles stability tests.

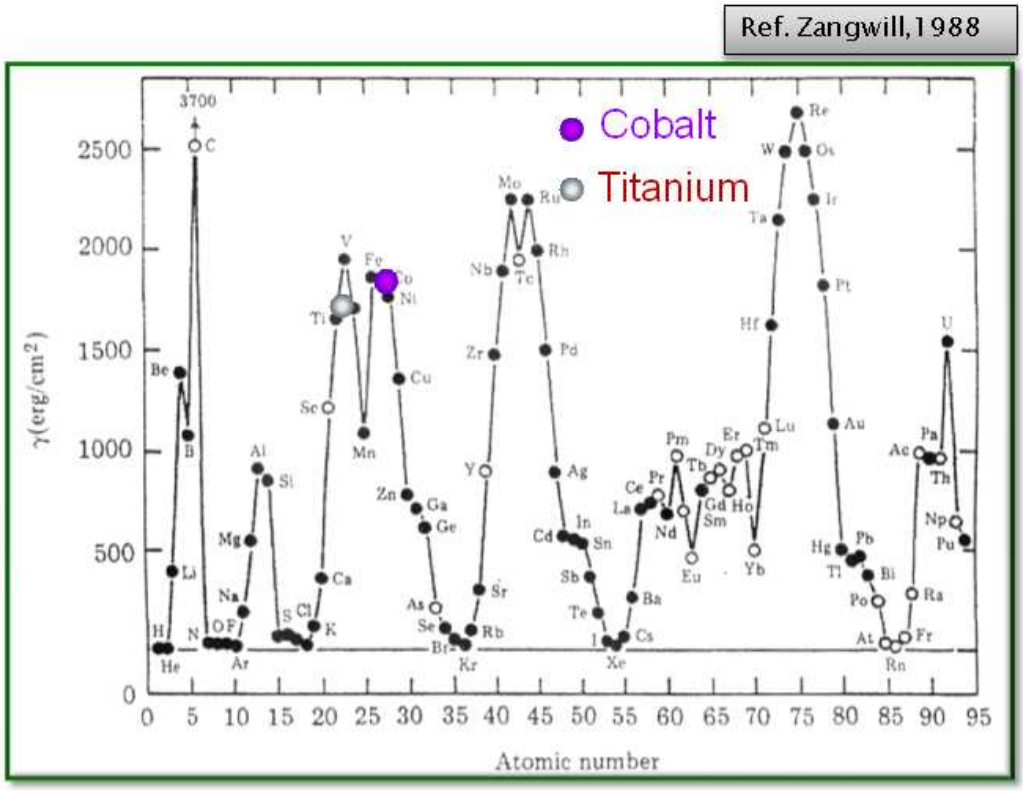

Figure 3-16 The various surface energy of different metals, where one can find that the surface energy of cobalt is familiar with that of titanium.

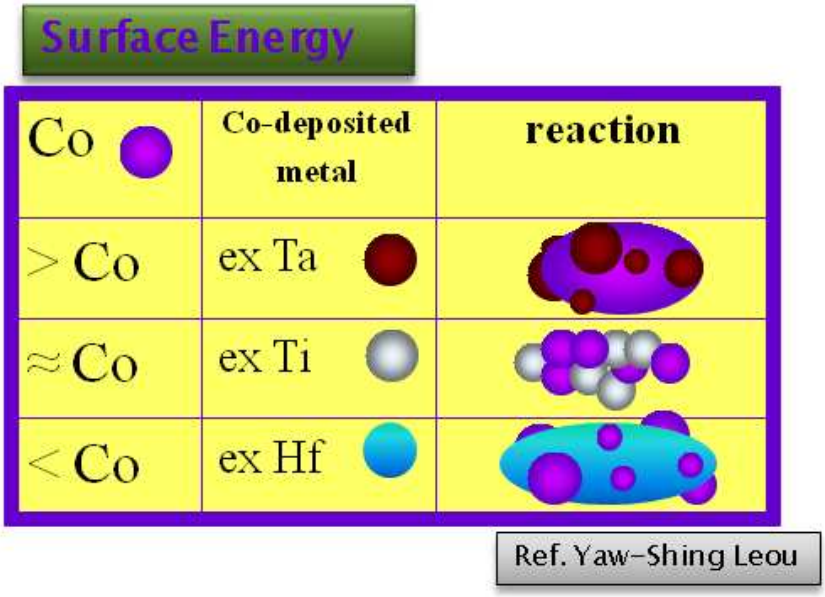

Figure 3-17 The diagram of different surface energy metals reacting with Cobalt as they coalescence into nanoparticles.

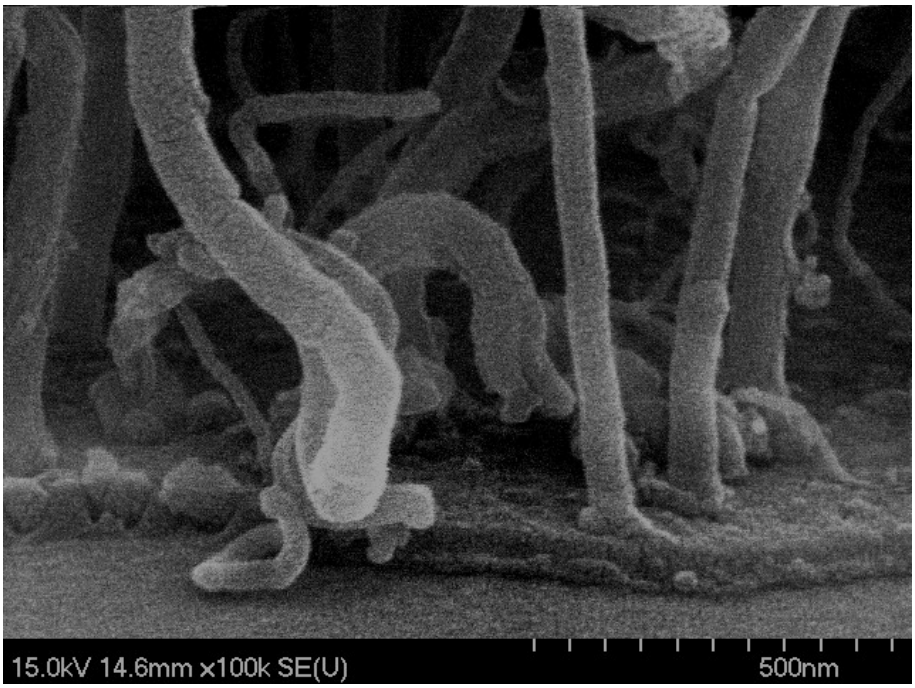

(a)

Figure 3-18 The images of SEM displayed the roots of the CNTs for both (a) the conventional samples without co-deposited catalyst and (b) the proposed samples with co-deposited catalyst. The proposed samples were cleaved across the patterned area and a CNT immersed partially into the co-deposited metal layer on the cleaved edge was marked by a circle in (c).

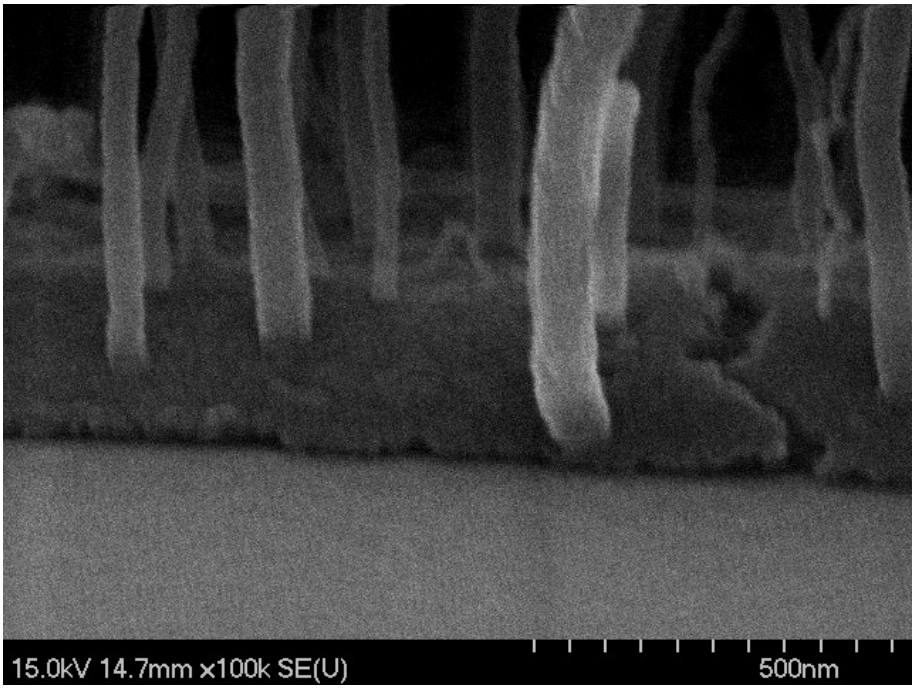

(b)

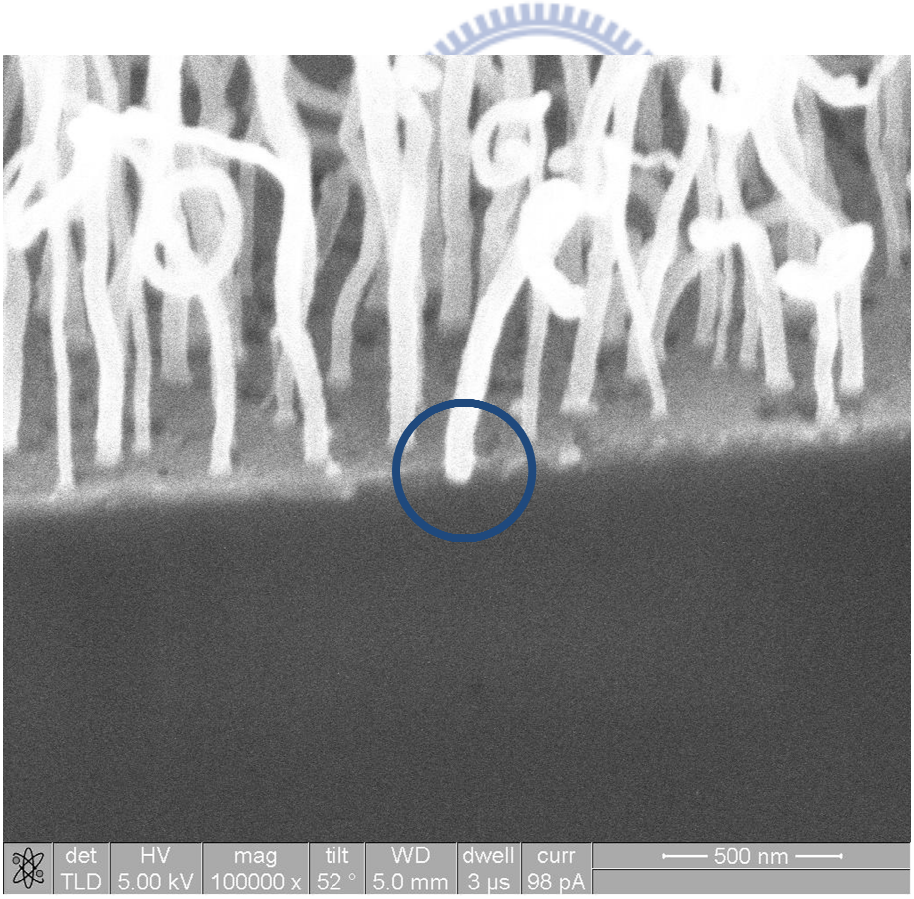

(c)

Figure 3-18 (cont.).

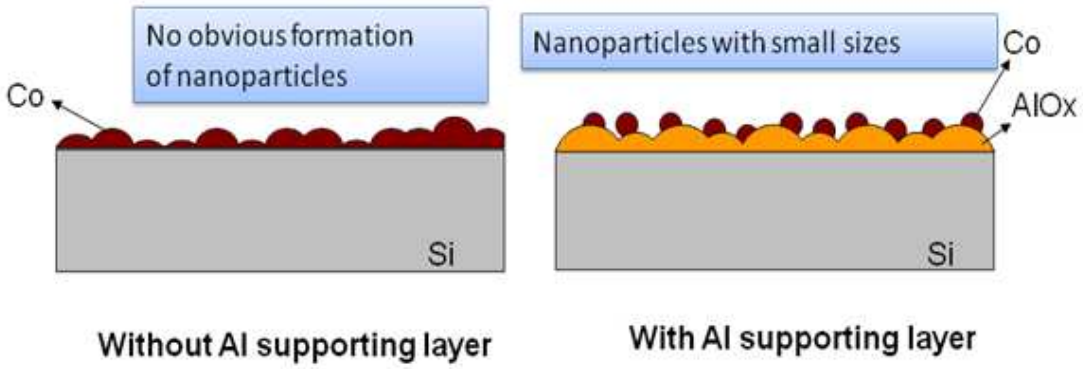

(a) **(b)**

Figure 3-19 The catalyst after pretreatment in reducing gas environment: (a) without Al supporting layer and (b) with Al supporting layer, where nanoparticles with small sizes could be achieved with Al supporting layer.

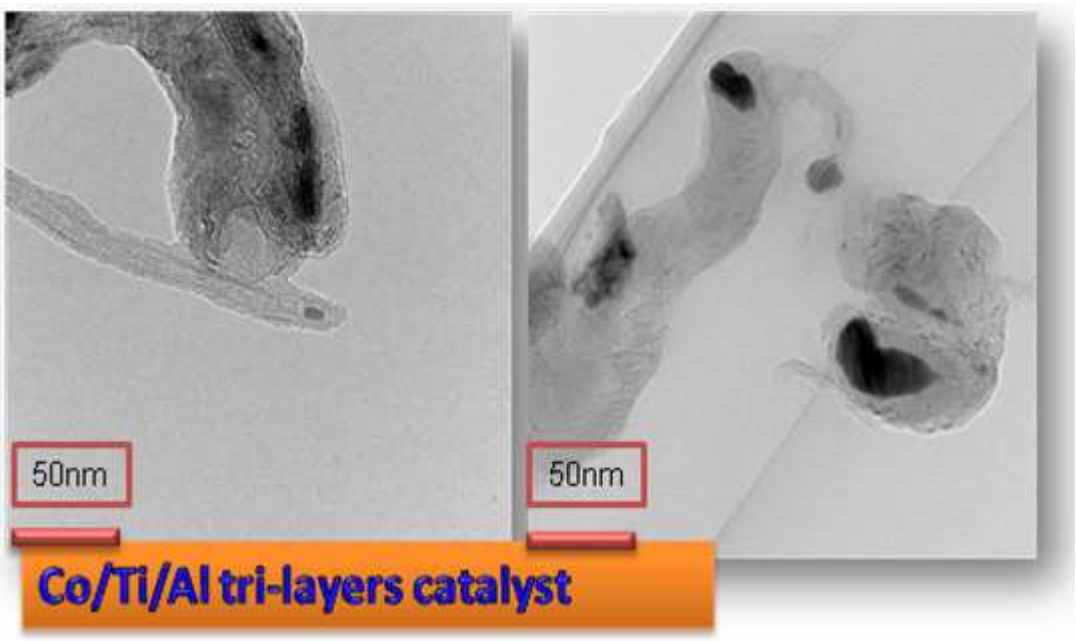

(a)

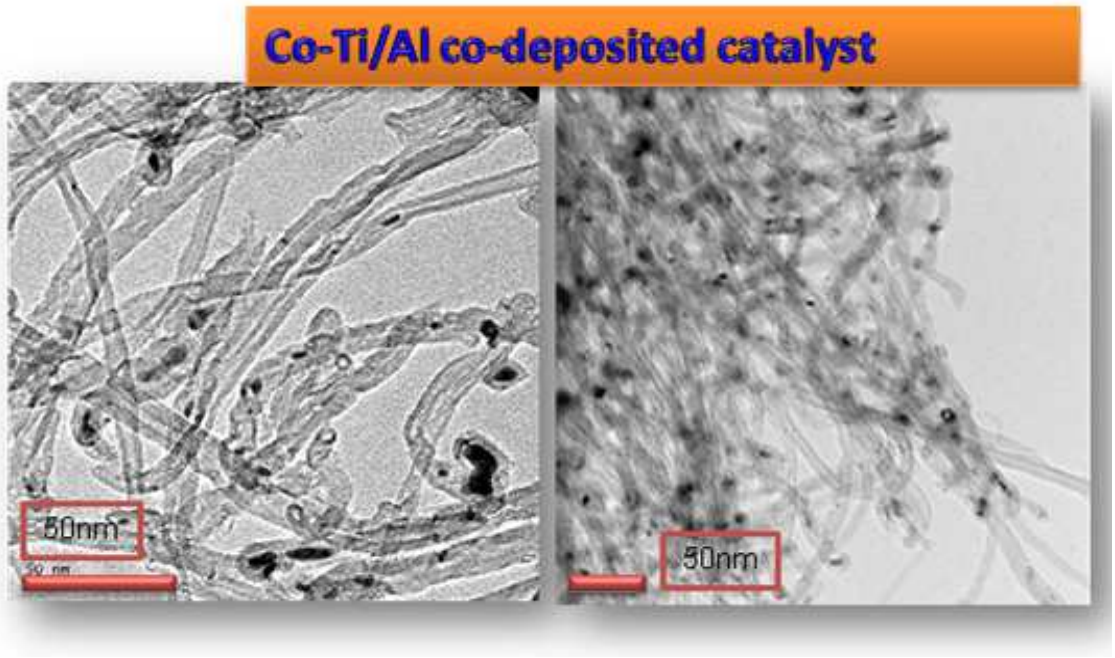

(b)

Figure 3-20 The Transmission Electron Microscopy (TEM) images of (a) using Co/Ti/Al catalyst structure and (b) using Co-Ti/Al co-deposited catalyst structure. It's obvious that the diameter of CNTs becomes smaller by using co-deposited catalyst structure.

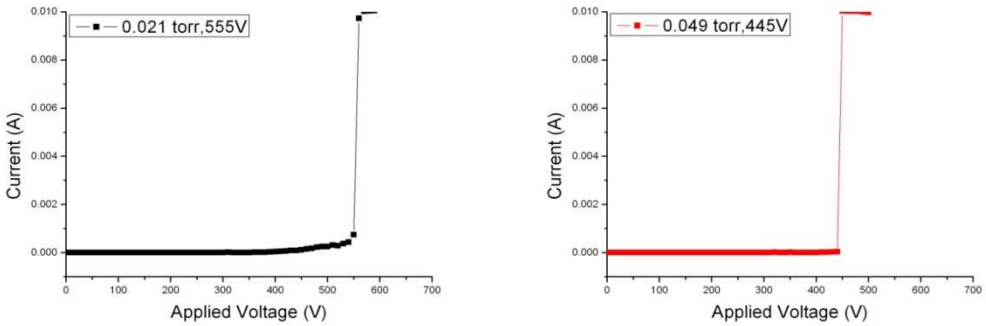

(a)

(b)

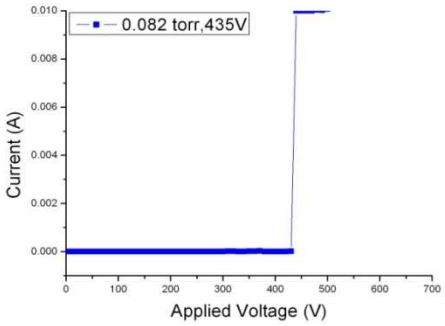

(c)

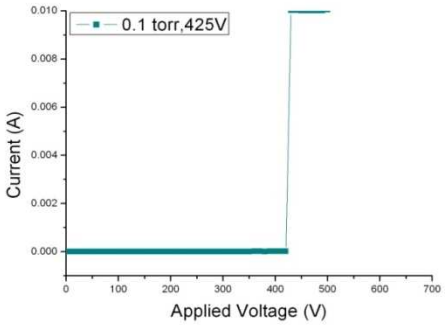

(d)

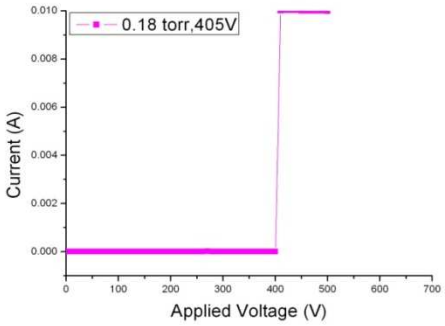

(e)

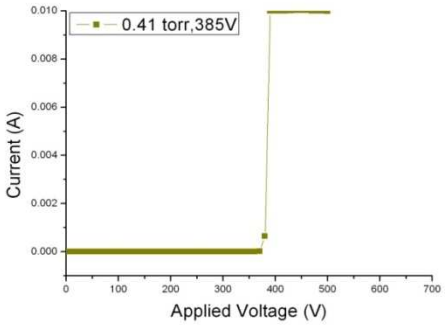

(f)

Figure 3-21 The gas breakdown characteristics of the CNTs-based film synthesized from the co-deposited catalyst structure under different gas pressures in the nitrogen environment. The pressures are (a) 0.0021 torr, (b) 0.0049 torr, (c) 0.082 torr, (d) 0.1 torr, (e) 0.18 torr, (f) 0.41 torr, (g) 0.8 torr, (h) 1.0 torr, (i) 2.1 torr and (j) 5.3 torr. The above is integrated into (k).

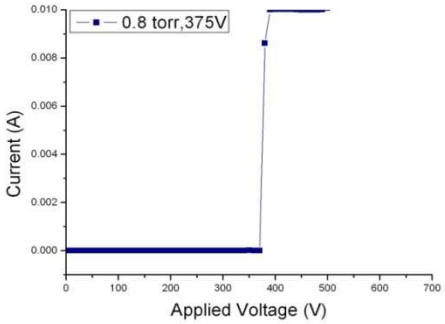

(g)

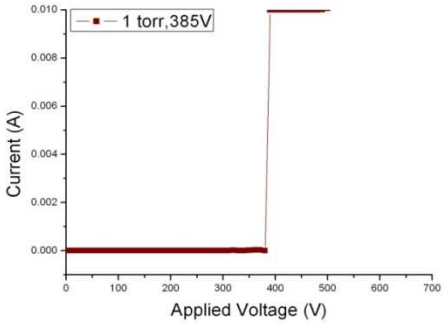

(h)

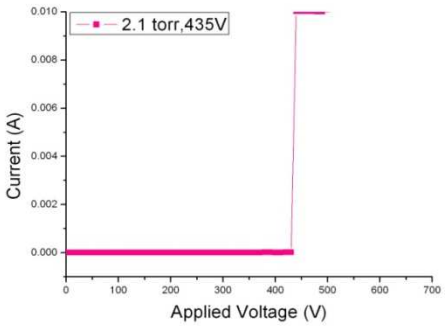

(i)

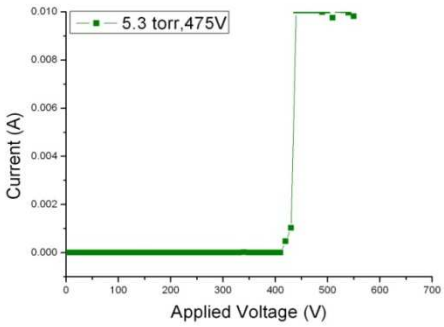

(j)

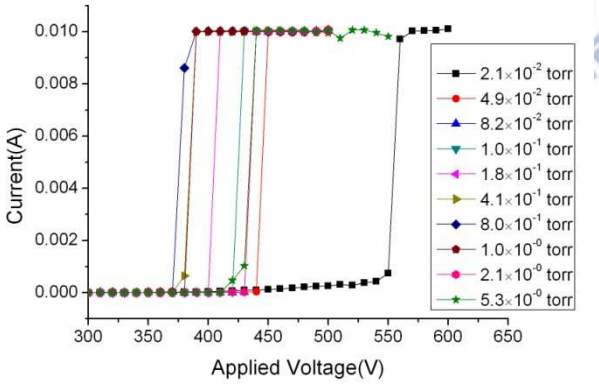

(k)

Figure 3-21 (cont.).

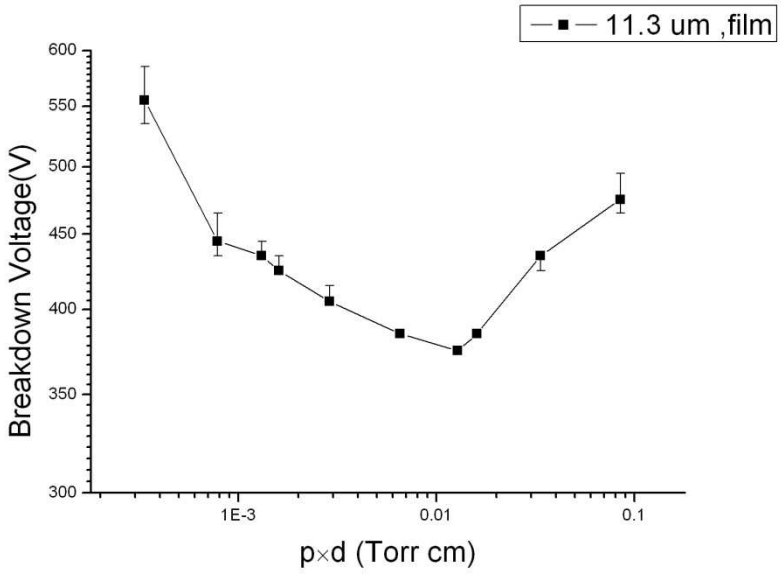

Figure 3-22 Breakdown voltages versus p×d characteristics of the CNTs-based film synthesized from the co-deposited catalyst structure under nitrogen environment (Paschen's curve). The variations of the breakdown voltages were improved obviously, which was related to the improvement of adhesion and contact resistance via the catalyst co-deposition.

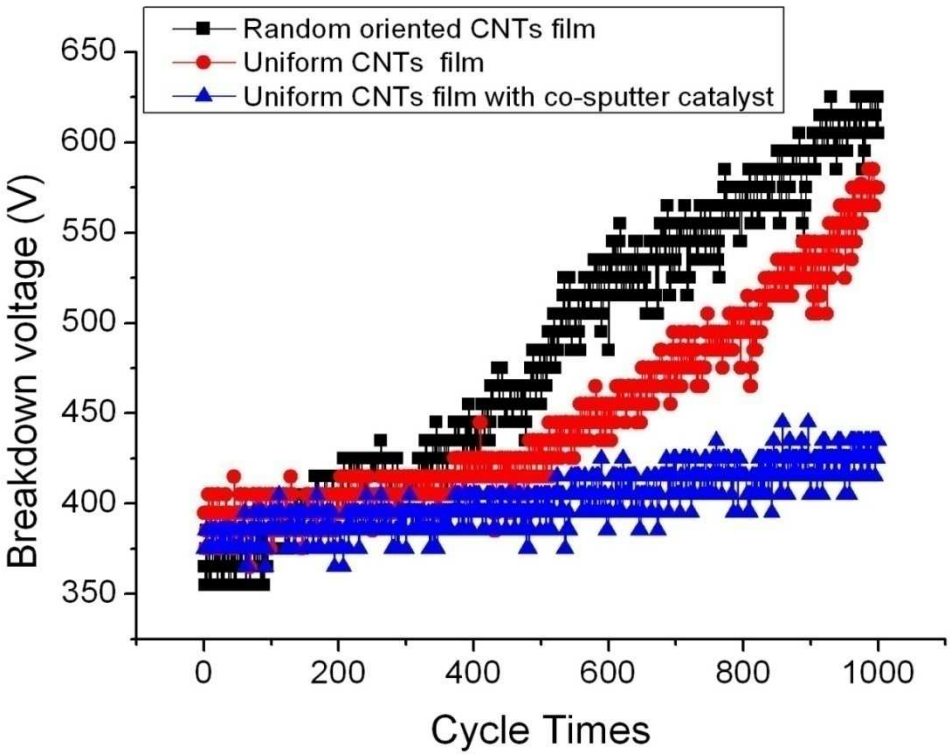

Figure 3-23 The stability test of gas breakdown characteristics under nitrogen environment with the Random oriented CNTs film, the Uniform CNTs film and the CNTs film with co-sputter catalyst. One can find that the Vbr of the CNTs film synthesized from Co-Ti co-deposited catalyst structure lifts up from 375V to 435V after 1000 cycles, 16% in increase, which is further improved than the first two CNTs film.

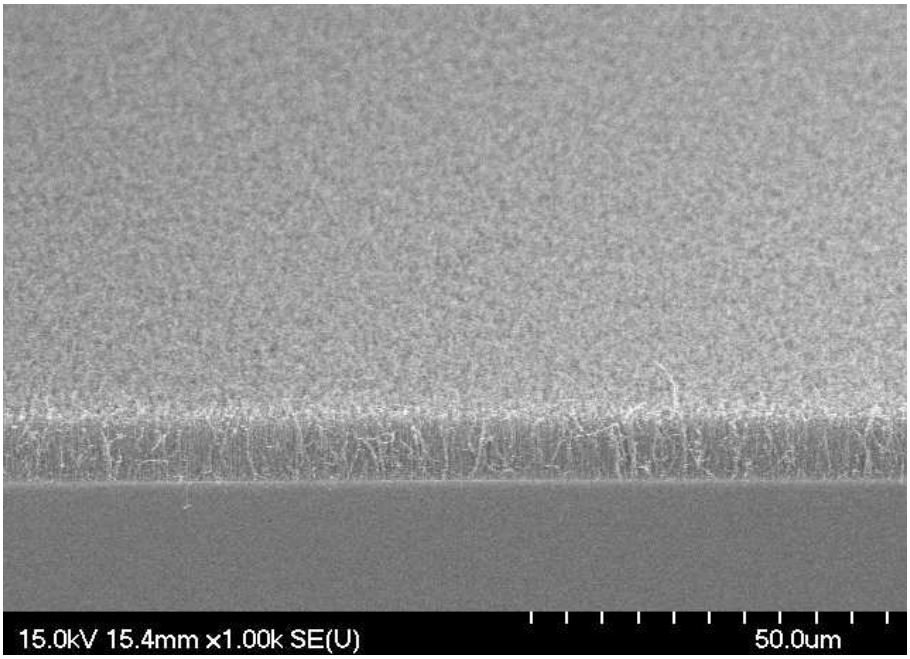

(a)

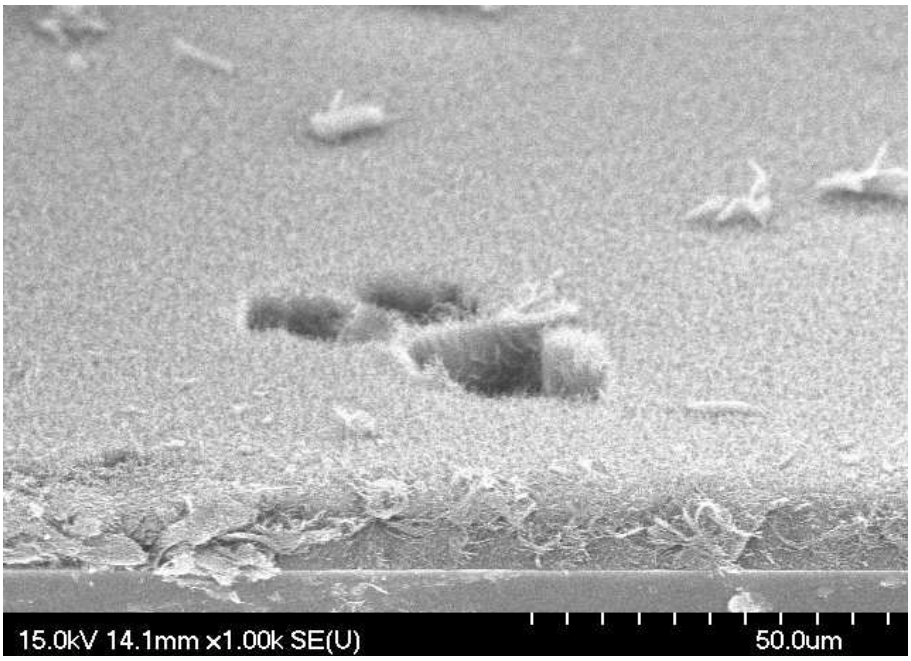

(b)

Figure 3-24 The SEM images before and after stability tests: (a), (b) and (c) are the images of the CNTs film synthesized from Co-Ti co-deposited catalyst structure before stability test, after 500 cycles stability tests and after 1000 cycles stability tests, respectively. The pull-off and evaporation of CNTs were not as serious as the conventional two samples, which are associated to the improvement of adhesion and contact resistance via the catalyst co-deposition.

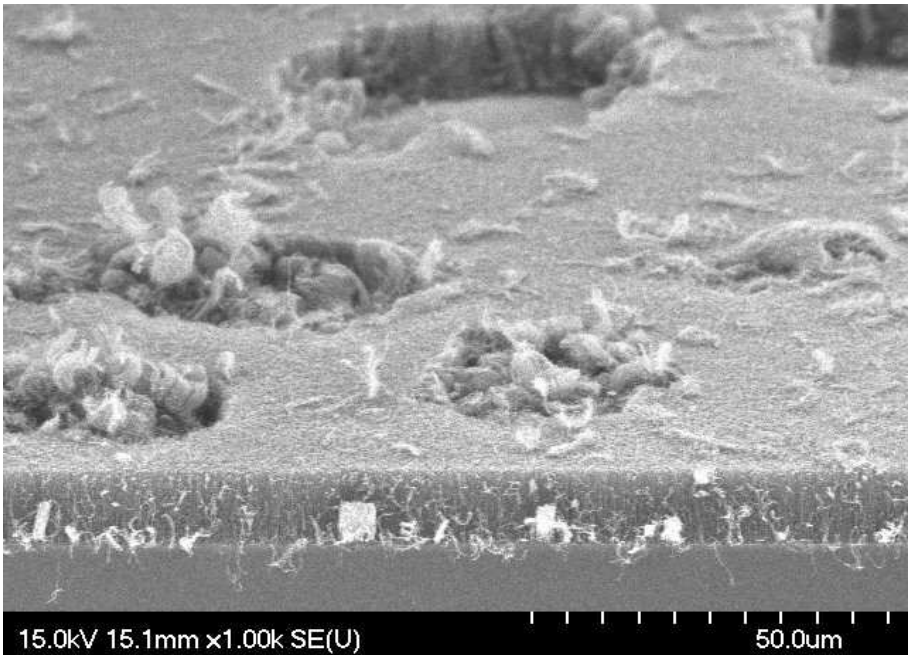

(c)

Figure 3-24 (cont.).

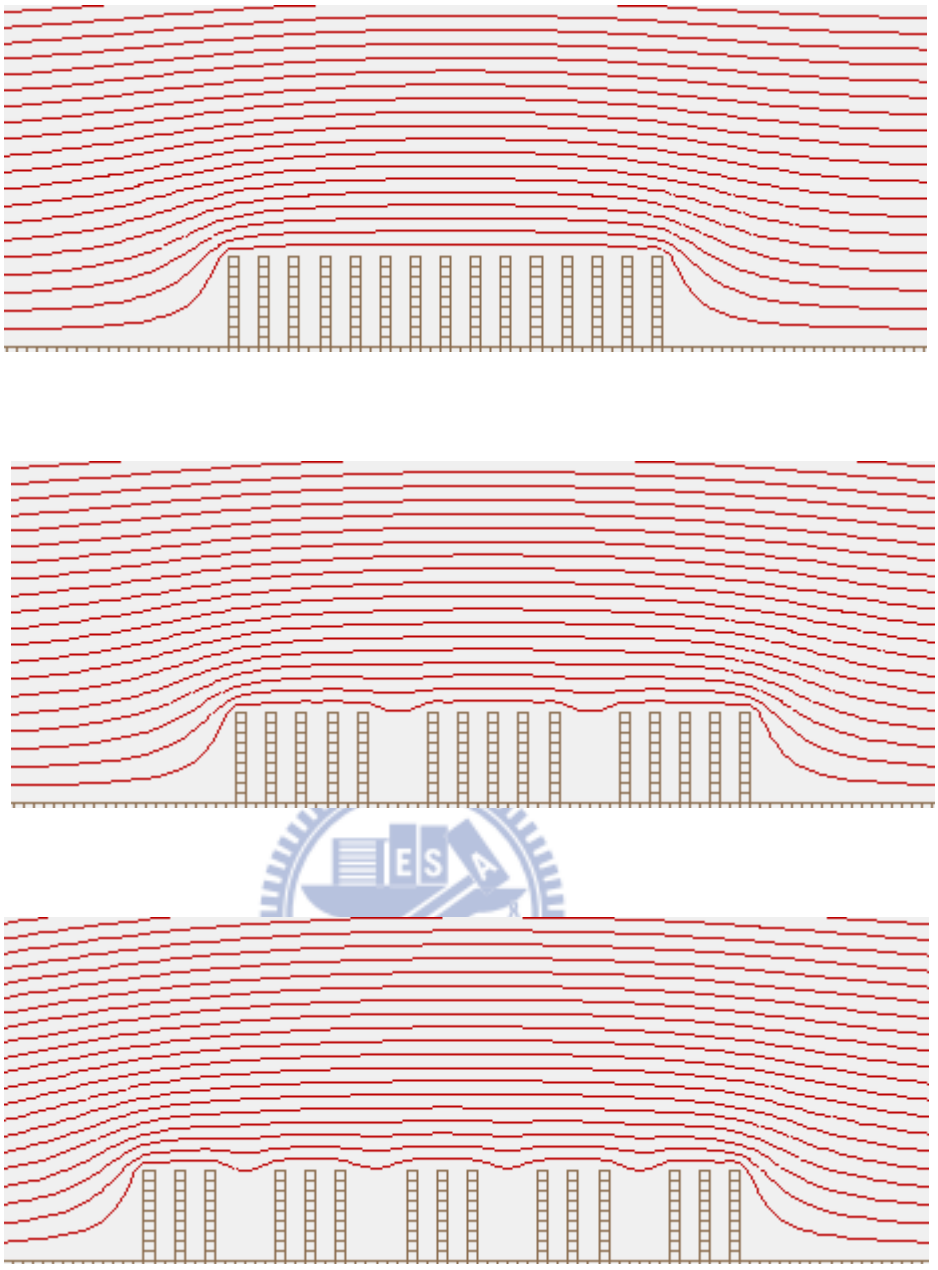

Figure 3-25 Simulation of the equipotential lines of the electrical field for tubes of different distances between each other [81].

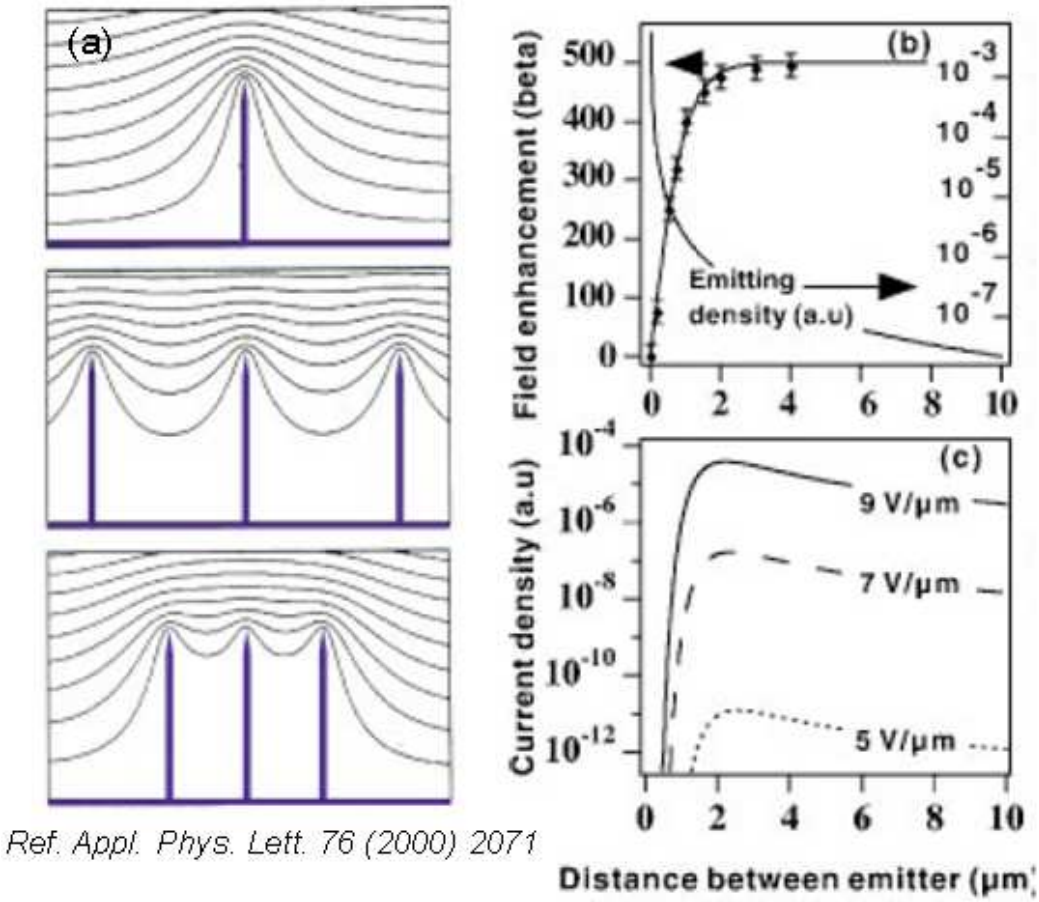

Ref. Appl. Phys. Lett. 76 (2000) 2071

Figure 3-26 (a) Simulation of the equipotential lines of the electrical field for tubes of 1 μm height and 2 nm radius, for distances of 4, 1, and 0.5 μm between tubes; along with (b) the corresponding changes of the field enhancement factor β and emitter density, and (c) current density as a function of the distance [53].

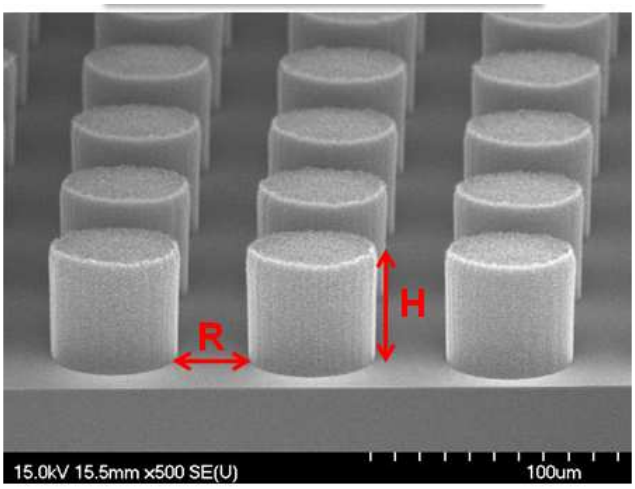

Figure 3-27 Definition of the R/H ratio, where R is the inter-pillar distance (spacer) and H is the height of a CNT pillar.

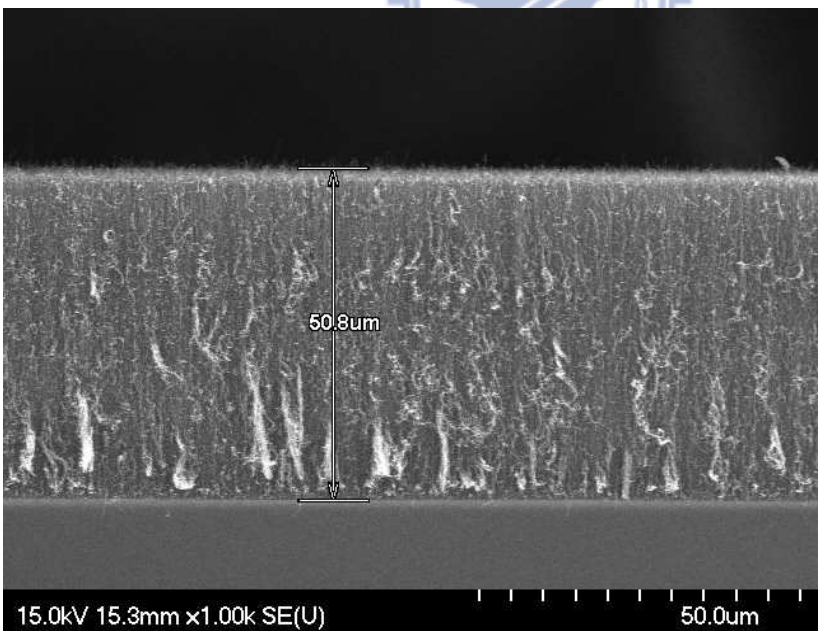

Figure 3-28 The cross-sectional view of CNTs film synthesized from Co-Ti co-deposited catalyst structure for 50.8 μm in height.

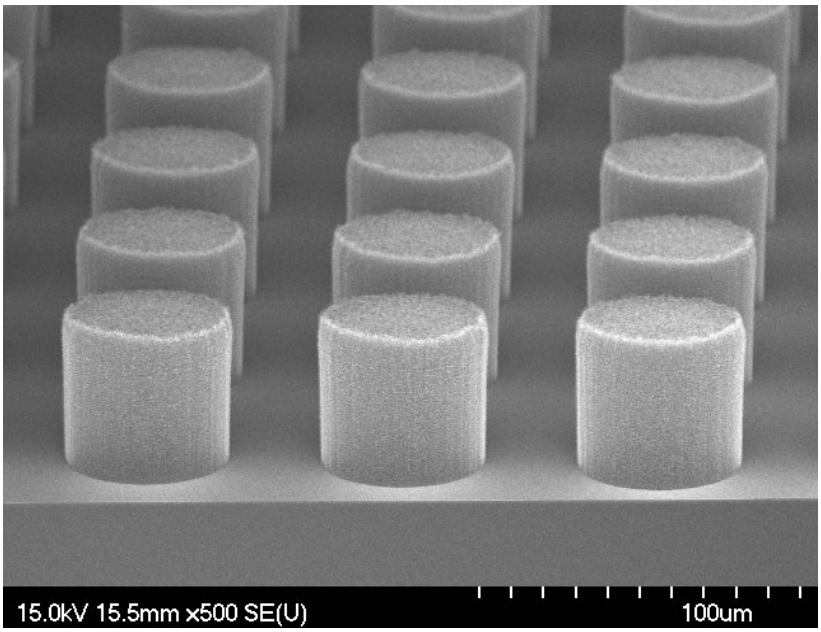

(a)

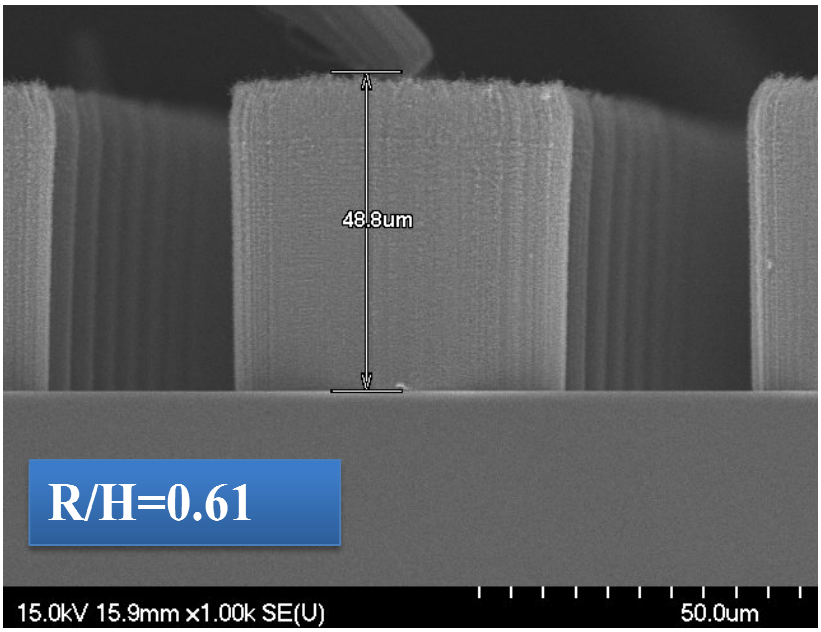

(b)

Figure 3-29 The pictures shown here were the tilted image (a) (about 45°)and the cross-sectional image (b) taken by the SEM for the48.8 μm high pillar-like CNTs synthesized from the Co-Ti co-deposited catalyst structure grown by thermal CVD. Here the R/H ratio is 0.61.

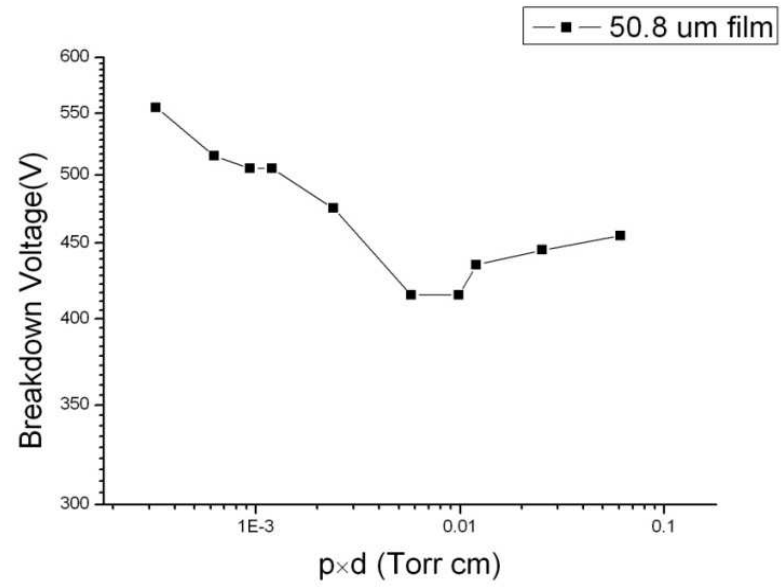

(a)

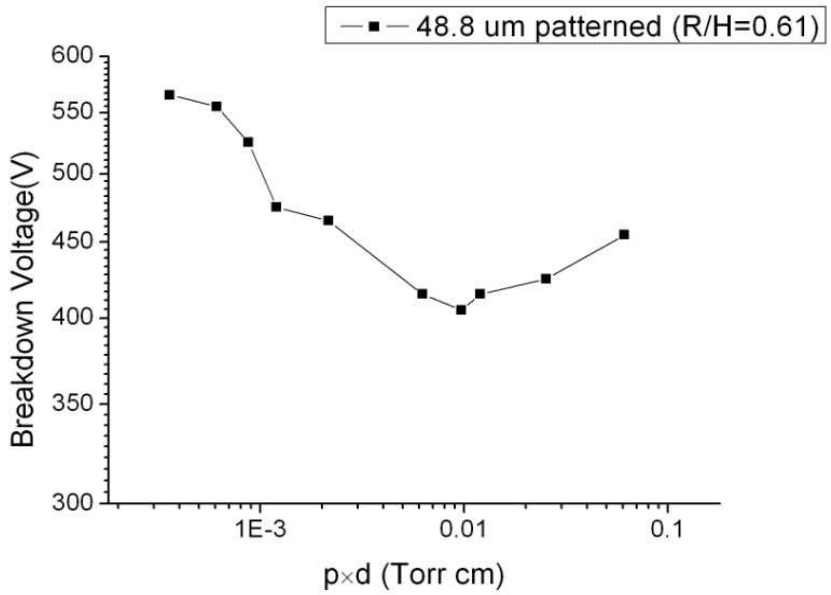

(b)

Figure 3-30 Breakdown voltages vs. p×d characteristics of (a) the film sample (50.8 μm) and (b) the pattern sample (48.8 μm, R/H =0.61) under nitrogen environment (Paschen's curve). One could find in (c) that there is no much difference of breakdown voltages between the film sample and the pattern sample at this R/H ratio.

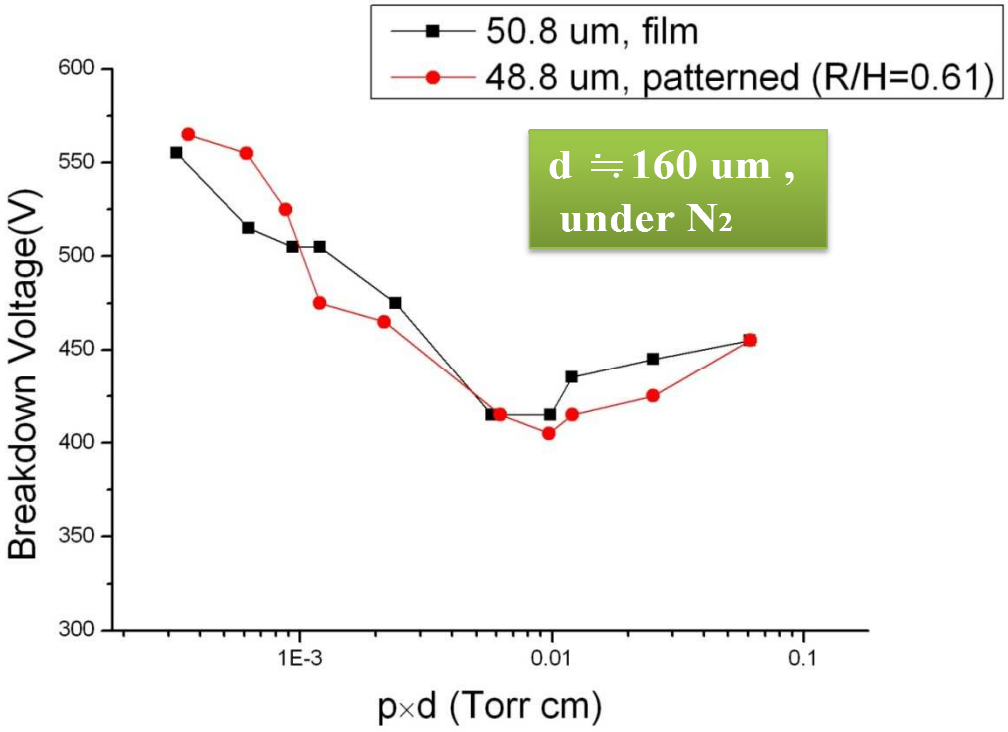

(c)

Figure 3-30 (cont.).

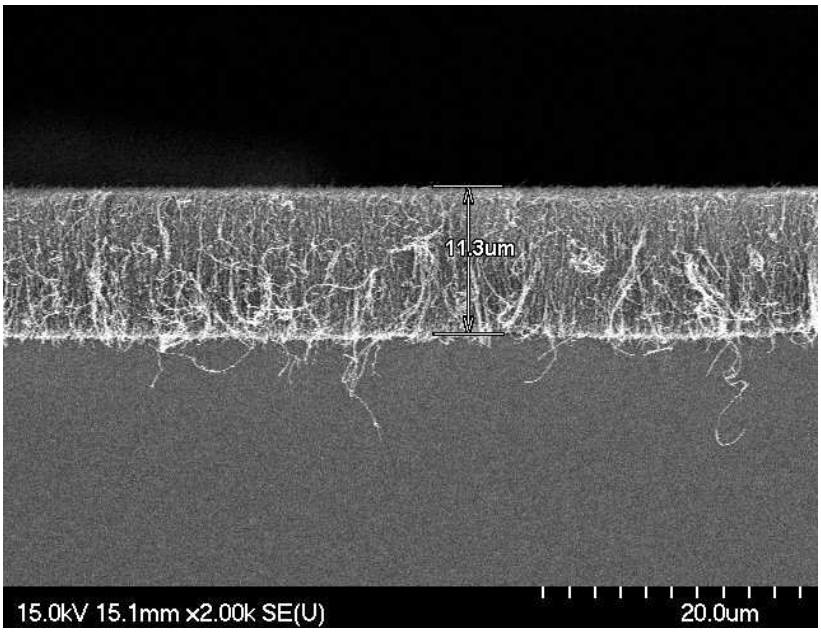

Figure 3-31 The cross-sectional view of CNTs film synthesized from Co-Ti co-deposited catalyst structure for 11.3 μm in height.

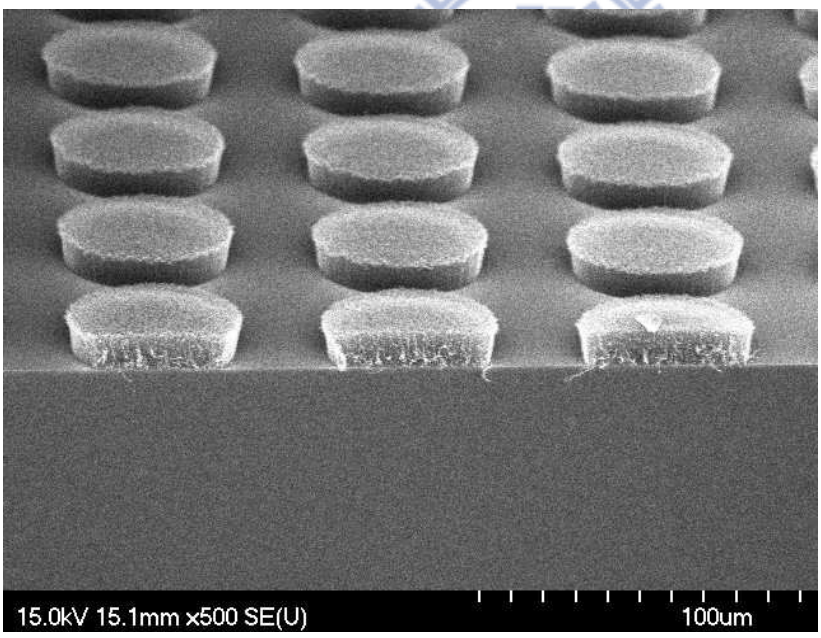

(a)

Figure 3-32 The pictures shown here were the tilted image (a) (about 45°)and the cross-sectional image (b) taken by the SEM for the 12.5 μm high pillar-like CNTs synthesized from the Co-Ti co-deposited catalyst structure grown by thermal CVD. Here the R/H ratio is 2.40.

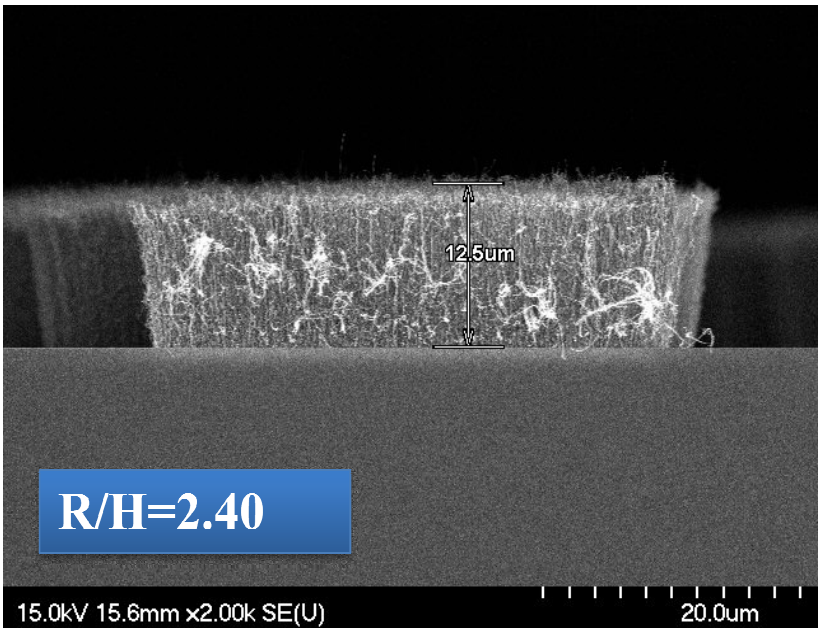

(b)

Figure 3-32 (cont.).

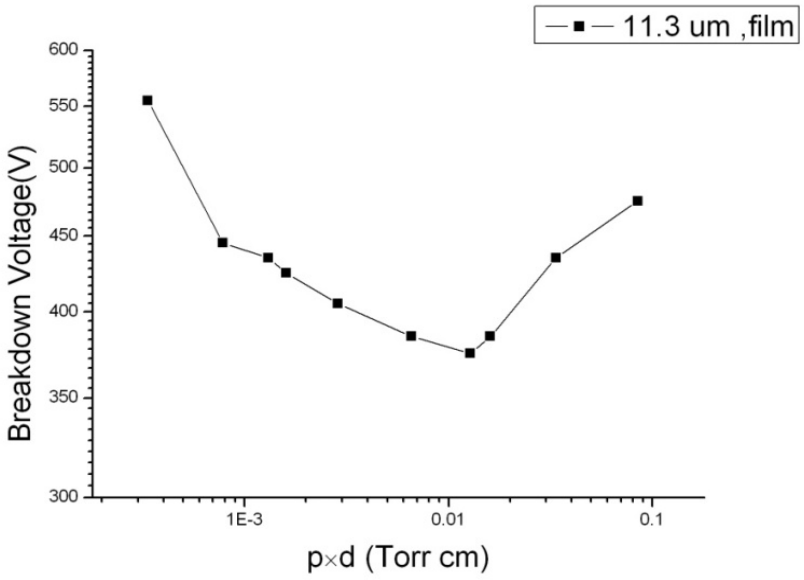

(a)

Figure 3-33 Breakdown voltages vs. p×d characteristics of (a) the film sample (11.3 μm) and (b) the pattern sample (12.5 μm, R/H =2.40) under nitrogen environment (Paschen's curve). One could found in (c) that the breakdown voltages of the patterned sample begin to lower than that of film sample at this R/H ratio.

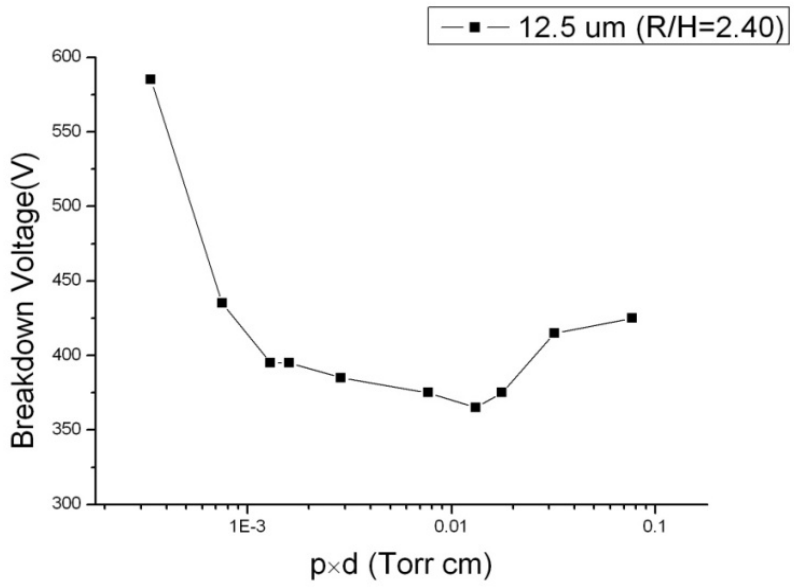

(b)

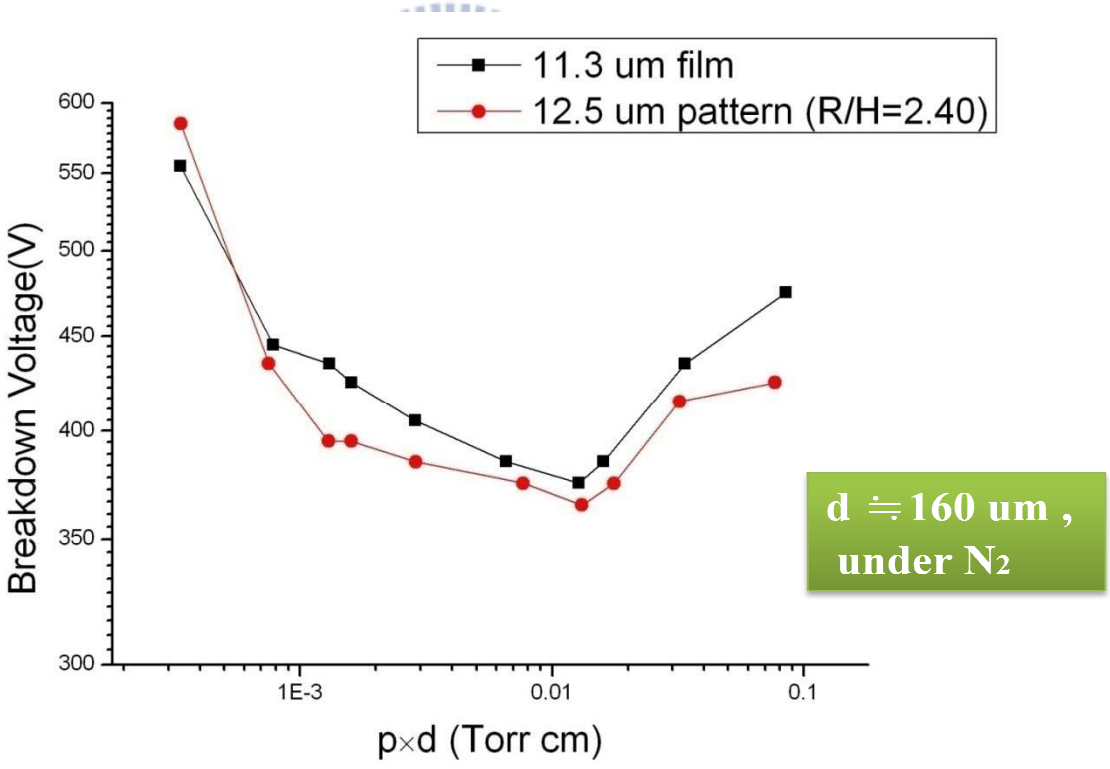

(c)

Figure 3-33 (cont.).

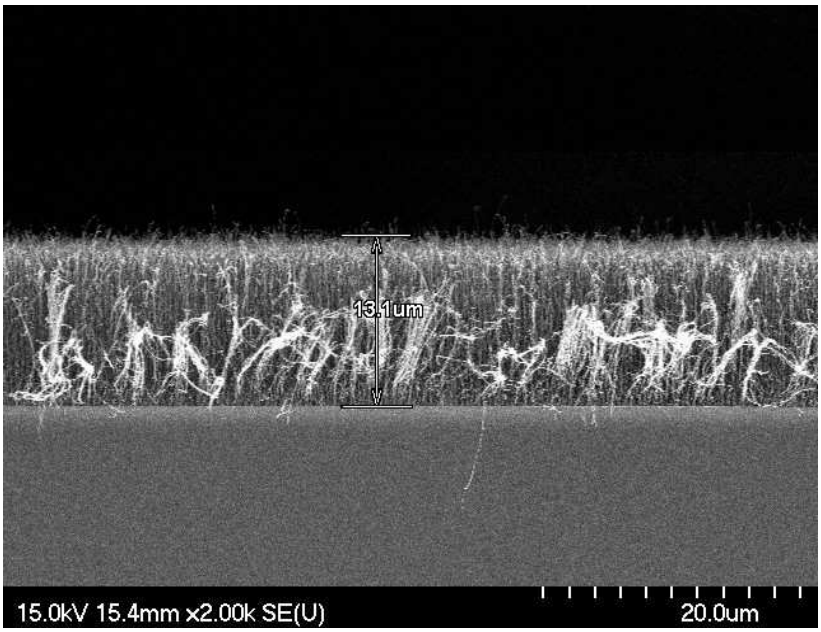

Figure 3-34 The cross-sectional view of CNTs film synthesized from Co-Ti co-deposited catalyst structure for 13.1 μm in height.

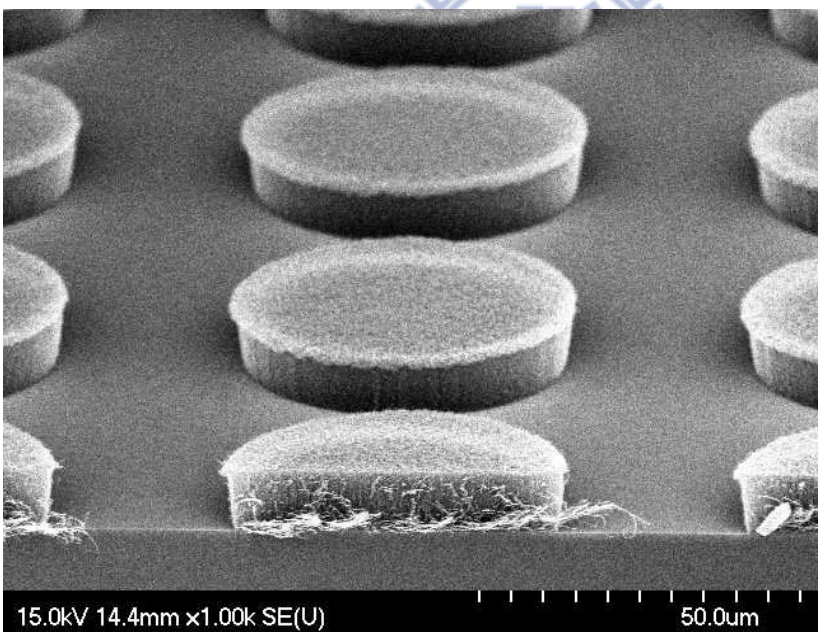

(a)

Figure 3-35 The pictures shown here were the tilted image (a) (about 45°)and the cross-sectional image (b) taken by the SEMfor the 10.3μmhigh pillar-like CNTs synthesized from the Co-Ti co-deposited catalyst structure grown by thermal CVD. Here the R/H ratio is 2.91.

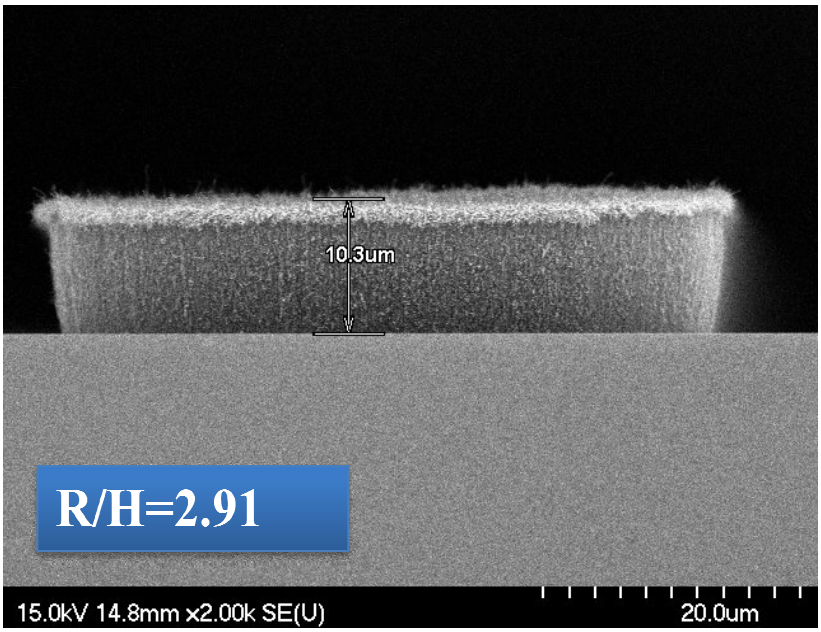

(b)

Figure 3-35 (cont.).

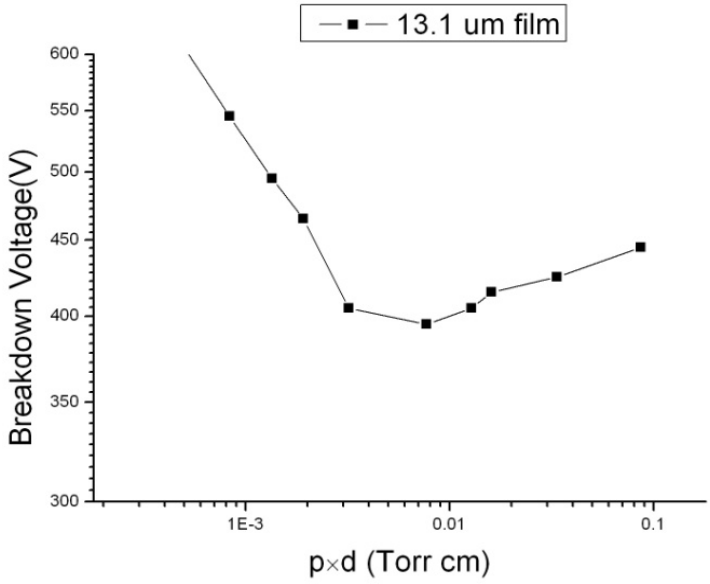

(a)

Figure 3-36 Breakdown voltages vs. p×d characteristics of (a) the film sample (13.1 μm) and (b) the pattern sample (10.3μm, R/H =2.91) under nitrogen environment (Paschen's curve). One could found in (c) that the breakdown voltages of patterned sample are greatly lower than film sample at this R/H ratio.

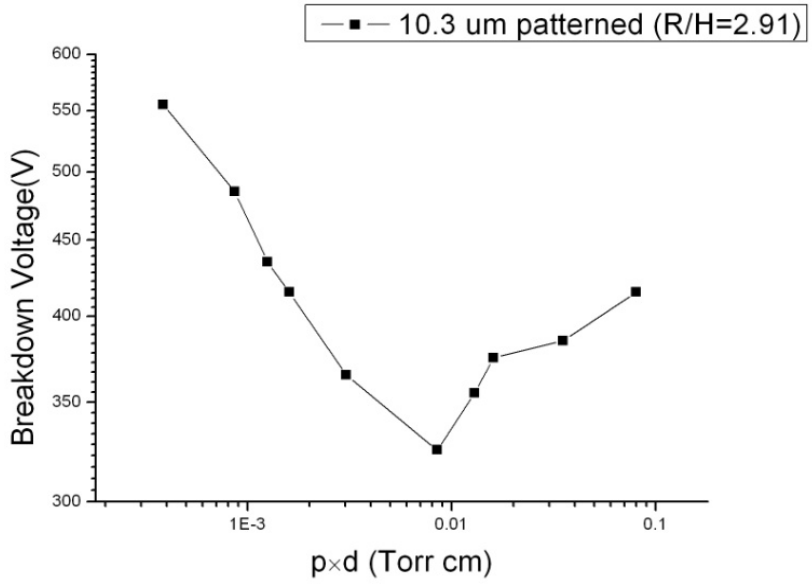

(b)

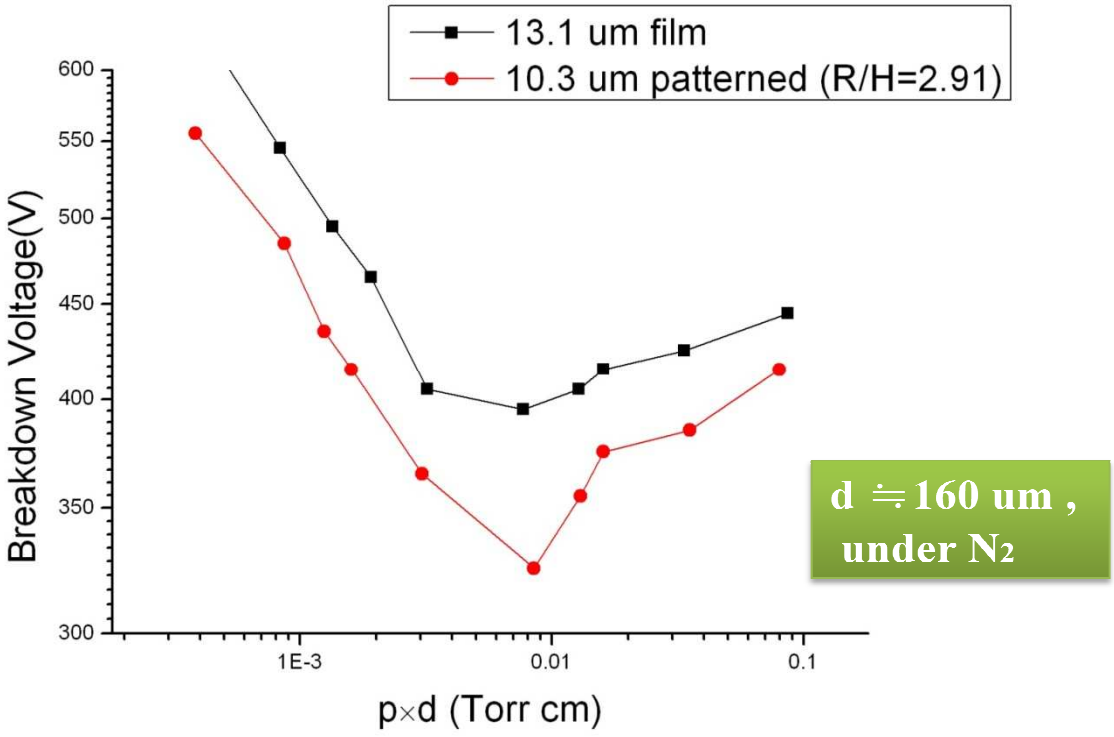

(c)

Figure 3-36 (cont.).

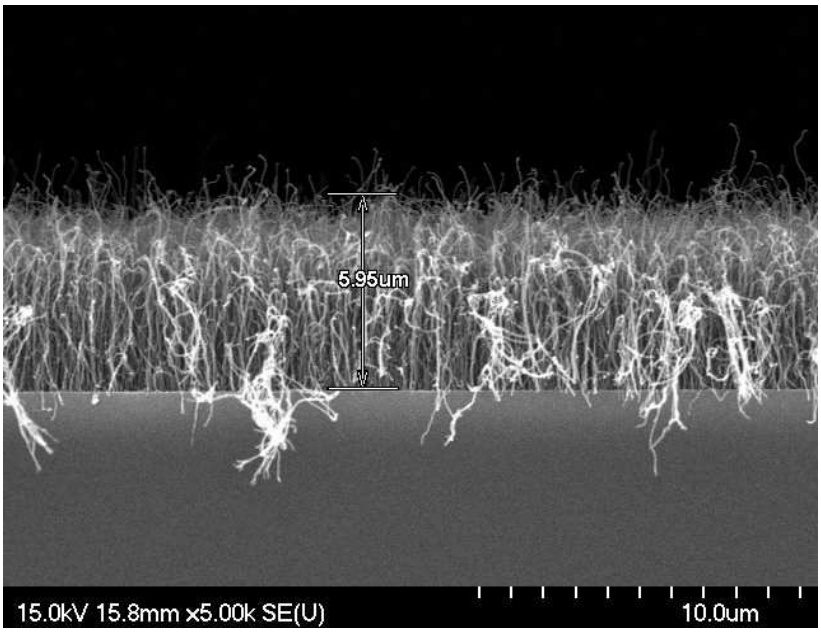

Figure 3-37 The cross-sectional view of CNTs film synthesized from Co-Ti co-deposited catalyst structure for 5.95 μm in height.

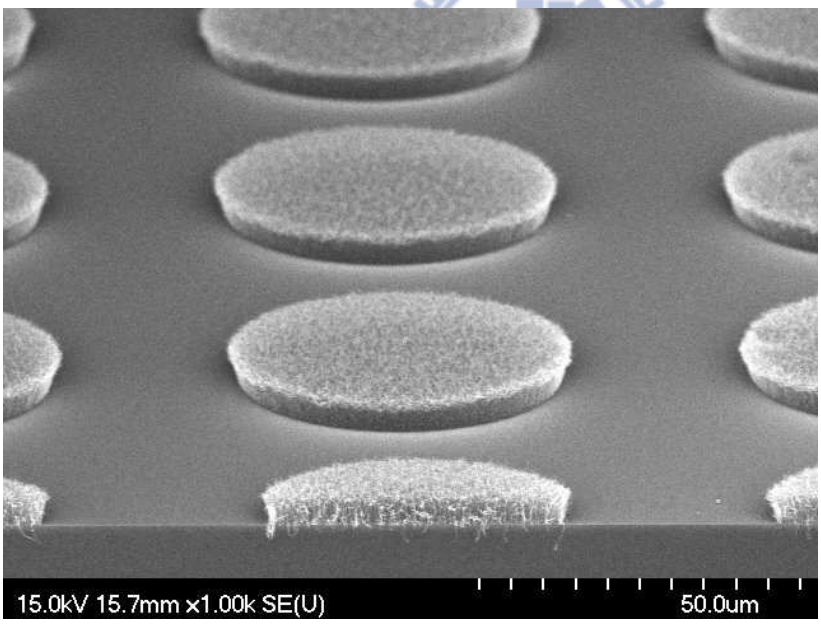

(a)

Figure 3-38 The pictures shown here were the tilted image (a) (about 45°)and the cross-sectional image (b) taken by the SEMfor the 5.95μmhigh pillar-like CNTs synthesized from the Co-Ti co-deposited catalyst structure grown by thermal CVD. Here the R/H ratio is 5.04.

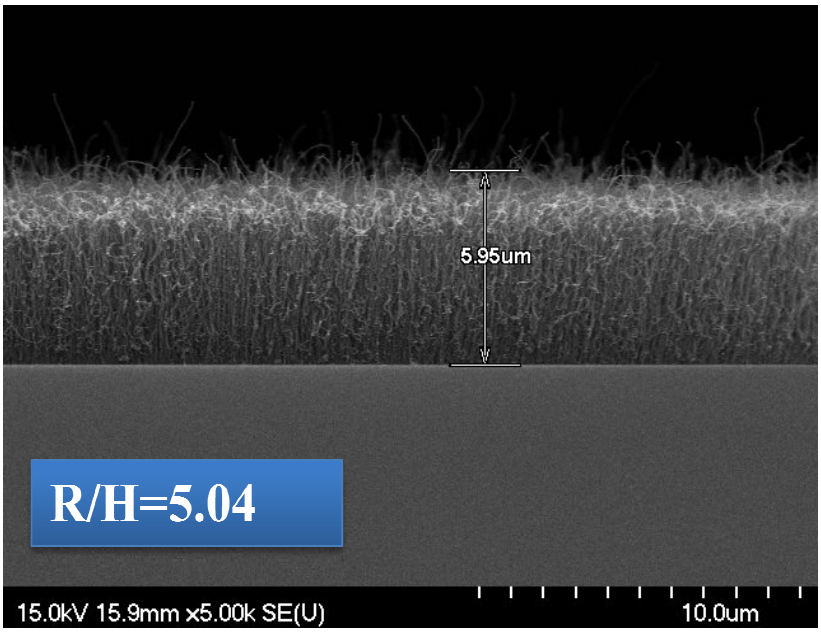

(b)

Figure 3-38 (cont.).

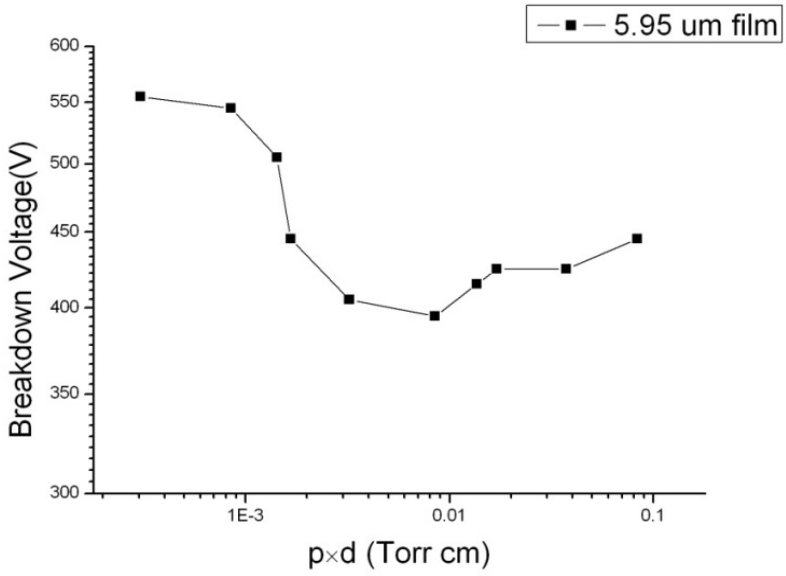

(a)

Figure 3-39 Breakdown voltages vs. p×d characteristics of (a) the film sample (5.95 μm) and (b) the pattern sample 5.95 μm, R/H =5.04) under nitrogen environment (Paschen's curve). One could found in (c) that the breakdown voltages of patterned sample is lower than film sample but not so much as R/H = 2.91 at this R/H ratio.

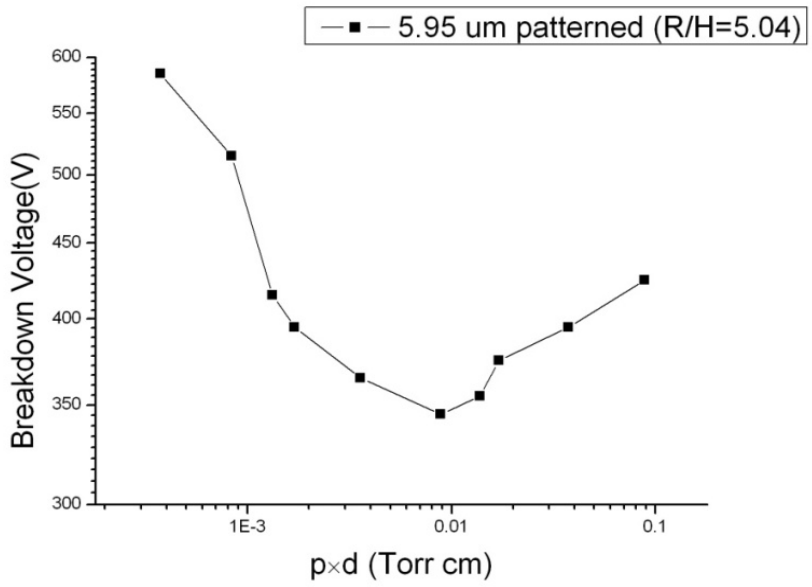

(b)

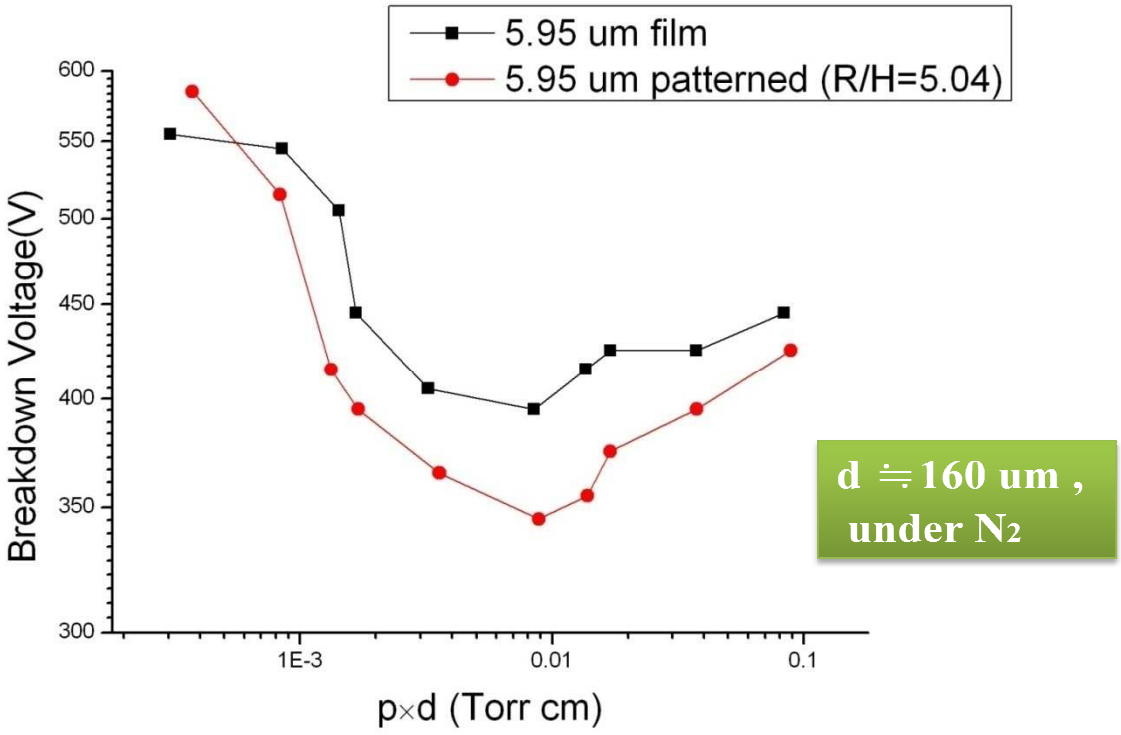

(c)

Figure 3-39 (cont.).

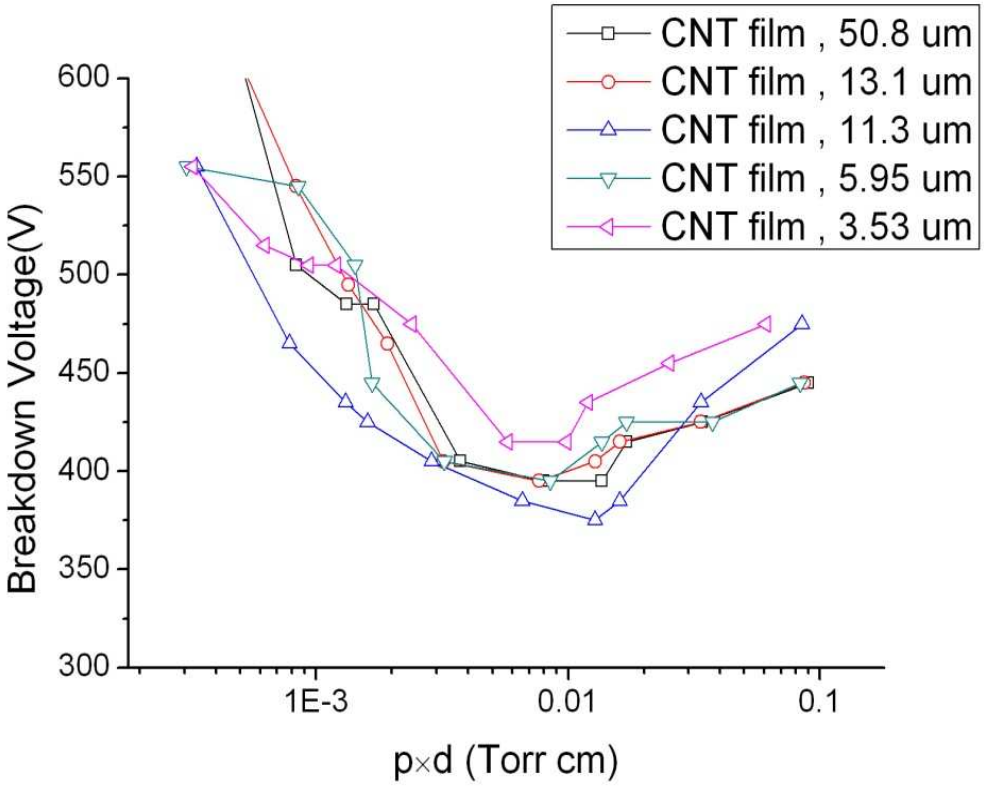

Figure 3-40 The comparison of the breakdown voltages characteristics of the film samples with different height. The lowest breakdown voltages were obtained at the height of CNTs around 11.3 μm to 13.1 μm. The breakdown voltage would increase when the height of the CNTs was too long or too short.

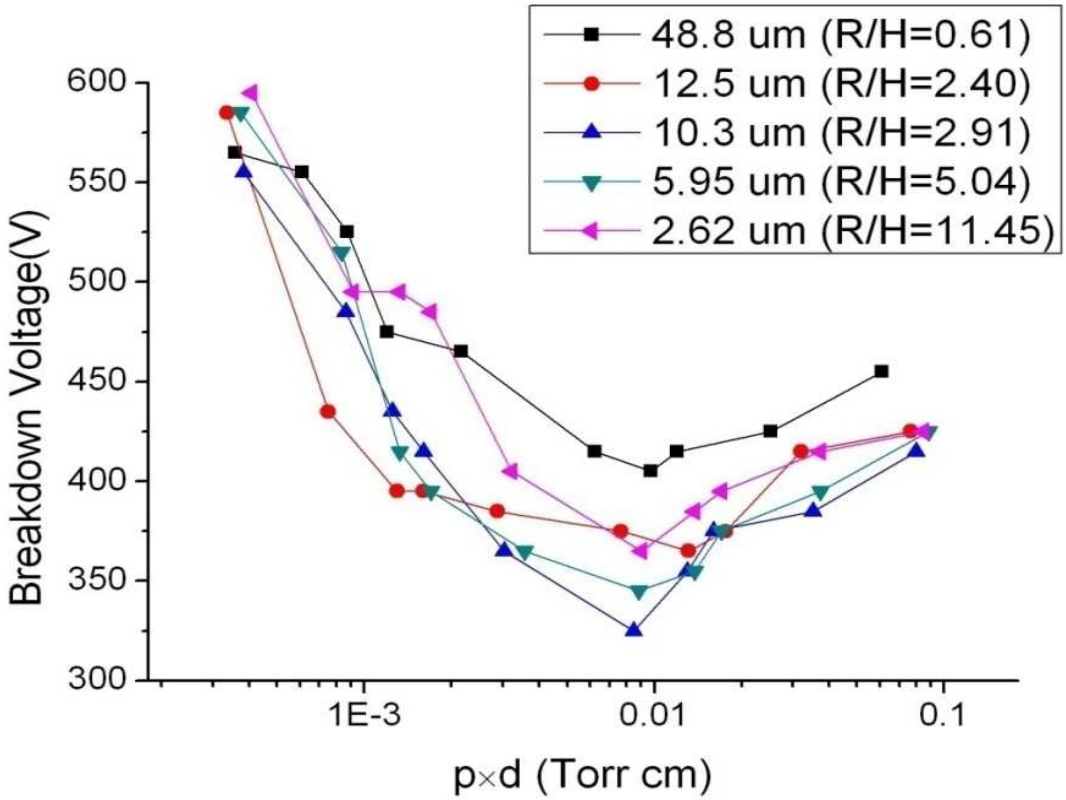

Figure 3-41 The comparison of the breakdown voltages characteristics of the pattern samples with different R/H ratio. It's obviously that the lowest breakdown voltages were approached as the R/H ratio was around 2.91. If the R/H ratio increases to 5.04 and 11.4, the breakdown voltages will raise up gradually.

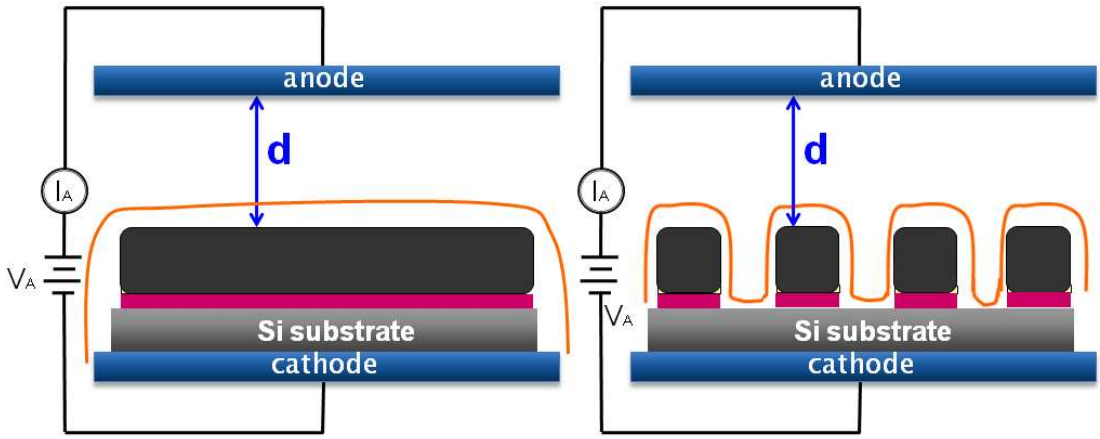

(a)

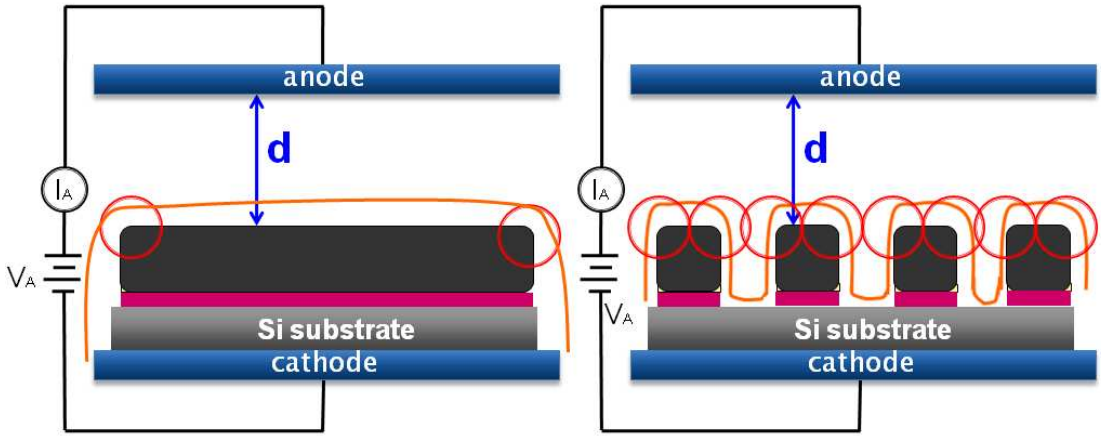

(b)

Figure 3-42 (a)The local electrical field distribution and (b) the emission corner of the film sample and the patterned sample for a constant anode-to-cathode distance and the same gas pressure.

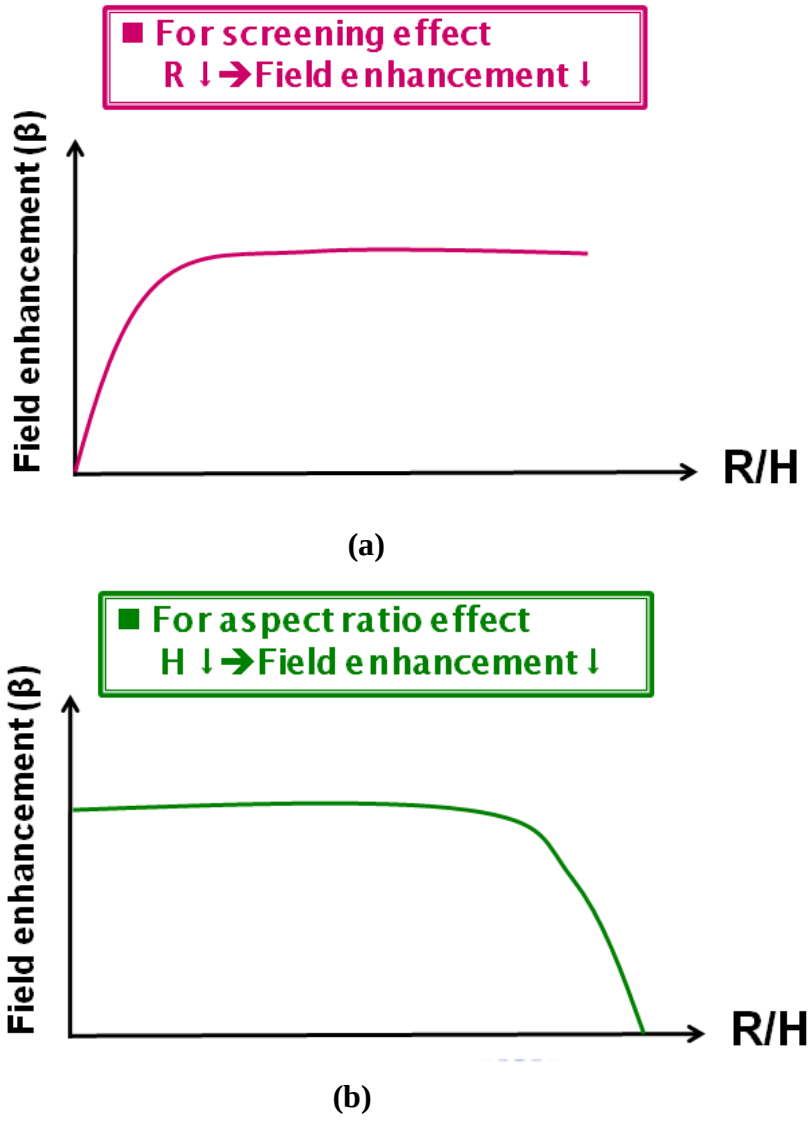

Figure 3-43 Corresponding changes of the field enhancement β as a function of the R/H ratio when considering (a) the screening effect, (b) the aspect ratio effect and (c) both of the two effects.

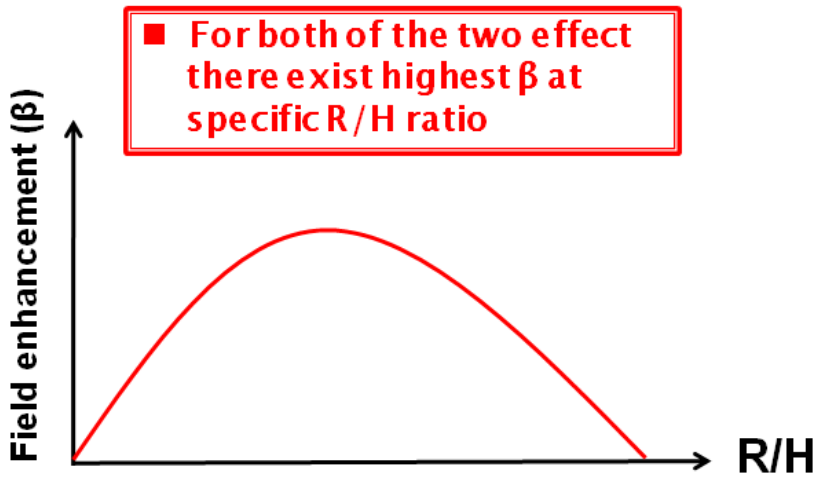

(c)

Figure 3-43 (cont.).

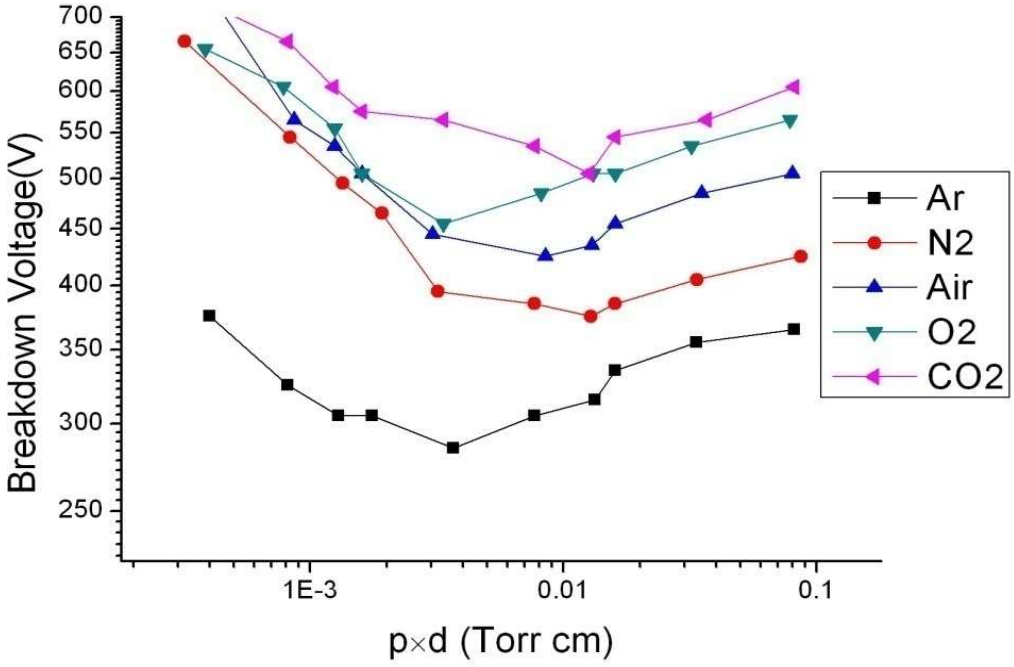

(a)

Figure 3-44 The breakdown characteristics of different gases for (a)the film sample with 11.3 μm in CNTs' height and (b)the patterned sample with R/H = 2.91. Different gas molecules have different mean free path, ionization energy and recombination rate, which causes their different breakdown characteristics in Paschen's curve.

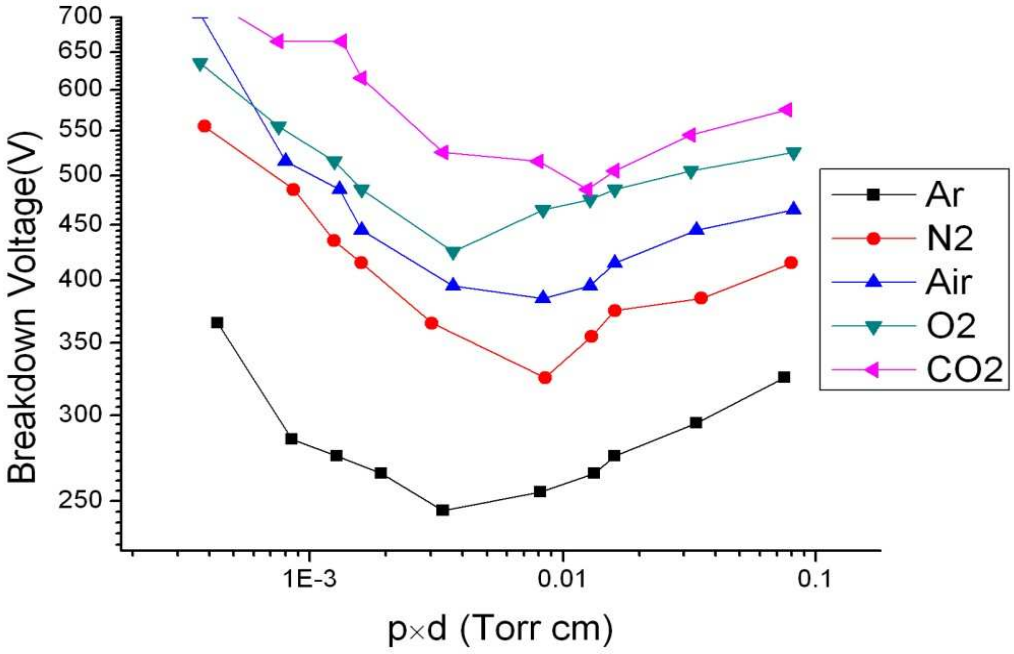

(b)

Figure 3-44 (cont.).

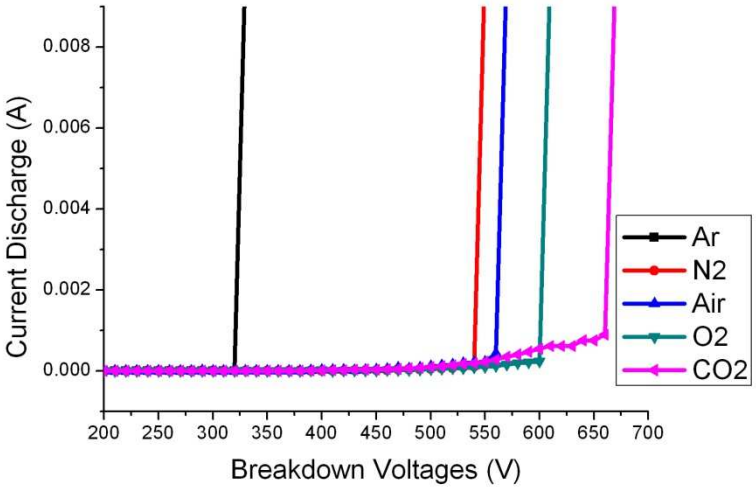

(a)

Figure 3-45 Discharge current versus breakdown voltage curves for Ar, N_2, Air, O_2 and CO_2 of the film sample with 11.3 μm in CNTs' height at p×d product value around (a)8×10^{-4} torr cm and (b) 8×10^{-3}torr cm, showing distinct breakdown voltages; carbon dioxide displays the highest and argon the lowest.

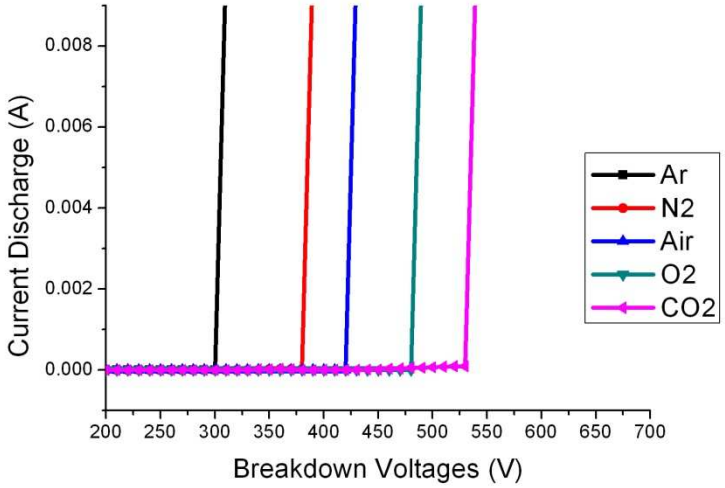

(b)

Figure 3-45 (cont.).

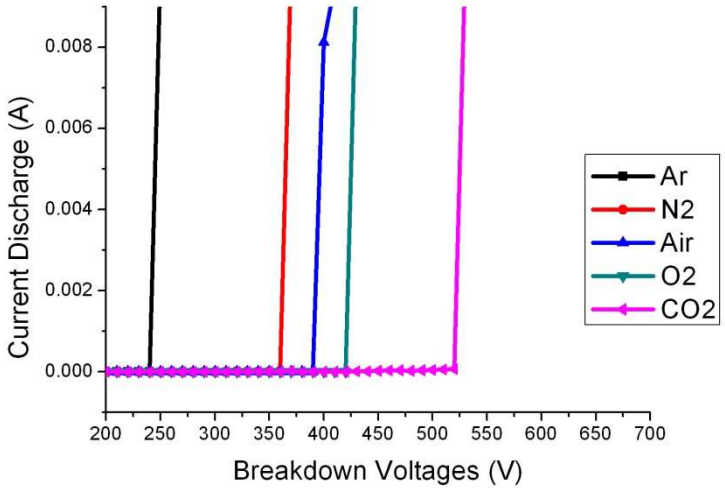

(a)

Figure 3-46 Discharge current versus breakdown voltage curves for Ar, N_2, Air, O_2 and CO_2 of the patterned sample with R/H = 2.91 at p×d product value around (a)8×10^{-4} torr cm and (b) 8×10^{-3}torr cm, showing distinct breakdown voltages; carbon dioxide displays the highest and argon the lowest. It's noticeably that the breakdown voltage windows of (b) were wider and at relatively low voltages.

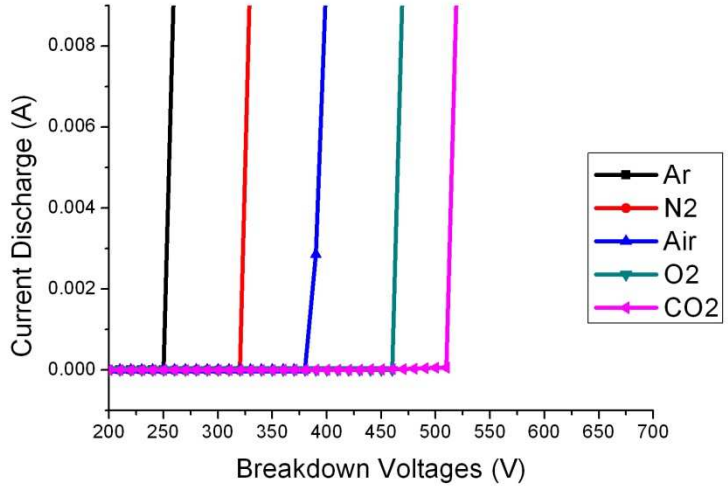

(b)

Figure 3-46 (cont.).

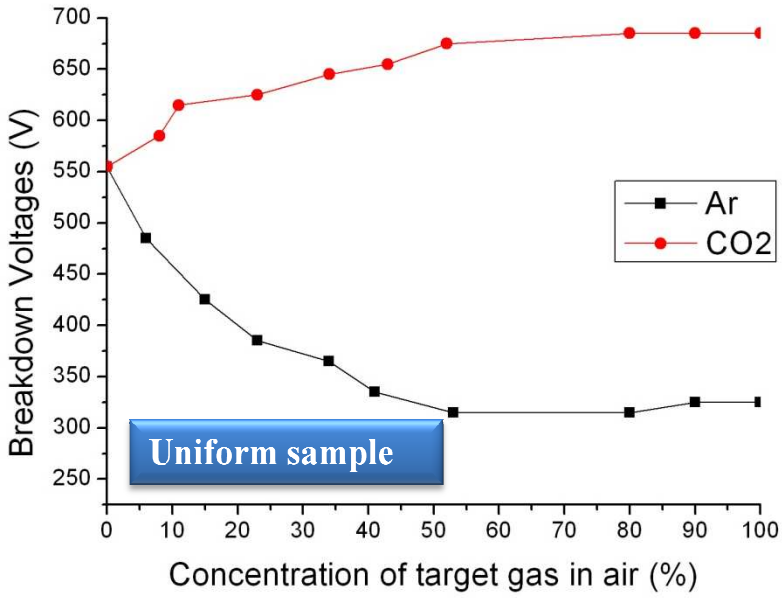

(a)

Figure 3-47 Breakdown voltages of Ar and CO_2 gases in mixture with air as a function of concentration for (a) film sample with 11.3 μm in CNTs' height and (b) patterned sample with R/H = 2.91.Breakdown voltage increases with increasing CO_2 concentration in the mixture, and decreases with increasing Ar concentration.

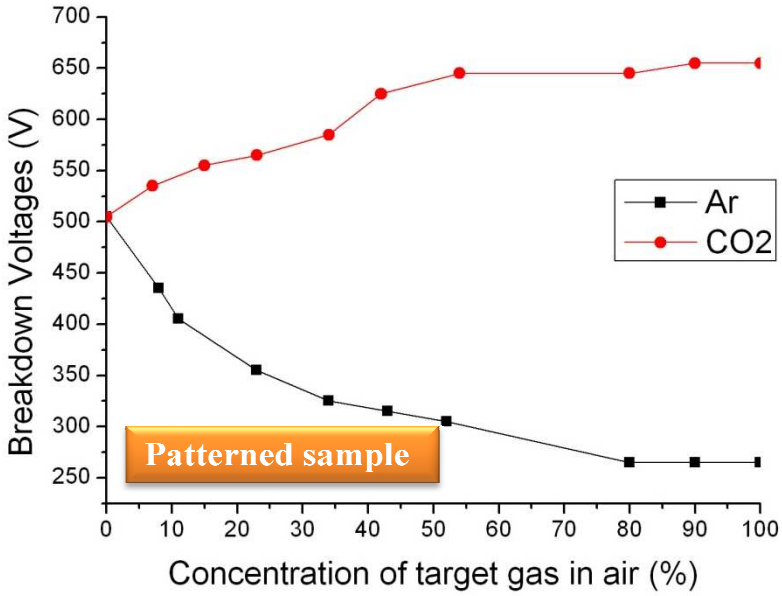

(b)

Figure 3-47 (cont.).

Chapter 4

==========

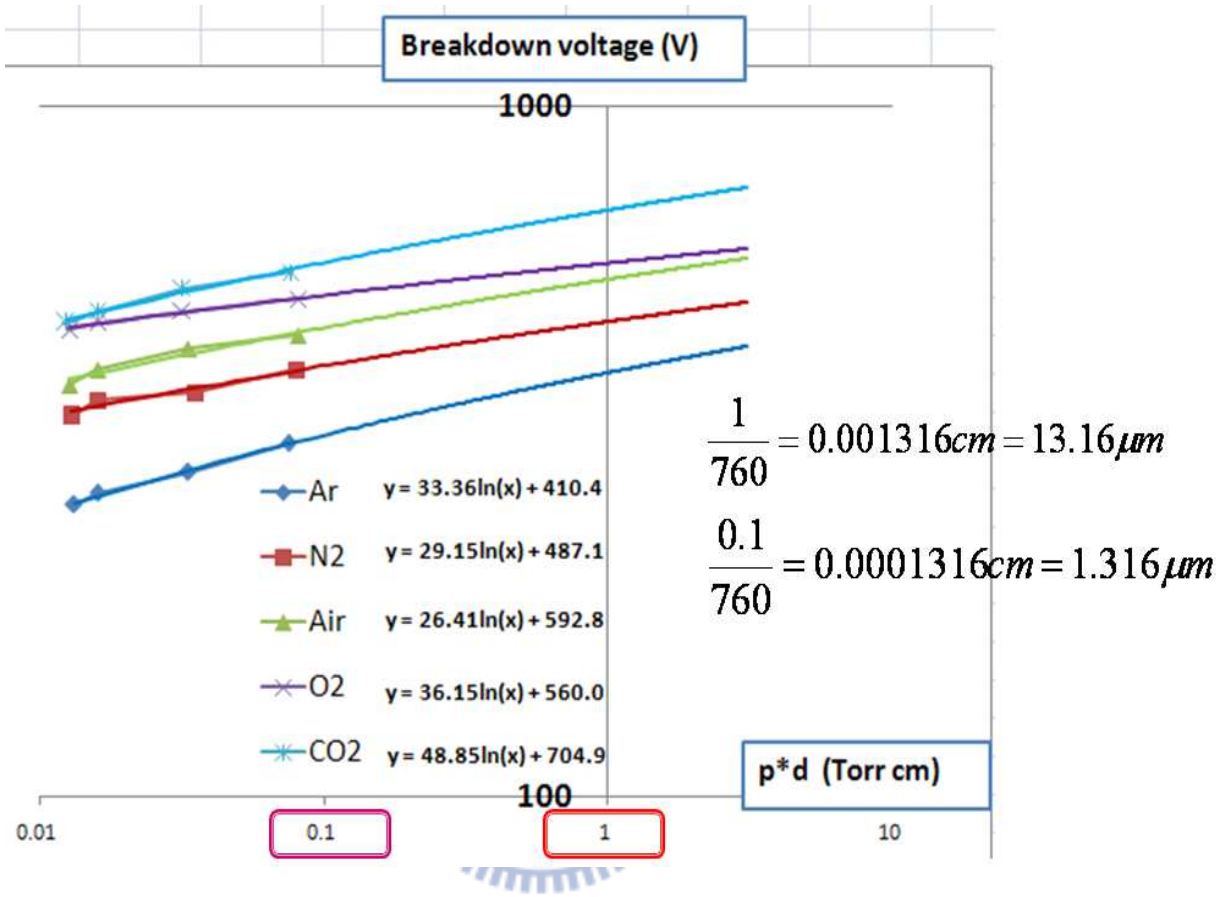

Figure 4-1 Extension of the linear region in the right side of the Paschen's curve

Reference

[1] Sander J. Tans, Alwin R. M. Verschueren & Cees Dekker, *"Room-temperature transistor based on a single carbon nanotube,"* NATURE | VOL 393 | 7 MAY 1998

[2] R. Martel, T. Schmidt, H. R. Shea, T. Hertel, and Ph. Avouris, *"Single- and multi-wall carbon nanotube field-effect transistors,"* APPLIED PHYSICS LETTERS VOLUME 73, NUMBER 17

[3] Auble, D.L.; Meyers, T.P. , *"An open path, fast response infrared absorption gas analyzer for H2O and CO2,"* Boundary-Layer Meteorology 59(3):pp.243–256.

[4] Ashish Modi, Nikhil Koratkar, Eric Lass, Bingqing Wei& Pulickel M. Ajayan, *" Miniaturized gas ionization sensors using carbon nanotubes,"* Nature Vol 424 10 JULY 2003

[5] Iijima S.," *Helical microtubules of graphitic carbon* ," Nature Vol. 354 (6348), pp.56–58, 1991.

[6] Baughman, Ray H., Zakhidov, Anvar A., de Heer, and Walt A. ," Carbon Nanotubes—The Route Toward Application ," Science, Vol.297 pp.787-790, 2002.

[7] Douglas R. Kauffman and Alexander Star, *"Carbon Nanotube Gas and Vapor Sensors"* Angew. Chem. Int. Ed. 2008, 47, pp.6550 – 6570

[8] M. S. Dresselhaus, G. Dresselhaus, K. Sugihara, L. I. Spain, and H. A. Goldberg, "*Graphite fibers and filaments,*" Springer-Verlag, New York, pp. 185-186, 1998

[9] P. M. Ajayan, *"Nanotubes from carbon,"* Chem. Rev., Vol. 99, pp. 1787-1790, 1999.

[10] S. Iijima and T. Ichihashi, "*Single-shell carbon nanotubes of 1-nm diameter,*" Nature, Vol. 363, pp. 603-605, 1993

[11] D. S. Bethune, C. H. Kiang, M. S. de Vries, G. Gorman, R. Savoy, J. Vazquez,

and R. Beyers, "*Cobalt-catalyzed growth of carbon nanotubes with single-atomic-layer walls*," Nature, Vol. 363, pp. 605-607, 1993

[12] "http://en.wikipedia.org/wiki/Image:CNTnames.png" 2006

[13] "http://online.itp.ucsb.edu/online/qhall_c98/dekker/" 2006

[14] Y. K. Kwon, T. H. Lee, S. G. Kim, P. Jund, D. Tomanek, and R. E. Smalley. "*Morphology and Stability of Growing Multiwall Carbon Nanotubes"* Phys Rev. Lett., Vol. 79, pp. 2065-2068, 1997

[15] Y. Saito, "*Carbon Nanotubes: Preparation and Physical Properties*," Asia Display/IDW'01, pp. 11-14, 2001

[16] Min-Feng Yu et al., "*Strength and Breaking Mechanism of Multiwalled Carbon Nanotubes Under Tensile Load*," Science, Vol. 287, pp. 637-640, 2000.

[17] Philip G. Collins and Phaedon Avouris, "*Nanotubes for Electronics- Scientific American December*", Vol. 69, 8 pages., 2000

[18] Gamaly EG and Ebbesen TW," *Mechanism of carbon nanotube formation in the arc discharge* ," Phys Rev B, 1995,52(3), pp.2083–2089.

[19] Guo T, Nikolaev P, Thess A, Colbert DT, and Smalley RE.," *Catalytic growth of single-walled nanotubes by laser vaporization* ," Chem Phys Lett, Vol. 243, pp.49–54, 1995.

[20] M. P. Siegal, D. L. Overmyer, and F. H. Kaatz ," *Controlling the site density of multiwall carbon nanotubes via growth conditions,"*App. Phys. Lett., Vol. 84, No. 25, pp. 5156-5158, 2004

[21] Yih-Ming Shyu and Franklin Chau-Nan Hong," *The effects of pre-treatment and catalyst composition on growth of carbon nanofibers at low temperature* ,"Diamond and Related Materials Vol.10, pp. 1241-1245, 2001

[22] Nolan, Peter E., Schabel, Michael J., Lynch, David C," *Hydrogen control of carbon deposit morphology* ,"Carbon , Vol. 33 , No. 1 , pp. 79-85 , 1995

[23] Mi Chen, Chieng-Ming Chen, and Chia-Fu Chen,” *Growth of carbon nanotubes by microwave plasma chemical vapor deposition using CH_4 and CO_2 gas mixture* ,”Thin Solid Films, Vol. 420/421, pp. 230-234. 2002

[24] Mi Chen, Chieng-Ming Chen, Shin-Chen Shi and Chia-Fu Chen,” *Low-Temperature Synthesis Multiwalled Carbon Nanotubes by Microwave Plasma Chemical Vapor Deposition Using CH_4-CO_2 Gas Mixture* ,”Jpn. J. Appl. Phys. Vol. 42, pp. 614–619, 2003

[25] Niraj Sinha, Jiazhi Ma, and John T. W. Yeow, ” *Carbon Nanotube-Based Sensors,”* Journal of Nanoscience and Nanotechnology Vol. 6, pp.573–590, 2006

[26] T. Ueda, M.M.H. Bhuiyan, H. Norimatsu, S. Katsuki, T. Ikegami, F. Mitsugi, *“Development of carbon nanotube-based gas sensors for NO x gas detection working at low temperature,”* Physica E 40 (2008) pp.2272–2277

[27] Yong Zhang, JunHua Liu, and Changchun Zhu, *“Novel Gas Ionization Sensors Using Carbon nanotubes,”* Sensor Letters Vol. 8, pp.219-227, 2010

[28] Alireza Nikfarjam, Azam Iraji zad, Fatemeh Razi, S. Zahra Mortazavi, *“Fabrication of gas ionization sensor using carbon nanotube arrays grown on porous silicon substrate,”* Sensors and Actuators A 162 (2010) pp.24–28

[29] Ashish Modi, Nikhil Koratkar, Eric Lass, Bingqing Wei& Pulickel M. Ajayan, ” *Miniaturized gas ionization sensors using carbon nanotubes,”* Nature Vol 424 10 JULY 2003

[30] Yang Doo Lee, Woo-Sung Cho, Seung-IL Moon, Yun-Hi Lee, Jai Kyeong Kim, Sahn Nahm, Byeong-Kwon Ju, *“Gas sensing properties of printed multiwalled carbon nanotubes using the field emission effect,”* Chemical Physics Letters 433 (2006) pp.105–109

[31] Abdel-Salam, M., et al. High Voltage EngineeringÐTheory and Practice (Dekker, New York, (2000).

[32] E.Kuffel, W.S. Zaengl, J.Kuffel (2004). *"High Voltage Engineering Fundamentals, Second edition,"* Butterworth-Heinemann. ISBN 0-7506-3634-3.

[33] Little, P.F. (1956). "Secondary effects". In Flügge, Siegfried. Electron-emission • Gas discharges I. Handbuch der Physik (Encyclopedia of Physics). XXI. Berlin-Heidelberg-New York: Springer-Verlag. pp. 574–663

[34] Emmanouel Hourdakis, Brian J. Simonds, and Neil M. Zimmerman (2006). *"Submicron gap capacitor for measurement of breakdown voltage in air"*. Rev. Sci. Instrum. 77 (3): 034702.

[35] 莊達人著，「VLSI 製造技術」，高立圖書股份有限公司，台北市，民國八十九年出版。

[36] C. A. Spindt, I. Brodie, L. Humpnrey, and E. R. Westerberg, "*Electrical Properties of Thin-film Field Emission Cathodes with Molybdenum Cones*," J. Appl. Phys., vol. 47, pp. 5248-5251, 1976

[37] V. V. Zhirnov and E. I. Givargizov, "*Field Emission from Silicon Spikes with Diamond Coating*," J. Vac. Sci. & Technol. B, vol. 13, no. 2, pp. 418-421, 1995.

[38] R. B. Marcus, T. S. Ravi, T. Gmitter, H. H. Busta, J. T. Niccum, K. K. Chin, and D. Liu, "*Atomically sharp silicon and metal field emitters*," IEEE Trans. Electron Devices, Vol. 38, pp. 2289-2291, 1991.

[39] Takahito Ono, Dong Youn Sim and Masayoshi Esashi, *"Micro-discharge and electric breakdown in a micro-gap,"* J. Micromech. Microeng. 10 (2000) pp.445–451

[40] Jiarui Huang, Junhai Wang, Cuiping Gu, Kun Yu, Fanli Meng, Jinhuai Liu, *"A novel highly sensitive gas ionization sensor for ammonia detection,"* Sensors and Actuators A 150 (2009) pp.218–223

[41] E. M. Burbidge, G. R. Burbidge, W. A. Fowler, and F. Hoyle (1957), *"Synthesis of the Elements in Stars"*. Reviews of Modern Physics **29** (4): 547

[42] 李勝利著，「各類型偵測感應器簡介」，勞工安全衛生簡訊第 76 期

[43] Douglas R. Kauffman and Alexander Star,” *Carbon Nanotube Gas and Vapor Sensors,”* Angew. Chem. Int. Ed. 2008, 47, pp.6550 – 6570

[44] Ting Zhang, Syed Mubeen, Nosang V Myung and Marc A Deshusses, *“Recent progress in carbon nanotube-based gas sensors,”* Nanotechnology 19 (2008) 332001 (14pp)

[45] Kim S J, Lee S H and Lee C J, *“Organic vapour sensing by current response of porous silicon layer, ”* 2001 J. Phys. D: Appl. Phys. 34 3505

[46] Sumanasekera G U, Adu C K W, Fang S and Eklund P C, *” Effects of Gas Adsorption and Collisions on Electrical Transport in Single-Walled Carbon Nanotubes,”* 2000, Phys. Rev. Lett. 85 pp.1096-9

[47] Kong J, Franklin N R, Zhou Ch, Chapline M G, Peng Sh, Cho K and Dai H,” *Nanotube Molecular Wires as Chemical Sensors,”* 2000, Science 287 pp.622-5

[48] Li J, Lu Y, Ye Q, Cinke M, Han J and Meyyappan M,” *Carbon Nanotube Sensors for Gas and Organic Vapor Detection,”* 2003, Nano Lett 3 pp.929-33

[49] Mina Baghgar, Yaser Abdi and Ezatollah Arzi, *” Fabrication of low-pressure field ionization gas sensor using bent carbon nanotubes,”* J. Phys. D: Appl. Phys. 42 (2009) 135502 (5pp)

[50] S J Kim, *“Gas sensors based on Paschen’s law using carbon nanotubes as electron emitters,”* J. Phys. D: Appl. Phys. 39 (2006) pp.3026–3029

[51] Jiarui Huang , Junhai Wang , Cuiping Gu , Kun Yu , Fanli Meng , Jinhuai Liu, *“A novel highly sensitive gas ionization sensor for ammonia detection,”* Sensors and Actuators A 150 (2009) pp.218–223

[52] Mina Baghgar, Yaser Abdi and Ezatollah Arzi, *“Fabrication of low-pressure field ionization gas sensor using bent carbon nanotubes,”* J. Phys. D: Appl. Phys. 42 (2009) 135502 (5pp)

[53] L. Nilsson, O. Groening, C. Emmenegger, O. Kuettel, E. Schaller, and L. Schlapbach, H. Kind, J-M. Bonard, and K. Kern, *"Scanning field emission from patterned carbon nanotube films,"* APPLIED PHYSICS LETTERS VOLUME 76, NUMBER 15

[54] Jessica L. Killian, Nathaniel B. Zuckerman, Darrell L. Niemann, Bryan P. Ribaya, Mahmud Rahman, Robert Espinosa, M. Meyyappan, and Cattien V. Nguyen, *"Field emission properties of carbon nanotube pillar arrays,"* JOURNAL OF APPLIED PHYSICS 103, 064312 2008

[55] Jung Sang Suh, Kwang Seok Jeong, and Jin Seung Lee, Intaek Han, *"Study of the field-screening effect of highly ordered carbon nanotube arrays,"* APPLIED PHYSICS LETTERS VOLUME 80, NUMBER 13

[56] W. B. Choi, D. S. Chung, J. H. Kang, H. Y. Kim, Y. W. Jin, I. T. Han, Y. H. Lee, J. E. Jung, N. S. Lee, G. S. Park, and J. M. Kim, *"Fully sealed, high-brightness carbon-nanotube field-emission display,"* APPLIED PHYSICS LETTERS VOLUME 75, NUMBER 20

[57] W. Zhu, C. Bower and O. Zhou, G. Kochanski and S. Jin,*" Large current density from carbon nanotube field emitters,"* APPLIED PHYSICS LETTERS VOLUME 75, NUMBER 6

[58] S.B. Sinnott , R. Andrews , D. Qian , A.M. Rao , Z. Mao , E.C. Dickey ,F. Derbyshire, *"Model of carbon nanotube growth through chemical vapor deposition,"* Chemical Physics Letters 315 1999 pp.25–30

[59] Y. Y. Wei, Gyula Eres, V. I. Merkulov, and D. H. Lowndes, *" Effect of catalyst film thickness on carbon nanotube growth by selective area chemical vapor deposition,"* APPLIED PHYSICS LETTERS VOLUME 78, NUMBER 10

[60] Kingsuk Mukhopadhyay , Akira Koshio , Toshiki Sugai , Nobuo Tanaka , Hisanori Shinohara , Zoltan Konya , Janos B. Nagy, *"Bulk production of*

quasi-aligned carbon nanotube bundles by the catalytic chemical vapour deposition (CCVD) method," Chemical Physics Letters 303 1999 pp.117–124

[61] Chuan-Ping JUAN, Kuo-Ji CHEN, Chun-Chien TSAI, Kao-Chao LIN, Wei-Kai HONG, Chen-Yu HSIEH,Wen-Pin WANG, Rui-Ling LAI, Kuei-Hsien CHE , Li-Chyong CHEN and Huang-Chung CHENG, *"Improved Field-Emission Properties of Carbon Nanotube Field-Emission Arrays by Controlled Density Growth of Carbon Nanotubes,"* J.J.A.P. Vol. 44, No. 1A, 2005, pp. 365–370

[62] Ke Yu, Ziqiang Zhu, Min Xu, Qiong Li, Wei Liu, Qun Chen, *"Soluble Carbon Nanotube Films Treated Using a Hydrogen Plasma for Uniform Electron Field Emission,"* Surface and Coating Technology, Vol. 179, pp.63, 2004.

[63] Zhixin Yu, De Chen, Ba°rd Tøtdal, and Anders Holmen, *"Effect of Catalyst Preparation on the Carbon Nanotube Growth Rate,"* Catalyst Today, Vol. 100, pp. 261, 2005.

[64] Hong-Zhang Geng, Ki Kang Kim, Kang Pyo So, Young Sil Lee, Youngkyu Chang, and Young Hee Lee, *"Effect of Acid Treatment on Carbon Nanotube-Based Flexible Transparent Conducting Films,"* J. AM. CHEM. SOC. 2007, 129, pp.7758-7759

[65] Yoshikazu Homma, Yoshiro Kobayashi, and Toshio Ogino, Daisuke Takagi and Roichi Ito, Yung Joon Jung and Pulickel M. Ajayan, *"Role of Transition Metal Catalysts in Single-Walled Carbon Nanotube Growth in Chemical Vapor Deposition,"* J. Phys. Chem. B 2003, 107, pp.12161-12164

[66] S.B. Sinnott, R. Andrews, D. Qian, A.M. Rao, Z. Mao, E.C. Dickey, F. Derbyshire, *"Model of carbon nanotube growth through chemical vapor deposition,"* Chemical Physics Letters 315 1999 pp.25–30

[67] Naiqin Zhao, Chunnian He, Zhaoyang Jiang, Jiajun Li, Yongdan Li, *"Fabrication and growth mechanism of carbon nanotubes by catalytic chemical*

vapor deposition," Materials Letters 60 (2006) pp.159 – 163

[68] H. Cui , G. Eres, J.Y. Howe, A. Puretkzy, M. Varela, D.B. Geohegan, D.H. Lowndes, *"Growth behavior of carbon nanotubes on multilayered metal catalyst film in chemical vapor deposition,"* Chemical Physics Letters 374 (2003) pp.222–228

[69] R. Andrews, D. Jacques, A.M. Rao, F. Derbyshire, D. Qian , X. Fan, E.C. Dickey , J. Chen, *"Continuous production of aligned carbon nanotubes: a step closer to commercial realization,"* Chemical Physics Letters 303 1999 pp.467–474

[70] A. M. Rao, D. Jacques, and R. C. Haddon, W. Zhu, C. Bower, and S. Jin, *"In situ-grown carbon nanotube array with excellent field emission characteristics,"* APPLIED PHYSICS LETTERS VOLUME 76, NUMBER 25

[71] Ge Li and Supriya Chakrabarti, Mark Schulz, Vesselin Shanov, *"Growth of aligned multiwalled carbon nanotubes on bulk copper substrates by chemical vapor deposition,"* J. Mater. Res., Vol. 24, No. 9, Sep 2009

[72] A Jorio, M A Pimenta, A G Souza Filho, R Saito, G Dresselhaus and M S Dresselhaus, *"Characterizing carbon nanotube samples with resonance Raman scattering,"* New Journal of Physics 5 (2003) pp.139.1–139.17

[73] Rui-Ling Lai, Jiun-Kai Shiu, Yao-Ren Chang, Kao-Chao Lin, Pei-Chi Chang, Chuan-Pin Juan, Han-Chung Tai, and Huang-Chung Cheng, *"Properties of Carbon Nanotubes Via a Thin Ti Capping Layer on the Pretreated Catalyst,"* Journal of The Electrochemical Society, 154 (3) J109-J115 (2007)

[74] Rui-Ling LAI, Jiun-Kai SHIU, Yao-Ren CHANG, Kao-Chao LIN, Pei-Chi CHANG, Chuan-Pin JUAN, Chien-Yin LEE, Shia-Wei CHEN, and Huang-Chung CHENG, *"The Reliability Improvements of Carbon Nanotubes Emitters by Utilizing an Fe–Ti Codeposited Catalyst,"* J.J.A.P. Vol. 46, No. 8A, 2007, pp. 5367–5372.

[75] S. H. Jo, Y. Tu, Z. P. Huang and D. L. Carnahan, D. Z. Wang and Z. F. Ren, *"Effect of length and spacing of vertically aligned carbon nanotubes on field emission properties,"* APPLIED PHYSICS LETTERS VOLUME 82, NUMBER 20

[76] L. Nilsson, O. Groening, C. Emmenegger, O. Kuettel, E. Schaller, and L. Schlapbach, H. Kind, J-M. Bonard, and K. Kern, *"Scanning field emission from patterned carbon nanotube films,"* APPLIED PHYSICS LETTERS VOLUME 76, NUMBER 15

[77] Shunjiro Fujii, Shin-ichi Honda, Hideyasu Kawai, Kazuhiro Ishida, Kenjiro Oura, Mitsuhiro Katayama, *"Effect of arrangement of pillar array of aligned carbon nanotube bundles on its field-emission characteristic,"* Diamond & Related Materials 17 (2008) pp.556–558

[78] Jung Sang Suh, Kwang Seok Jeong, and Jin Seung Lee, Intaek Han, *"Study of the field-screening effect of highly ordered carbon nanotube arrays,"* APPLIED PHYSICS LETTERS VOLUME 80, NUMBER 13

[79] Jessica L. Killian, Nathaniel B. Zuckerman, Darrell L. Niemann, Bryan P. Ribaya, Mahmud Rahman, Robert Espinosa, M. Meyyappan, and Cattien V. Nguyen, *"Field emission properties of carbon nanotube pillar arrays,"* JOURNAL OF APPLIED PHYSICS 103, 064312 (2008)

[80] 邱源成，李榮宗，趙啟盛，「惰性氣體中直流電器銀接點電弧特性和損耗機制之研究」，國立中山大學機械與機電工程研究所碩士論文，高雄市，民國九十一年。

[81] 魏英彰，「利用二段式熱化學氣相沉積法成長不同間距高度比之奈米碳管柱列之場發射特性研究」，國立交通大學電子研究所碩士論文，新竹市，民國九十八年。

Vita

姓 名: 黃均宇

性 別: 男

生 日: 民國七十六年二月十九日

籍 貫: 彰化縣

地 址: 屏東縣恆春鎮中正路 232 巷 147 弄 19 號 3 樓

學 歷: 國立交通大學電子工程學系

(94 年 9 月～98 年 7 月)

國立交通大學電子工程研究所碩士班

(98 年 9 月～100 年 7 月)

論文題目:

利用共鍍催化金屬與不同間距高度比之奈米碳管柱列改善氣體游離式感測器之特性研究

Study on the improvement of carbon nanotubes gas ionization sensors via co-deposited catalyst and pillar array with different spacer / height ratios